PREPARATION AND CHARACTERIZATION OF VINYL SILANE CROSSLINKED THERMOPLASTIC COMPOSITES FILLED WITH NATURAL FIBRES

by

TEBOHO CLEMENT MOKHENA (B.Sc. Hons.)

Submitted in accordance with the requirements for the degree

MASTER OF SCIENCE (M.Sc.)

Department of Chemistry

Faculty of Natural and Agricultural Sciences

at the

UNIVERSTY OF THE FREE STATE (QWAQWA CAMPUS)

SUPERVISOR: Prof AS Luyt

December 2012

DECLARATION

We, the undersigned, hereby declare that the research in this thesis is Mr Mokhena's own original work, which has not partly or fully been submitted to any university in order to obtain a degree.

_____ _____

TC Mokhena Prof AS Luyt

DEDICATION

This work is dedicated to my late parents, Letsatsi Ramateka Mokhena and Maboteng Agnes Nondlala. I will always love and remember them as pillars of my life.

To the entire Mokhena family “Bakgatla ba batle Maananong”.

ABSTRACT

In this work sisal nanowhiskers (SNW) extracted from sisal fibres were used to reinforce polyethylene matrices, high-density polyethylene (HDPE) and low-density polyethylene (LDPE). The nanocomposites were prepared by solution casting from toluene and melt-mixing, both followed by melt pressing. In the case of melt mixing, the surfaces of the SNW were also chemically modified with 1 phr of triethoxy vinyl silane (VTES) to improve their dispersibility and compatibility with the matrices. The nanocomposites and sisal nanowhiskers were characterized by Fourier transform infrared (FTIR) spectroscopy, transmission electron microscopy (TEM), scanning electron microscopy (SEM), thermogravimetric analysis (TGA), differential scanning calorimetry (DSC), dynamic mechanical analysis (DMA) and X-ray diffractometry (XRD). The sisal nanowhiskers, obtained through sulphuric acid hydrolysis treatment, had average lengths of 197 ± 75 nm and diameters of 12.2 ± 3.7 nm, and a crystallinity index of 89%. FTIR confirmed the surface chemical modification of the sisal nanowhiskers. The microscopic techniques demonstrated a fairly good dispersion of the whiskers in the matrices, regardless of the treatment or the preparation method. The storage modulus for the solution mixed nanocomposites was better than the untreated melt mixed nanocomposites. This behaviour was ascribed to the formation of a rigid cellulosic network during processing. For the treated melt mixed samples, the reinforcing effect was worse, suggesting the absence of a strong mechanical network because of the good interaction between the whiskers and the host polymer matrix. TGA revealed that there was no significant influence on the degradation behaviour of both polymers. The crystallization behaviour of the polymers was found to strongly depend on their morphologies. The melting and crystallization behaviour of the LDPE nanocomposites were almost unchanged, while an increase in crystallinity was observed for all the HDPE nanocomposites. The tensile properties depended on the type of polymer, the treatment, and the preparation method. Generally there was an improvement in tensile modulus, and a decrease in elongation at break, but the stress at break only improved for the HDPE nanocomposites.

TABLE OF CONTENTS

LIST OF ABBREVIATIONS

AFM	Atomic force microscopy
aPP	Atactic propylene
ATR-FTIR	Attenuated total reflectance Fourier-transform infra-red spectroscopy
CN	Cellulose nanowhiskers
DCP	Dicumyl peroxide
DDLS	Depolarized dynamic light scattering
DLS	Polarized dynamic light scattering
DMA	Dynamic mechanical analysis
DSC	Differential scanning calorimetry
FTIR	Fourier transform infra-red
FWHM	Full width at half maximum
HDPE	High-density polyethylene
IXS	Inelastic X-ray scattering
LDPE	Low-density polyethylene
MA	Maleic anhydride
MAPP	Maleic anhydride grafted polypropylene
MCC	Microcrystalline cellulose
MFC	Microfibrillated cellulose
PE	Polyethylene
PP-g-MA	Maleic anhydride grafted polypropylene
PP	Polypropylene
RH	Relative humidity
SAXS	Small-angle X-ray scattering
SEM	Scanning electron microscopy
SCN	Spherical cellulose nanowhiskers
SNW	Sisal nanowhiskers
T_c	Crystallization temperature
TEM	Transmission electron microscopy
TGA	Thermogravimetric analysis
T_g	Glass transition temperature

T_m	Melting temperature
VTES	Vinyl triethoxysilane
XRD	X-ray diffractometry
WAXD	Wide angle X-ray diffractometry
ΔH_f	Enthalpy of fusion
ΔH_m	Melting enthalpy
ΔH_m^{norm}	Normalised melting enthalpy
ΔH_m^{obs}	Observed melting enthalpy
ΔH_∞	Melting enthalpy of 100% crystalline polymer
χc	Crystallinity

LIST OF TABLES

LIST OF FIGURES

Chapter 1: General introduction

1.1 Background

The need for the development of environmentally friendlier materials has drawn much interest from many scientists, in the industrial and academic communities, due to the consciousness about the conservation of the environment. This was led by increased pressure from governments and customer needs globally to produce environmentally benign and sustainable materials, which was driven by the consumption rate of petroleum-based materials and the fear of their exhaustion in the future. It is estimated that the rate of consumption of these materials is 100 000 times higher than nature can replenish, and their production is 20 times more than the combination of all metals since their introduction into the market [1-6].

A possible solution is the introduction of fillers that are cheaper and less harmful to the environment. Various types of fillers such as aramid, natural fibres, carbon, and glass have been used as reinforcing materials for polymers with the main aim to increase some of the properties of the resulting products. The manmade or engineering fillers (e.g. glass fibre and aramid) are too expensive and harmful to our ecosystem, thus they are not good from an economical and ecological viewpoint [7-10]. Natural fibres render some advantageous properties such as biodegradability, sustainability, low abrasion and they are abundantly available and therefore cheaper. Natural fibre reinforced composites have low densities, good specific strength, high toughness and good acoustic properties. The fibres are, however, inherently incompatible with hydrophobic polymer matrices and they have scattered mechanical properties, even if they are from the same source. The natural fibres' properties are reliable on factors such as weather, soil type, age and the external stimuli which affect the plant during its growth [11-16].

Nanocomposites are generally defined as composites in which one of the components has at least one or more dimensions in the nanorange (< 100 nm). The nanocomposites technology became one of the interesting fields of study and occupied most of the reinforcement arena, thanks to the Toyota group from Japan. Their introduction of nanofiller reinforcement in the early 1990s led to a huge paradigm shift from micro- to nano-scale fillers. Nanofillers offer excellent mechanical and optical properties at low contents, due to large surface areas which

lead to better interaction with the matrix. The resulting nanocomposites also have improved stiffness, strength, toughness, thermal stability, barrier properties and flame retardancy compared to the pure polymers. Nowadays, the recognition of these nano-sized fillers increased the choice of fillers [17,18].

Cellulosic nanofillers have some advantages compared to other nanofillers, such as biodegradability, and abundant availability, hence lower cost. Besides their renewability, cellulose whiskers merit special consideration due to their remarkable reinforcing capability. Cellulose whiskers already act as the reinforcing elements in plants and animals. It consists of slender parallelepiped rods with nanometric lateral dimensions and hence high aspect ratios. Depending on the processing route one can have either microfibrillated cellulose or cellulose nanocrystals. Microfibrillated cellulose results from mechanical treatments such as high pressure homogenization, while the acid hydrolysis of biomass yields cellulose nanocrystals. Acid hydrolysis treatment dissolves the less lateral ordered part (amorphous region), leaving behind a water-insoluble highly crystalline residue which is converted into a stable suspension through mechanical treatment. The resulting rod-like particles are known as cellulose nanocrystals, whiskers, nanowhiskers or micro-crystallites. Their morphology and dimensions depend on the nature of the source and the controlled acid hydrolysis conditions, such as concentration of the acid, temperature and time. Their diameters range between 2 and 20 nm and their lengths vary between 100 nm and several tens of microns. Because of a small number of defects their axial Young's modulus is estimated to be close to that of Kevlar and more than that of steel. Depending on the analysis technique, their axial Young's modulus may range between 137 and 143 GPa, and their strength may be in the order of 7 GPa [19-22].

The exploitation of all the above-mentioned advantages of natural nanofillers as reinforcement in thermoplastics and thermosets is governed by their inherent polar character resulting in incompatibility with and poor dispersion in non-polar polymer matrices. This results in poor adhesion, durability and mechanical properties. The reinforcement of synthetic and natural polymers by natural nanofillers is still limited to either water-soluble or aqueous suspensions of polymer, such as latex. However, several attempts have been made to improve their dispersion and compatibility, such as graft copolymerization and surface treatment of cellulose nanofibres, either with surfactants or by modifying their surface with chemicals such as chlorosilanes, silanes, maleated propylene and isocyanates. The production of

cellulose whiskers is also time consuming and give low yields, hence their availability is still limited. A viable method for industrial production (through melt compounding or extrusion) of natural nanocellulose reinforced materials is required [23-26].

1.2 Objective of the study

The objective of this study was to investigate the effect of triethoxy vinyl silane treatment on the dispersion of sisal nanowhiskers in polyethylene matrices. High-density polyethylene (HDPE) and low-density polyethylene (LDPE) were chosen because of their wide utilization, and because of the differences between their morphologies and properties. Solution casting of polyethylene/sisal whiskers suspensions, and melt-mixing of the different components, both followed by hot melt pressing, were carried out to compare the effect of the processing method on the properties of the resulting nanocomposites. The morphology, thermomechanical, mechanical, and thermal properties of the nanocomposites were investigated by using scanning (SEM) and transmission (TEM) electron microscopy, dynamic mechanical analysis (DMA), tensile testing, thermogravimetric analysis (TGA), differential scanning calorimetry (DSC), and X-ray diffractometry (XRD).

1.3. Thesis outline

The outline of this thesis is as follows:

- Chapter 1: General introduction
- Chapter 2: Literature review
- Chapter 3: Materials and methods
- Chapter 4: Results and discussion
- Chapter 5: Conclusions

1.4 References

1. N.L.G. de Rodriguez, W. Thielemans, A. Dufresne. Sisal cellulose whiskers reinforced polyvinyl acetate nanocomposites. Cellulose 2006; 13:261-270. DOI: 10.1007/s10570-005-9039-7

2. M.P. Hekkert, L.A.J. Joosten, E. Worrell, W.C. Turkenburg. Reduction of CO_2 emissions by improved management of material and product use: The primary case of packaging. Resources, Conservation and Recycling 2000; 29:33-64.
DOI: 10.1016/S0921-3449(99)00056-7.

3. J. Lu, T. Wang, L.T. Drzal. Preparation and properties of microfibrillated cellulose polyvinyl alcohol composites materials. Composites: Part A, 2008; 39:738-746.
DOI: 10.1016/j.compositesa.2008.02.003.

4. A. Bendahou, H. Kaddami, H. Sautereau, M. Raihane, F. Erchiqui, A. Dufresne. Shortpalm tree fibers polyolefin composites: Effect of filler content and coupling agent on physical properties. Macromolecular Materials and Engineering 2008; 293:140-148.
DOI: 10.1002/mame.200700315.

5. J.K. Pandey, W.S. Chu, C.S. Kim, C.S. Lee, S.H. Ahn. Bio-nano reinforcement of environmentally degradable polymer matrix by cellulose whiskers from grass. Composites: Part B 2009; 40:676-680.
DOI: 10.1016/j.compositesb.2009.04.013.

6. K. Oksman, A.P. Mathew, D. Bendeson, I. Kvein. Manufacturing process of cellulose whiskers/polylactic acid nanocomposites. Composites Science and Technology 2006; 66:2276-2784.
DOI: 10.1016/j.compscitech.2006.03.002.

7. P. Chen, J. Wang, B. Wang, W. Li, C. Zhang, H. Li, B. Sun. Improvement of interfacial adhesion for plasma-treated aramid fiber-reinforced poly(phthalazinone ether sulfone ketone) composite and fiber surface aging effects. Surface and Interface Analysis 2009; 41:38-43.
DOI: 10.1002/sia.2972

8. X.C. Ge, X.H. Li, Y.Z. Meng. Tensile properties, morphology, and thermal behaviour of PVC composites containing pine flour and bamboo flour. Journal of Applied Polymer Science 2004; 93:1804-1811.
DOI:10.1002/app.20644

9. R. Velmurugan, V. Manikandan. Mechanical properties of palmyra/glass fiber hybrid composites. Composites: Part A 2007; 38:2216-2226.
DOI: 10.1016/j.compositesa.2007.06.006

10. X. Li, L.P. Tabil, S. Panigrahi. Chemical treatments of natural fiber for use in natural fiber-reinforced composites: A review. Journal of Polymers and the Environment 2007; 15:25-33.
DOI: 10.1007/s10924-006-0042-3.

11. N. Ljungberg, J.–Y. Carvaillé, L. Heux. Nanocomposites of isotactic propylene reinforced with rod-like cellulose whiskers. Polymer 2006; 47:6285-6292.
DOI: 10.1016/j.polymer.2006.07.013.

12. F.P. La Mantia, M. Morreale. Green composites: A brief review. Composites: Part A 2011; 42:579-588.
DOI: 10.1016/j.compositesa.2011.01.017.

13. A.J. de Menezes, G. Siqueira, A.A.S. Curvelo, A. Dufresne. Extrusion and characterization of functionalized cellulose whiskers reinforced polyethylene nanocomposites. Polymer 2009; 50:4552-4563.
DOI: 10.1016/j.polymer.2009.07.038.

14. H-S. Yang, H. Kim, H. Park, B. Lee, T. Hwang. Water absorption behaviour and mechanical properties of lignocellulosic filler-polyolefin biocomposites. Composite Structures 2006; 72:429-437.
DOI: 10.1016/j.compstruct.2005.10.013

15. A. Arbelaiz, B. Fernández, J.A. Ramos, A. Retegi, R. Llano-Ponte, I. Mondragon. Mechanical properties of short flax fibre bundle/polypropylene composites: Influence of matrix/fibre modification, fibre content, water uptake and recycling. Composites Science and Technology 2005; 65:1582-1592.
DOI: 10.1016/j.compscitech.2005.01.008.

16. A.K. Bledzki, M. Letman, A. Viksne, L. Rence. A comparison of compounding processes and wood type for wood fibre-PP composites. Composites: Part A 2005; 36:789-797.
DOI: 10.1016/j.compositesa.2004.10.029.

17. L. Petersson, K. Oksman. Biopolymer based nanocomposites: Comparing layered silicates and microcrystalline cellulose as nanoreinforcement. Composites Science and Technology 2006; 66:2187-2196.
DOI: 10.1016/j.compscitech.2005.12.010

18. A. Ranade, N.A. D'Souza, B. Gnade. Exfoliated and intercalated polyamide-imide nanocomposites with montimorillonite. Polymer 2002; 43:3759-3766.
DOI: 10.1016/S0032-3861(02)00106-4

19. S.J. Eichhorn, A. Dufresne, M. Aranguren, N.E. Marcovich, J.R. Capadona, S.J. Rowan, C. Weder, W. Thielemans, M Roman, S. Renneckar, W. Gindl, S. Viegel, J. Keckes, H. Yano, K. Abe, M. Nogi, A.N. Nakagaito, A. Mangalam, J. Simonsen, A.S. Benight, A. Bismarck, L.A. Berglund, T. Peijs. Review: Current international research into cellulose nanofibres and nanocomposites. Journal of Materials Science 2010; 45:1-33.
DOI:10.1007/s10853-009-3874-0.

20. B. Braun, J.R. Dorgan. Single-step method for the isolation and surface functionalization of cellulosic nanowhiskers. Biomacromolecules 2009; 10:334-341.
DOI: 10.1021/bm8011117.

21. J. Lu, P. Askeland, L.W. Drzal. Surface modification of microfibrillated cellulose for epoxy composite applications. Polymer 2008; 49:1285-1296.
DOI: 10.1016/j.polymer.2008.01.028.

22. J.B. Zhong, J. Lv, C. Wei. Mechanical properties of sisal fibre reinforced ureaformaldehyde resin composites. eXPRESS Polymer Letters 2007; 1:681-687.
DOI:10.3144/expresspolymlett.2007.93.

23. C. Goussé, H. Chanzy, G. Excoffier, L. Soubeyrand, E. Fleury. Stable suspensions of partially silylated cellulose whiskers dispersed in organic solvents. Polymer 2002; 43:2645-2651.
DOI: 10.1016/S0032-3861(02)00051-4.

24. A.N. Frone, S.-F.Chailan, D.M. Panaitescu, D. Donescu. Cellulose fiber-reinforced polylactic acid. Polymer Composites 2011; 32:977-985.
DOI: 10.1002/pc.21116.

25. N. Ljungberg, C. Bonini, F. Bortolussi, L. Heux, J.Y. Cavaillé. New nanocomposites materials reinforced with cellulose whiskers in actatic propylene: Effect of surface and dispersion characteristics. Biomacromolecules 2005; 6:2732-2739.
DOI: 10.1021/bm050222v.

26. G. Siqueira, J. Bras, A. Dufresne. Cellulose whiskers versus microfibrils: Influence of the nature of the nanoparticle and its surface functionalization on the thermal and mechanical properties of the nanocomposites. Biomacromolecules 2009; 10:425-432.
DOI: 10.1021/bm801193d.

Chapter 2: Literature review

2.1 Cellulose nanowhiskers

2.1.1 Classification and sources

A lot of work has been done on the preparation and characterization of cellulose nanowhiskers during the past decade [1-17]. A wide of variety of cellulose-containing sources were used for the production of cellulose nanowhiskers such as sisal, wood, flax, cotton, tunicates, bacterial and microcrystalline cellulose, ramie and valonia [1-11]. Several methods were used to extract cellulose nanocrystals from the sources such as mechanical processes [11,12], and acid and enzymatic hydrolysis [1-11,13,14]. These processes were often used separately or in combination depending on the desired morphology or geometrical dimensions. In general, there are two forms or types of cellulose nanoparticles, depending on the method applied and the resulting morphology and dimensions. The first one is a web-like network structure of long cellulose fibrils which is well-known in the literature as microfibrillated cellulose (MFC), and which is produced by mechanical treatment or by omitting acid hydrolysis treatment [11]. However, mild acid hydrolysis was reported to also produce microfibrillated cellulose [12]. The second type is known as cellulose nanoparticles, microcrystals, microcrystallites, nanowhiskers, nanocrystals, or nanofibers [1-11,13,14]. In this study, cellulose nanowhiskers will be used to present these remarkable materials. The commercial applications of these materials include food texturing, pharmaceutics and paper production.

2.1.2 Preparation and morphology

Acid hydrolysis is the classic method used to isolate cellulose nanowhiskers from a variety of sources [1-11]. It is worth noting that this step is considered as the second stage in the overall treatment, since a pretreatment step is required. Pretreatment include purification and homogenation of the source material, so that it reacts more consistently during the acid hydrolysis treatment. Pretreatment is dependent on the nature of the source and to a lesser degree on the desired morphology. Pretreatment of plants, for instance, consists of complete or partially removing the matrix materials (hemicellulose, lignin, etc.). The second stage

involves the separation of the purified material into nanocrystals. The pretreated material is then exposed to harsh acid hydrolysis at a given concentration, time and temperature. Sulphuric acid and hydrochloric acid are the most used acids, but the use of other acids such as bromic acid and maleic acid has also been reported. When sulphuric acid is used to prepare cellulose nanowhiskers, it reacts with the surface hydroxyl groups of cellulose *via* esterification, giving a stable suspension in water. This is limited in hydrochloric acid as a hydrolyzing agent, and these suspensions tend to flocculate. During acid hydrolysis the amorphous regions are dissolved, leaving behind intact crystalline regions. This is attributed to faster hydrolysis kinetics of the amorphous regions with respect to the crystalline ones. The hydronium ions easily penetrate the microfibrils in the amorphous regions, promoting hydrolytic cleavage of glycosidic links and leaving behind the highly crystalline particles. The resulting suspension is diluted with ice cubes to quench the reaction. The suspension then undergoes successive washing by centrifugation, followed by dialysis against deionized water to remove the remaining acid. A final centrifuge or filtration step may be performed to remove any aggregates in the suspension. Ultrasonication treatment is often used to facilitate the dispersion of the crystalline cellulose [5-7].

Microscopic techniques such as transmission electron microscopy (TEM), scanning electron microscopy (SEM) and atomic force microscopy (AFM) are the most used techniques to establish the shape and dimensions of the cellulose nanowhiskers. However, polarized dynamic light scattering (DLS), depolarized dynamic light scattering (DDLS) and small-angle X-ray scattering (SAXS) were also used for this purpose [6-15]. The cellulose nanowhiskers prepared *via* acid and enzymatic hydrolysis appear as elongated rod-like crystalline nanoparticles, regardless of the source. The resulting morphology and crystallinity are similar to those of original cellulose fibres. The dimensions and morphology were found to depend on the nature of the source and the controlled acid hydrolysis conditions such as time, temperature and acid concentration. In general, the sulphuric acid concentration does not vary much from 65% and the hydrolysis time may vary from 30 minutes to 24 hours depending on the temperature and the nature of the source material. However, the concentration of hydrochloric acid may vary from 9 to 15%. The cellulose nanowhiskers' diameters range between 2 to 20 nm, and their lengths vary between 100 nm and several tens of microns. Microfibrillated cellulose (MFC) appears as long hairy fibrils of cellulose. MFC is usually prepared by mechanical means such as a high pressure homogenizer, but mild acid conditions may lead to this kind of nanoparticle [11-12]. In addition, spherical cellulose

nanowhiskers were also reported to be produced by a mixture of hydrochloric acid and sulphuric acid [16-18].

Cellulose nanowhiskers were found to appear as spheroids or ovaloids. It was reported that at low contents cellulose nanowhisker particles are randomly oriented in aqueous suspension as an isotropic phase, and when the concentration reaches a critical value, they form a chiral nematic ordering, where these suspensions transform from an isotropic to an anisotropic chiral nematic liquid crystalline phase. Further increases in concentration of the cellulose nanowhisker particles showed a birefringence phenomenon. These phases depend on the surface charge density and mainly on the aspect ratio. These investigations showed that the chiral nematic order can be retained after water evaporation when observed between cross-polarizers [19-24].

Bendeson *et al.* [8] studied the effect of preparation conditions (concentration of microcrystalline cellulose (MCC) and sulphuric acid, the hydrolysis time and temperature, and the ultrasonication treatment time) on the ensuing cellulose nanowhiskers' structure for sulphuric acid hydrolysis of microcrystalline cellulose derived from Norwegian spruce (*Picea abies*). The authors used response surface methodology to find the optimum conditions to produce cellulose nanocrystals. They observed a decrease in the length of the MCC and an increase in the surface charge with prolonged hydrolysis. They also found that the optimum conditions to produce cellulose nanowhiskers were sulphuric acid (63.5%) for about 2 hours at ~45 °C. The nanowhiskers' length ranged between 200 and 400 nm, the width was less than 10 nm, and the yield was 30% (with respect to the initial fibre weight). The ultrasonication time and initial concentration of MCC, however, did not have any influence. For a concentration of 0.1 g cellulose/100 ml a clear flow birefringence of a nematic liquid crystalline phase was observed between two crossed polarizing films.

Beck-Candanedo *et al*. [4] compared the properties of cellulose nanocrystals obtained by acid hydrolysis of softwood and hardwood and investigated the influence of hydrolysis time and acid-to-pulp ratio. They found that the nanocrystals displayed similar dimensions, surface charge, and critical concentrations required to form an anisotropic liquid phase. They found that prolonged hydrolysis conditions and higher acid-to-pulp ratios yield shorter nanocrystals with narrower polydispersity indices and that the anisotropic concentration increased. However, the cellulose nanocrystal dimensions did not dependent on time and temperature.

The temperature and time were varied during the preparation of cellulose nanocrystals from commercial cotton fibres by sulphuric acid hydrolysis, and the cellulose nanowhiskers showed similar dimensions [5]. Different nanowhisker dimensions from two cellulose sources (wood and cotton) were reported by Pakzad *et al*. [25]. The authors used the same conditions as Beck-Candanedo *et al*. [4]. They found that the wood nanowhiskers were longer and thinner than the cotton cellulose nanowhiskers.

Wang *et al*. [16,18] prepared spherical cellulose nanowhiskers (SCN) by acid hydrolysis of microcrystalline cellulose with a mixture of acid composed of sulphuric acid, hydrochloric acid and water at a ratio of 3:1:6 under ultrasonication. The authors obtained spherical cellulose nanowhiskers with diameters in the range of 10-180 nm, but mostly between 20 and 90 nm. The average diameter was 62 nm with polydispersity (standard deviation of the particle size distribution by the average size) going up to 49%. They also found that at a low solid content the SCN suspension displayed an isotropic phase and showed a flow birefringence pattern after injection, but that this pattern disappeared after the suspension stood still. At higher solids contents the suspensions displayed a chromatic birefringence at rest. They observed a liquid crystalline phase under polarized optical microscopy at solids contents above 3.9%. At higher solids contents a crosshatch pattern was observed. Similar shapes was reported by Zhang *et al*. [17], using similar preparation conditions.

2.1.3 Thermal properties

The thermal properties of materials are important for their applications and processing conditions. Most researchers used TGA to study the thermal behaviour of cellulosic nanowhiskers [5,7,13,19-23,26,27]. A small mass loss (~1%) was observed below 100 °C and was attributed to water evaporation. A second step associated with depolymerisation, dehydration and decomposition of glycosyl units occurred between 100 and ~300 °C. This step represents the thermal stability of cellulose nanocrystals with a weight loss of ~50%. The last step consisted of the formation of charred residue which is oxidized and degraded at temperatures above 400 °C. All these events were dependent on several factors such as the extraction method, post-treatment, the drying method, crystallinity, analysis atmosphere (inert or oxidizing) and heating rate. Beside the fact that sulphuric acid hydrolysis yield stable suspensions in water, the thermostability of the resulting cellulose nanowhiskers were found

to be reduced. Prolonged sulphuric acid hydrolysis was found to introduce a large number of sulphate ions on the surface of the cellulose nanowhiskers, and the removal of these ions requires less energy compared to hydroxyl groups. This resulted in less thermally stable cellulose nanowhiskers. Treatment with stronger bases such as sodium hydroxide was found to neutralize the sulphate ions and increase the thermostability of the whiskers. An alternative was to use hydrochloric acid (HCl), which does not introduce acidic groups. The problem of CN obtained from HCl acid hydrolysis was their flocculation in water. This was ascribed to a lack of surface charges [5,7,13,21,22,23,26].

Martins *et al*. [5] compared the effect of preparation and drying methods on the properties of the cellulose nanocrystals derived from commercial cotton by sulphuric acid hydrolysis. The cellulose nanocrystals showed lower thermal stability with respect to native cotton, and they showed several degradation steps. It was pointed out that extraction at high temperatures led to less thermally stable cellulose nanowhiskers because of the greater number of sulphates ions introduced on the cellulose nanocrystals' surfaces. Freeze dried cellulose whiskers showed high crystallinity and better thermal stability than the oven dried whiskers due to the low temperatures involved during drying. It was also reported that enzymatic hydrolysis led to thermally stable cellulose nanowhiskers compared to sulphuric acid hydrolysis [13]. Post-treatment of the cellulose nanowhiskers with sodium hydroxide, however, was found to increase their thermostability and crystallinity [26].

The effect of different surface treatments of cellulose nanowhiskers on their thermal properties was studied Petersson *et al*. [27]. The nanowhiskers were modified with tert-butanol, coated with surfactant (Beycostat AB09) and compared with unmodified ones. All the nanowhiskers displayed a mass loss below 150 °C which was attributed to water evaporation. The unmodified and tert-butanol treated nanowhiskers degraded earlier than the native MCC and the surfactant coated ones. This was attributed to the acid hydrolysis treatment with sulphuric acid. It was reported that the surfactant coated the nanowhiskers and delayed their degradation which gave rise to high residual masses.

2.1.4 Mechanical properties of cellulose nanowhiskers

The nanosize of these materials makes it difficult to use available techniques to characterize their mechanical properties. Some work was done on the incorporation of the nanowhiskers

in epoxy resins or dispersing them in mica (in the case of atomic force microscopy (AFM)) in order to investigate these properties [29-34]. The experimental results and theoretical models were compared in these studies. The mechanical properties were investigated by AFM, inelastic X-ray scattering (IXS), Raman spectroscopy and tensile testing. The elastic modulus in the axial and transverse directions was found to be in the range of 140-220 GPa and 9-15 GPa, respectively. These values depended on the technique used, the type of cellulose nanowhiskers used, and the analysis conditions. Šturcová *et al*. [32] studied the elastic modulus of tunicate cellulose nanowhiskers using Raman spectroscopy. The modulus was calculated using the characteristic peak (1095 cm^{-1}) during the deformation of the nanowhiskers in an epoxy resin using a four-bending bending test. They reported an experimental modulus of 143 GPa and a theoretical modulus of 145 GPa. An elastic modulus ranging between 18 and 50 GPa at 0.1% RH for wood cellulose nanowhiskers was reported by Lahiji *et al*. [29], using AFM. The elastic modulus of flax microfibrils was reported to be approximately 15 GPa, and the axial modulus 220 GPa, as determined by inelastic X-ray scattering (IXS) [30]. A Young's modulus of ~5 GPa was reported for tunicate cellulose nanowhiskers films obtained from water casting using tensile testing [34].

2.2 Sisal nanowhiskers

Sisal fibre is an interesting high tensile strength fibre known for its short renewable times. It is obtained from the leaves of the sisal plant (*Agave sisalana*). Brazil and India are regarded as the main producers of sisal fibres, but countries like Tanzania are also known as producers. Many studies have been done on the development of new composite materials using sisal fibre [35-36]. Recent studies show that sisal fibres have the potential to be used for the production of cellulose nanoparticles such as nanowhiskers and microfibrillated MFC [1-2,11,37-39]. It was reported in the literature that through acid hydrolysis sisal nanowhiskers with an aspect ratio of about 60 can be produced from sisal fibres. The resulting diameters ranged between 5 and 6 nm and the lengths between 200 and 250 nm. MFCs with the diameters of about 52 nm was also produced by passing the fibres through a microfluidizer ten times [11,37]. Several polymers such as polyvinyl acetate and polycaprolactone were used to prepare nanocomposites using the sisal nanowhiskers and MFC as a reinforcing phases [1,37]. Significant improvements in the mechanical and thermal properties were observed by incorporating sisal nanowhiskers into these polymer matrices. This showed the

reinforcing capability of sisal nanoparticles, which can be improved by chemical modification for better dispersion and hence improved mechanical and thermal properties.

2.3 Polyolefin/cellulose nanowhiskers nanocomposites

Nowadays, the incorporation of nanofiller in synthetic polymers has been an attractive scientific topic because of the improved properties at low filler contents (<10 wt%) [40-42]. Addition of these nanosize fillers into polymeric materials results in products exhibiting exceptional properties, that are not observed in either component. These properties include improved mechanical and electrical properties, higher thermal stability, and good barrier properties, compared to the pure polymer or conventional micro-composites. This increases the number of applications of the synthetic polymers and reduces the cost, especially when natural nanofillers are used [9,33,49-52].

2.3.1 Preparation and morphology

The stability of cellulose nanowhisker suspensions after acid hydrolysis treatment has been the controlling factor in preparing cellulosic nanocomposites. This led to more studies exploring water as processing medium in order to maintain the stability and dispersed state of the nanowhiskers, which makes hydrosoluble polymers to be the most studied host polymers [1,3,51]. The use of aqueous dispersed polymers (i.e. latexes) was the first alternative that opened doors to explore hydrophobic polymers [3,6,45-46]. The second alternative consisted of the modification of cellulose nanowhisker surfaces with surfactants or other chemicals in order to disperse them in an adequate organic solvent in order to be included in a suitable polymer matrix. The processing of the nanocomposites consisted of aqueous nanowhisker suspensions mixed with dispersed or dissolved polymers. The three most used techniques to prepare composites films are casting followed by solvent evaporation, freeze drying and hot-pressing, and freeze drying, extrusion and hot-pressing of the mixture. These techniques result in different morphologies which control the resulting mechanical and thermal properties [1,3,51-60]. Polyolefin/cellulose nanowhiskers nanocomposites have not been investigated as thoroughly as the microcomposites [9,33,47-52]. This is the result of the processing techniques that require processing temperatures very close to the onset temperatures of thermal degradation of the cellulosic nanowhiskers. It was also attributed to the difficulty of achieving reasonable dispersion of the strongly hydrophilic cellulose

nanowhiskers in the hydrophobic thermoplastics because of the incompatibility between the two. The cellulose nanowhiskers, however, were chemically modified to enhance their dispersion and compatibility, and these nanocomposites were compared with the nanocomposites prepared with unmodified nanowhiskers. The modified cellulose nanowhiskers resulted in homogeneity and improved properties of the resulting nanocomposites [9,33,49,51,52].

Although it was possible to observe the dispersion and homogeneity of these nanocomposites, SEM was used for detailed structural examinations. The film surfaces, depending on the homogeneity, appeared either similar to that of the neat polymer or opaque. The opacity was ascribed to the lack of homogeneity, the presence of aggregates in micrometric size, or remaining bubbles. It was pointed out that the composite films that look similar to the neat polymer resulted from homogeneity and good dispersion. The cellulose nanowhiskers generally appeared as white dots and their concentration was found to be a direct function of the cellulose content in the nanocomposites. The homogeneity was dependent on the type modification used and the processing technique [1,3,51-52].

Organic acid chloride-grafted cellulose nanowhiskers were extruded with low density polyethylene (LDPE) by de Menezes *et al*. [9]. The photographs of the unmodified nanowhisker nanocomposites showed black dots. However, the nanowhisker composites modified with acid chlorides with longer aliphatic chains (stearoyl chloride) appeared the same as that of the unfilled LDPE films. This was attributed to better dispersion of the nanowhiskers in the polymer, even at higher nanowhisker contents.

Ljungberg *et al*. [34] studied the effect of filler characteristics on the overall properties of the final nanocomposites. The cellulose nanowhiskers surface characteristics were varied by maintaining the nanowhiskers' surfaces without modification, or by grafting maleated polypropylene to the nanowhiskers' surfaces, or by dispersing them with a surfactant. The nanocomposite films were obtained by mixing atactic propylene (aPP) dissolved in hot toluene at 110 °C with 6 wt% of different kinds of fillers dispersed in toluene. The solvent was then evaporated at 110 °C. The nanocomposite films from the whiskers without modification and from the MAPP grafted suspensions were opaque, and this was ascribed to aggregates of micrometric size or to voids. The nanocomposites reinforced with nanowhiskers coated with a surfactant were transparent as a result of improved dispersion.

The fractured surfaces of the films observed through SEM showed aggregates of nanowhiskers with thicknesses of 0.5-1.0 μm in the case of unmodified and MAPP grafted nanocomposites, while the ones with surfactant showed no aggregates. Similar results were reported where the MAPP grafted nanowhiskers did not improved dispersibility of the nanowhiskers in a polypropylene matrix prepared by solution casting from toluene. Micropores and white dots with dimensions of 200 nm were observed [51].

Nanowhiskers were directly incorporated into PE or PP matrices through melt mixing using a Brabender at 170 °C, followed by compression moulding at 180 °C. Ethylene-acrylic oligomer was used as a dispersant. The SEM images revealed white spots which were not well dispersed, but the authors did not mention whether these spots represent the reinforcement phase or not. They did, however, report that the cellulose nanowhiskers may have been degraded during processing and pointed out that more work was needed to understand the dispersion of cellulose nanowhiskers in semicrystalline polymers [48]. Similar observations were reported by Lee *et al*. [47] on the extruded polypropylene-nanowhiskers composites. They could, however, not locate the cellulose nanowhiskers in the polymer nanocomposites.

2.3.2 Thermal properties

A number of researchers studied the influence of cellulose nanowhiskers on the thermal properties of the host polymer matrices [1,3,9,11,12,34,39,43-52]. In amorphous polymers the glass-rubber transition temperature has been an interesting event studied by either DSC or DMA [1,3,11,12,34,39]. In crystalline polymers the research was focused on the melting temperature and heat of fusion, supported by X-ray diffraction results [9,43-52]. Not much has been done on the thermal stability of cellulose bionanocomposites, but this topic is important when considering the processing and applications of these materials [9,51,52].

2.3.2.1 Melting and crystallization behaviour

Several authors reported that the addition of unmodified cellulose nanowhiskers into semicrystalline polymers has no influence on the melting temperature (T_m) [9,48,51]. Similar behaviour was reported for modified cellulose nanowhiskers. However, the heat of fusion and degree of crystallinity were reported to increase with the content of the cellulose

nanowhiskers, whether modified or not [9,48]. This effect was attributed to the cellulose nanowhiskers' nanosize and crystalline structure, which make them act as nucleating agents in the polymer matrix and promote crystallization. Spoljaric *et al*. [51] used different surface modifications for microcrystalline cellulose (MCC). The melt and crystallization temperatures showed to increase with an increase in unmodified MCC content, but the heat of fusion and crystallinity were reduced. This was attributed to the MCC having a cellulose II form which does not transcrystallize PP. Surface treatment with silicone oil and stearic acid showed marginal changes in the crystallization temperature (T_c), while PP-g-MA showed a slight increase on the T_c onset temperature. The T_c further increased with an increase in MCC content, which is the result of an increase in the number of nucleation sites. The authors suggested that the crystallization properties depended more on the MCC content than on the type of modification used to treat the MCC surfaces. The same behaviour was observed for the melting temperature (T_m).

De Menezes *et al*. [9] reported a significant increase in crystallinity with an increase in cellulose nanowhiskers content regardless of the type of surface modification. The T_m, however, remained roughly constant between 103 and 105 °C. They pointed out that the cellulose nanowhiskers acted as nucleating agents independent of their surface modification. The nucleation efficiency, however, was found to depend on the surface character of the cellulose nanowhiskers [49]. The nanocomposites with MAPP-modified nanowhiskers, however, inhibited the nucleating effect, while the unmodified and surfactant-modified nanowhiskers enhanced it. Both the unmodified and surfactant-modified nanocomposites showed two crystallization peaks (α- and β-phase). These results were supported by X-ray diffraction patterns in which the unmodified and surfactant grafted samples displayed peaks corresponding to the β-phase.

Very recently, Bahar *et al*. [51] reported that the melting and crystallization temperatures remained roughly constant with an increase in the MAPP-modified cellulose nanowhiskers concentration. In contrast to other reports where it was found that MAPP inhibited the nucleation efficiency of the PP matrix, these authors found that the 15 wt% MAPP-modified cellulose nanocomposites exhibited a 50% higher crystallinity than that of the neat polymer. Gray [50] studied the transcrystallization of PP on cellulose nanocrystals' surfaces by polarized optical microscopy. The author reported that the cellulose nanowhiskers acted as a nucleating agents and that this behaviour is influenced by their dispersion.

2.3.2.2 Thermal stability

There were only a few papers that reported on the thermal degradation behaviour of polyolefin/cellulose nanowhiskers composites [9,51,52]. Generally the presence of the cellulose nanowhiskers increased the decomposition temperature of the matrix. The initial degradation temperature, which is usually associated with water evaporation from the cellulose nanowhiskers, is however increased by the polymer. This is because the polymer covered the cellulose nanowhiskers and delayed their degradation temperature. These observations depended on the cellulose nanowhiskers contents and on the surface modification of the cellulose nanowhiskers.

The thermal degradation of PP/cellulose nanowhiskers composites were studied by Bahar *et al*. [51], using TGA. The authors observed that an increase in cellulose nanowhiskers content led to an increase in the decomposition temperature at 5% mass loss of the samples. The composites with 15 wt% nanofibres showed an ~15 °C higher temperature than pure PP at this mass loss. Similar behaviour was observed for the temperatures at 50% mass loss. This was ascribed to the presence of maleated polypropylene which enhanced the compatibility between the nanowhiskers and the PP matrix, and the thermal stability. In contrast, de Menezes *et al*. [9] reported that the onset temperatures of degradation of the LDPE/cellulose nanowhiskers nanocomposites were lower than that of the neat polymer. The latter happened independent of surface modification. Similar behaviour was observed at temperatures associated with 2% mass loss. This was attributed to the water content of the cellulosic filler. The T_d maximum (maximum of derivative signal), however, remained roughly constant regardless of the cellulose nanowhiskers content and their surface modification.

Spoljaric *et al*. [52] used different surface treatments of microcrystalline cellulose (MCC) to prepare the composites. They prepared MCC grafted with maleated propylene MAPP, and MCC treated with silicone oil, stearic acid and alkyltitanate. The polymer shielded the degradation of MCC which led to a higher decomposition temperature of the MCC, but an increase in MCC content slightly reduced the decomposition temperatures. The onset of decomposition of the polymers was not affected by the presence of the MCC. The authors reported that the thermal stability of the composites containing MCC modified with stearic acid and silicone oil was only marginally improved compared to those of their unmodified

counterparts. The thermal stability of the nanocomposites reinforced with MAPP grafted MCC, however, increased.

2.3.3 Mechanical properties

The mechanical properties of cellulose nanowhiskers reinforced polymers received considerable interest after the first announcement made by Favier *et al*. [6]. They reported a significant improvement in storage modulus above the glass-rubber transition temperatures with only 6 wt% of tunicin nanowhiskers incorporated in thermoplastic poly(styrene-co-butylacrylate). This led to more studies focussing on the improvement of the mechanical properties of polymers reinforced with cellulose nanowhiskers. These investigations were done through tensile testing and dynamic mechanical analysis (DMA) [9,11,12,34,39,43-52].

2.3.3.1 Non-linear mechanical properties

The tensile properties were found to strongly depend on the content and dispersion of nanowhiskers, and on the morphology of the nanowhiskers [9,34,49,51]. Bahar *et al*. [51] varied the hydrolysis and sonication times of the nanowhiskers in maleated polypropylene (MAPP), as well as the concentration of the MAPP. The tensile strength increased with the nanowhiskers content and it was more significant when the concentration of the MAPP was increased. This resulted from better compatibility and adhesion between the nanowhiskers and the polymer matrix. The strain at break increased while the modulus decreased up to 10% nanowhiskers content, after which the reverse was observed. This was ascribed to the addition of the nanowhiskers resulting in two competing effects: (i) micropores and (ii) the reinforcing effect of the fillers. The micropores were more effective at lower contents, while the reinforcing effect predominated at higher contents. Shorter sonication times led to lower tensile strengths and this was attributed to the incomplete dispersion of the nanowhiskers. Shorter hydrolysis times, however, led to slight increases in tensile strength which was ascribed to larger dimensions of the nanowhiskers. In contrast, a slight decrease in tensile strength with increase in nanowhiskers content was reported by Menezes *et al.* [9], while the modulus slightly increased, regardless of the surface modification. However, a significant improvement in elongation at break was observed when sufficiently long chains were grafted on the surface of the nanoparticles. This was ascribed to the better dispersion that resulted from the modification, giving rise to better stress transfer.

Ljungberg *et al*. [34] produced nanocomposites using atactic PP as apolar polymer reinforced with nanowhiskers without and with two different surface modifications. The modified nanowhiskers were (i) coated with surfactant and (ii) grafted with MAPP. The mechanical properties were significantly improved by the presence of the whiskers in all the nanocomposites. The authors pointed out that the tensile properties were not only dependent on filler-filler interaction, but also on the dispersion of the nanowhiskers. In another study [49], they used isotactic PP as the matrix with the same three unmodified and modified nanowhiskers. They reported that the quality of the nanowhiskers dispersion was a controlling factor in the tensile properties of these nanocomposites. The surfactant-modified whiskers improved the mechanical properties of the polymer more than the other whiskers.

2.3.3.2 Linear mechanical properties

Various researchers reported on the dynamic mechanical properties of polyolefin/cellulose nanowhiskers [9,49,51]. They found that these properties depend on the interwhisker interaction and the nanowhisker contents. In these studies chemical modifications were used to enhance the dispersion of whiskers and improve the properties of the product, but this process counteracted the interwhisker interaction which is believed to be responsible for the reinforcing effect. DMA results from these studies can be summarized into different observations. Firstly, no reinforcing effect was observed below T_g, while above T_g an increase in modulus was observed. These observations depended on the surface modification of the cellulose nanowhiskers and the competition between filler-filler and filler-polymer interaction. It was concluded that the modification of cellulose nanowhiskers must be mild not to destroy the hydrogen bonding between the nanowhiskers.

Ljungberg *et al*. [49] reported lower storage modulus values of the nanocomposites below T_g, and a significant reinforcing effect above T_g, depending on the surface modification. The storage modulus was higher for nanowhiskers coated with surfactant, followed by maleated propylene grafted nanowhiskers, and lastly the unmodified nanowhiskers. All the composites showed irremediable modulus reduction at higher temperatures than that of the neat polymer, and this was more obvious for the surfactant coated nanowhiskers. This was ascribed to mechanical coupling between the polypropylene crystallites and filler-filler interaction. In another investigation [34] they used atactic polypropylene as matrix and reported that there

was no significant reinforcing effect below T_g, but at higher temperatures the modulus was 50 times higher for all the composites, regardless of the surface modification. This effect was ascribed to a rigid network with filler-filler interactions.

De Menezes *et al*. [9] grafted different aliphatic organic acid chlorides, presenting different lengths, on ramie cellulose nanowhiskers by an esterification reaction. The authors prepared the nanocomposites by extrusion mixing of unmodified and grafted nanowhiskers with low density polyethylene. They reported that the storage modulus of the unmodified and grafted nanowhiskers composites was roughly the same as that of the neat polymer at temperatures below the glass transition, independent of the nanowhiskers content. A slight increase was observed in the rubbery region with respect to the neat polymer. This was ascribed to a reinforcing effect of the cellulose nanowhiskers and/or to the increase of the degree of crystallinity they observed in their DSC results. The chemical grafting of aliphatic chains onto the surface of the nanowhiskers, however, did not seem to have any effect. This was attributed to improved nanowhiskers dispersion which decreased the possibility of interwhiskers interactions. These interactions are believed to be the major factor responsible for the reinforcing effect in cellulose reinforced nanocomposites. Bahar *et al*. [51], however, reported that the storage modulus increased with the nanowhiskers content over the whole temperature range because of the surface modification of the nanowhiskers with maleated polypropylene.

2.4 References

1. N.L.G. de Rodriguez, W. Thielemans, A. Dufresne. Sisal cellulose whiskers reinforced polyvinyl acetate nanocomposites. Cellulose 2006; 13: 261-270.
   DOI: 10.1007/s10570-005-9039-7
2. J.I. Morán, V.A. Alvarez, V.P. Cyras, A. Vázquez. Extraction of cellulose and preparation of nanocellulose from sisal fibers. Cellulose 2008; 15:149-159.
   DOI: 10.1007/s10570-007-9145-9
3. X. Cao, H. Dong, C.M. Li. New nanocomposites materials reinforced with flax cellulose nanocrystals in waterborne polyurethane. Biomacromolecules 2007; 8:899-904.
   DOI: 10.1021/bm0610368

4. S. Beck-Candanedo, M. Roman, D.G. Gray. Effect of reaction conditions on the properties and behavior of wood cellulose nanocrystal suspensions. Biomacromolecules 2005; 6:1048-1054.
DOI: 10.1021/bm049300p
5. M.A. Martins, E.M. Texeira, A.C. Corrêa, M. Ferreira, L.H.C. Mattoso. Extraction and characterization of cellulose whiskers from commercial cotton fibers. Journal of Materials Science 2011; 46:7858-7864.
DOI: 10.1007/s10853-011-5767-2
6. V. Favier, H. Chanzy, J.Y. Cavaillé. Polymer nanocomposites reinforced by cellulose nanowhiskers. Macromolecules 1995; 28:6365-6367.
DOI: 10.1021/ma00122a053
7. M. Roman, W.T. Winter. Effect of sulfate groups from sulfuric acid hydrolysis on the thermal behavior of bacterial cellulose. Biomacromolecules 2004; 5:1671-1677.
DOI: 10.1021/bm034519
8. D. Bondeson, A. Mathew, K. Oksman. Optimization of the isolation of nanocrystals from microcrystalline cellulose by acid hydrolysis. Cellulose 2006; 13:171-180.
DOI: 10.1007/s10570-006-9061-4
9. A.J. de Menezes, G. Siqueira, A.A.S. Curvelo, A. Dufresne. Extrusion and characterization of functionalized cellulose whiskers reinforced polyethylene nanocomposites. Polymer 2009; 50:4552-4563.
DOI: 10.1016/j.polymer.2009.07.038
10. A.A. Baker, W. Helbert, J. Sugiyama. High-resolution atomic force microscopy of native valonia cellulose I microcrystals. Journal of Structural Biology 1997; 119:129-138.
DOI:10.1006/jsbi.1997.3866
11. G. Siqueira, J. Bras, A. Dufresne. Cellulose whiskers versus microfibrils: Influence of the nature of the nanoparticle and its surface functionalization on the thermal and mechanical properties of nanocomposites. Biomacromolecules 2009; 10:425-432.
DOI: 10.1021/bm801193d
12. M.A.S.A. Samir, F. Alloin, M. Paillet, A. Dufresne. Tangling effect in fibrillated cellulose reinforced nanocomposites. Macromolecules 2004; 37:4313-4316.
DOI: 10.1021/ma035939u

13. J. George, K.V. Ramana, A.S. Bawa, Siddaramaiah. Bacterial cellulose nanocrystals exhibiting high thermal stability and their polymer nanocomposites. International Journal of Biological Macromolecules 2011; 48:50-57.
DOI:10.1016/j.ijbiomac.2010.09.013
14. P. Satyamurthy, P. Jain, R.H. Balasubramanya, N. Vignesshwaran. Preparation and characterization of cellulose nanowhiskers from cotton fibres by controlled microbial hydrolysis. Carbohydrate Polymers 2011; 83:122-129.
DOI:10.1016/j.carbpol.2010.07.029
15. O.M. Astley, A.M. Donald. A small-angle X-ray scattering study of the effect of hydration on the microstructure of flax fiber. Biomacromolecules 2001; 2:672-680.
DOI: 10.1021/bm0056431
16. N. Wang, E. Ding, R. Cheng. Preparation and liquid crystalline properties of spherical cellulose nanocrystals. Langmuir 2008; 24:5-8.
DOI: 10.1021/la702923
17. J. Zhang, T.J. Elder, Y. Pu, A.J. Ragauskas. Facile synthesis of spherical cellulose nanoparticles. Carbohydrates Polymers 2007; 69:607-611.
DOI:10.1016/j.carbpol.2007.01.019
18. N. Wang, E. Ding, R. Cheng. Thermal degradation behaviors of spherical cellulose nanocrystals with sulfate groups. Polymer 2007; 48:3486-3493.
DOI: 10.1016/j.polymer.2007.03.062
19. D.-Y. Kim, Y. Nishiyama, M. Wada, S. Kuga. High yield carbonization of cellulose by sulfuric acid impregnation. Cellulose 2001; 8:29-33.
DOI: 10.1023A:1016621103245
20. P. Terech, L. Chazeau, J.Y. Cavaillé. A small-angle scattering study of cellulose whiskers in aqueous suspensions. Macromolecules 1999; 32:1872-1875.
DOI: 1021/ma9810621
21. O.M. Astley, A.M. Donald. A small-angle X-ray scattering study of the effect of hydration on the microstructure of flax fiber. Biomacromolecules 2001; 2:672-680.
DOI: 10.1021/bm0056431
22. Y. Habibi, L.A. Lucia, O.J. Rojas. Cellulose nanocrystals: Chemistry, self-assembly, and applications. Chemical Reviews 2010; 110:3479-3500.
DOI: 10.1021/cr900339w

23. L. Heux, G. Chauwe, C. Bonini. Nonflocculating and chiral-nematic self-ordering of cellulose microcrystals suspensions in nonpolar solvents. Langmuir 2000; 16:8210-8212. DOI: 10.1021/la9913957
24. M.M. de Souza Lima, R. Borsali. Rodlike cellulose microcrystals: Structure, properties, and applications. Macromolecular Rapid Communication 2004; 25:771-787. DOI: 10.1002/marc.200300268
25. A. Pakzad, J. Simonsen, P.A. Heiden, R.S. Yassar. Size effects on the nanomechanical properties of cellulose I nanocrystals. Journal of Materials Research 2012; 27:528-536. DOI: 10.1557/jmr.2011.288
26. M. Martínez-Sanz, A. Lopez-Rubio, J.M. Lagaron. Optimization of the nanofabrication by acid hydrolysis of bacterial cellulose nanowhiskers. Carbohydrate Polymers 2011; 85:228-236. DOI: 10.1016/j.carbpol.2011.02.021
27. L. Petersson, K. Kvien, K. Oksman. Structure and thermal properties of poly(lactic acid)/cellulose whiskers nanocomposite materials. Composites Science and Technology 2007; 67:2535-2544. DOI: 10.1016/j.compscitech.2006.12.012
28. J.K. Pandey, W.S. Chu, C.S. Kim, C.S. Lee, S.H. Ahn. Bio-nano reinforcement of environmentally degradable polymer matrix by cellulose whiskers from grass. Composites: Part B 2009; 40:676-680. DOI: 10.1016/j.compositesb.2009.04.013
29. R.R. Lahiji, X. Xu, R. Reifenberger, A. Raman, A. Rudie, R.J. Moon. Atomic force microscopy characterization of cellulose nanocrystals. Langmuir 2010; 26:4480-4488. DOI: 10.1021/la903111j
30. I. Diddens, B. Murphy, M. Krisch, M. Müller. Anisotropic elastic properties of cellulose measured using inelastic X-ray scattering. Macromolecules 2008; 41:9755-9759. DOI: 10.1021/ma801796u
31. S. Tanpichai, F. Quero, M. Nogi, H. Yano, R.J. Young, T. Lindström, W.W. Sampson, S.J. Eichhorn. Effective Young's modulus of bacterial and microfibrillated cellulose fibrils in fibrous networks. Biomacromolecules 2012:1340-1349. DOI: 10.1021/bm300042t
32. A. Šturcová, G.R. Davies, S.J. Eichhorn. Elastic modulus and stress-transfer properties of tunicates cellulose whiskers. Biomacromolecules 2005; 6:1055-1061.

DOI: 10.1021/bm049291k

33. S. Iwamoto, W. Kai, A. Isogai, T. Iwata. Elastic modulus of single cellulose microfibrils from tunicate measured by atomic force microscopy. Biomacromolecules 2009; 10:2571-2576.
DOI: 10.1021/bm900520n

34. N. Ljungberg, C. Bonini, F. Bortolussi, C. Boisson, L. Heux, J.Y. Cavaillé. New nanocomposite materials reinforced with cellulose whiskers in atactic polypropylene: Effect of surface and dispersion characteristics. Biomacromolecules 2005; 6:2732-2739.
DOI: 10.1021/bm050222v

35. G. Kalaprasad, B. Francis, S. Thomas, C.R. Kumar, C. Pavithran, G. Groeninckx, S. Thomas. Effect of fibre length and chemical modifications on the tensile properties of intimately mixed short sisal/glass hybrid fibre reinforced low density polyethylene composites. Polymer International 2004; 53:1624-1638.
DOI: 10.1002/pi.1453

36. J.B. Zhong, J. Lv, C. Wei. Mechanical properties of sisal fibre reinforced ureaformaldehyde resin composites. eXPRESS Polymer Letters 2007; 1:681-687.
DOI: 10.3144/expresspolymlett.2007.93

37. G. Siqueira, J. Bras, A. Dufresne. New process of chemical grafting of cellulose nanoparticles with a long chain isocyanate. Langmuir 2010; 26:402-411.
DOI: 10.1021/la9028595

38. F. Alloin, A. D'Aprea, N.E. Kissi, A. Dufresne, F. Bossard. Nanocomposites polymer electrolyte based on whisker or microfibrils polyoxyethylene nanocomposites. Electrochimica Acta 2010; 55:5186-5194.
DOI: 10.1016/j.electacta.2010.04.034

39. M. Roohani, Y. Habibi, N.M. Belgacem, G. Ebrahim, A.N. Karimi, A. Dufresne. Cellulose nanowhiskers reinforced polyvinyl alcohol copolymers nanocomposites. European Polymer Journal 2008; 44:2489-2498.
DOI: 10.1016/j.eurpolymj.2008.05.024

40. S. Pavlidou, C.D. Papaspyrides. A review on polymer-layered silicate nanocomposites. Progress in Polymer Science 2008; 33:1119-1198.
DOI:10.1016/j.progpolymsci.2008.07.008

41. C. Costache, M.J. Heidecker, E. Manias, G. Camino, A. Frache, G. Beyer, R.K. Gupta, C.A. Wilkie. The influence of carbon nanotubes, organically modified montmorillonites

and layered double hydroxides on the thermal degradation and fire retardancy of polyethylene, ethylene-vinyl acetate copolymer and polystyrene. Polymer 2007; 48:6532-6545.
DOI: 10.1016/j.polymer.2007.08.059

42. M.J. Faucheu, C. Gauthier, L. Chazeau, J.-Y. Cavaillé, V. Mellon, E.B. Lami. Miniemulsion polymerization for synthesis of structured clay/polymer nanocomposites: Short review and recent advances. Polymer 2010; 51:6-17.
DOI:10.1016/j.polymer.2009.11.044
43. G. Gong, J. Pyo, A.J. Mathew, K. Oksman. Tensile behavior, morphology and viscoelestic analysis of cellulose nanofiber-reinforced polyvinyl acetate (PVAc). Composites: Part A 2011; 42:1275-1282.
DOI: 10.1016/j.compositesa.2011.05.009
44. W. Helbert, J.Y. Cavaillé, A. Dufresne. Thermoplastic nanocomposites filled with wheat straw cellulose whiskers. Part I: Processing and mechanical behavior. Polymer Composites 1996; 17:604-611.
DOI:10.1002/pc.10650
45. K.G. Nair, A. Dufresne. Crab shell chitin whisker reinforced natural rubber nanocomposites. 2. Mechanical behavior. Biomacromolecules 2003; 4:666-674.
DOI: 10.1021/bm0201284
46. K.G. Nair, A. Dufresne. Crab shell chitin whisker reinforced natural rubber nanocomposites. 3. Effect of chemical modification of chitin whiskers. Biomacromolecules 2003; 4:1835-1842.
DOI: 10.1021/bm030058g
47. S.-H. Lee, Y. Teramoto, T. Endo. Cellulose nanofiber-reinforced polycaprolactone/ polypropylene hybrid nanocomposites. Composites: Part A 2011; 42:151-156.
DOI: 10.1016/j.compositesa.2010.10.014
48. B. Wang, M. Sain. Isolation of nanofibers from soybean source and their reinforcing capability on synthetic polymers. Composites Science and Technology 2007; 67:2521-2527.
DOI:10.1016/j.compscitech.2006.12.015
49. N. Ljungberg, J.-Y. Cavaillé. Nanocomposites of isotactic polypropylene reinforced with rod-like cellulose whiskers. Polymer 2006; 47:6285-6292.
DOI: 10.1016/j.polymer.2006.07.013

50. D.G. Gray. Transcrystallization of polypropylene at cellulose nanocrystals surfaces. Cellulose 2008; 15:297-301.
DOI: 10.1007/s10570-007-9176-2

51. E. Bahar, N.Ucar, A. Onen, Y. Wang, M. Oksüz, O. Ayaz, M. Ucar, A. Demir. Thermal and mechanical properties of polypropylene nanocomposite materials reinforced with cellulose nano whiskers. Journal of Applied Polymer Science 2012; 125:2882-2889.
DOI: 10.1002/app.36445

52. S. Spoljaric, A. Genovese, R.A. Shanks. Polypropylene-microcrystalline cellulose composites with enhanced compatibility and properties. Composites: Part A 2009; 40:791-799.
DOI: 10.1016/j.compositesa.2009.03.011

Chapter 3: Materials and methods

3.1 Materials

3.1.1 Polyethylene

Low-density polyethylene (LDPE) was supplied in pellets by Sasol Polymers, Johannesburg, South Africa. It has a melt flow index of 7 g/10 min (ASTM D-1238), density = 0.918 g cm^{-3}, a melting point of 108 °C and a molecular weight of 96 000 g mol^{-1}.

High density polyethylene (HDPE) was supplied in granular form by Safripol, Sasolburg, South Africa. It has a melt flow index of 3 g/10 min (ISO 1133), density = 0.949 g cm^{-3}, melting point of 130-133 °C and a molecular weight of 230 489 g mol^{-1}.

3.1.2 Sisal fibres

Sisal fibres (*Agave sisalana*) were obtained from the National Sisal Marketing Committee in Pietermaritzburg, South Africa.

3.1.3 Vinyl triethoxy silane

Vinyl triethoxy silane (VTES) was supplied by Merck Chemicals (Pty) Ltd, Germiston, South Africa. It has an assay of 98%.

3.1.4 Other chemicals

3.4.1.1 Dibutyltin dilaurate

Dibutyltin dilaurate was supplied by Merck Chemicals (Pty) Ltd, Germiston, South Africa. It has an assay of 96%.

3.1.4.2 Dicumyl peroxide (bis(α,α-dimethylbenzyl)peroxide)

Dicumyl peroxide (DCP) was supplied by Merck Chemicals (Pty) Ltd, Germiston, South Africa. It has an assay of 99%.

3.1.4.3 Glacial acetic acid

Glacial acetic acid was supplied by Merck Chemicals (Pty) Ltd, Germiston, South Africa. It has an assay of 98%.

3.1.4.4 Toluene

Toluene was supplied by Associated Chemical Enterprises (Pty) Ltd, Johannesburg, South Africa. It has an assay of 99.5%. It was dried by distillation over sodium and benzophenone at 110 °C and left over a 3 Å molecular sieve for 24 hours before use.

3.1.4.5 Sulphuric acid

Sulphuric acid was supplied by Merck Chemicals (Pty) Ltd, Germiston, South Africa. It has an assay of 95-99%.

3.1.4.6 Sodium hydroxide

Sodium hydroxide was supplied by Associated Chemical Enterprises (Pty) Ltd, Johannesburg, South Africa. It has an assay of 97%.

3.1.4.7 Sodium hypochlorite

Sodium hypochlorite was obtained from the local markets (JIK-household bleach, which contains sodium hypochlorite as an active ingredient with concentration of 3.5% (w/v), Reckitte Benckiser (Pty) Ltd., South Africa).

3.1.4.8 Sodium metal lumps

Sodium metal lumps in paraffin were supplied by Saarchem (Pty) Ltd, Krugersdorp, South Africa.

3.1.4.9 Benzophenone (Diphenyl ketone)

Benzophenone was supplied by Associated Chemical Enterprises (Pty) Ltd, Johannesburg, South Africa. It has assay of 95 %.

3.2 Preparation of sisal nanowhiskers

Sisal fibres were powderized with a Fritsch pulverisette mill. The powder was then treated four times with 4 wt% sodium hydroxide at 80 °C for four hours under mechanical stirring. The latter was performed to remove constituents other than cellulose from the fibres. After each treatment, the fibres were filtered and rinsed with distilled water until alkali was completely removed. Subsequent bleaching of the fibres was carried out at 80 °C for 6 h under mechanical stirring. The bleaching solution used consisted of equal parts of aqueous chlorite (1.7 wt% sodium chlorite ($NaClO_2$) in water) and an acetate buffer (27 g of sodium hydroxide (NaOH) and 75 ml glacial acetic acid, diluted to one liter using distilled water). This treatment was repeated four times with filtering and rinsing with distilled water between each step. The fibers were then dried for 24 hours at 40 °C in a vacuum oven. The dried treated fibers were ground again to a finer powder. Acid hydrolysis was carried out at 50 °C with 65 wt% sulphuric acid (H_2SO_4) for 50 minutes under mechanical stirring. The sisal fibre content during all these chemical treatments was in the range of 5-6 wt %. The suspension obtained was diluted with ice cubes to prevent any further reaction and washed by successive centrifugations at 10 °C and 5000 rpm for 30 minutes and a subsequent dialysis against distilled water was performed to remove the free acid from the suspension. A complete dispersion of the nanowhiskers was obtained by a sonication step using Cole Parmer Ultrasonic Processor for 15 minutes (5 minutes times three). The dispersion was filtered over a No. 1 fritted glass filter to remove any residual aggregates and stored at 4 °C after addition of a few drops of chloroform. The last step consisted of drying the sisal nanowhiskers using a freeze dryer (Flex-Dry^{TM} μP-Microprocessor Control, FTS Systems, Inc., USA).

3.3 Preparation of nanocomposites

3.3.1 Melt mixing

Table 3.1 shows the composition of the polyethylene/sisal nanowhiskers nanocomposite samples used in this study. The freeze dried whiskers was chemically modified using vinyl triethoxy silane (VTES). A desired amount of sisal whiskers were treated with 1 phr silane and DCP, with the ratio 12:1 of silane:DCP, and dibutyltin dilaurate was added as catalyst. All components were mixed for 10 min using mechanical stirring. Polyethylene powder was added to the mixture and further mixed for 10 minutes. The mixture was transferred into the 55 mL mixing chamber of a Brabender Plastograph and the mixing was conducted for 10 min at a rotor speed of 60 rpm and at 140 and 160 $^{\circ}$C respectively for LDPE and HDPE. The melt pressing of the prepared samples was carried out at the same temperatures at 50 bar for 10 min to form sheets with dimensions of 130 x 130 x 1.5 mm. Pure LDPE and HDPE as well as untreated samples were prepared under the same conditions.

3.3.2 Solution casting

An aqueous suspension of sisal nanowhiskers (1 wt %) was solvent-exchanged to acetone and then to dry toluene. This process was performed four times by centrifugation at 10 °C and 5000 rpm for 10 minutes. After each solvent exchange step re-dispersion was performed for 5 minutes using ultrasonication treatment to avoid aggregation. However, the suspension in toluene was not stable over time.

The sisal whiskers in dry toluene were mixed with the polyethylenes and sonicated for 10 minutes for better dispersion. The mixing was carried out manually in an oil bath for 20 minutes at 110 and 120 $^{\circ}$C respectively for LDPE and HDPE. The mixture was kept overnight in a vacuum oven at 80 $^{\circ}$C and melt pressed for 10 minutes at 50 bar pressure at 130 and 140 $^{\circ}$C respectively for LDPE and HDPE.

Table 3.1 Compositions of the different nanocomposite samples

Melt mixing	
LDPE/sisal nanowhiskers (w/w)	**HDPE/sisal nanowhiskers (w/w)**
100/0	100/0
99/1	99/1
95/5	95/5
VTES (1 phr) treated LDPE/sisal nanowhiskers	**VTES (1 phr) treated HDPE/sisal nanowhiskers**
100/0	100/0
99/1	99/1
95/5	95/5
Solution mixing	
LDPE/sisal nanowhiskers (w/w)	**HDPE/sisal nanowhiskers (w/w)**
100/0	100/0
99/1	99/1
95/5	95/5

3.4 Characterization methods

3.4.1 Transmission electron microscopy (TEM)

TEM is used for structure characterization. The basic components of TEM are the source of electrons (electron gun), a condenser system, a specimen stage, an objective lens and a projector system. The emitted electrons, from the electron gun, are changed by an electromagnetic lens and metal apertures to electron beams with well-defined energies that pass through the specimen. Some of the electrons will be scattered or disappear depending on the different densities within the sample. The unscattered electrons hit a fluorescent screen, which gives rise to a 'shadow image' of the specimen with varying darkness according to different densities within the specimen. The specimens, with thickness less than 1 μm, are normally placed on copper grids having square holes with edge length of 50 μm for viewing

through. The grids provide thermal and electrical conduction to the specimen stage, minimizing problems of overheating and charging. TEM is used to establish the crystallographic structures of polymers and to study polymer matrices filled or reinforced with minerals, glass, carbon, natural nanofibres to obtain detailed information about their nanostructures and dispersion within the nanocomposites materials [1-3].

The dimensions of the cellulose nanowhiskers and their dispersion in the nanocomposites were established by TEM. Cellulose nanowhiskers were diluted with water to 0.01 % w/v. The suspension was deposited on a carbon grid, stained with 2 wt% of uranyl acetate and allowed to dry at ambient temperature. The grids were observed with a Philips CM 200 microscope operated at an accelerating voltage of 80 kV. The nanocomposites were examined by cutting very thin sections from the samples using ultramicrotomy. A 2 % uranyl acetate solution was used to stain these sections before they were viewed under TEM.

3.4.2 Scanning electron microscopy (SEM)

SEM is a widely used electron beam technique in which electron scattering is used to image the topography of the sample surface. The basic components of SEM are a lens system, an electron gun, an electron collector, visual and photo-recording cathode ray tubes (CRTs), and the associated electronics. In SEM the electron beam is rastered across the sample surface, which must be conductive (which may be achieved by coating), with the signal from the emitted secondary electrons detected and displayed. SEM has the potential to generate images with a few nanometers spatial resolution, and has a relatively large field depth. This provides information on the sample surface [1,3]. SEM is widely applied to characterize multi-component polymers and blends by examining the fracture surfaces. Such images can provide information about the interfacial region and adhesion of the various phases in the blend. Furthermore, SEM examinations of the polymer matrices filled or reinforced with minerals, glass, carbon, natural fibres, or polymer fibres can provide detailed information about the microstructure and dispersion in the resulting composite or nanocomposite materials.

The morphology and dispersion of the sisal nanowhiskers in the resulting nanocomposites were examined by SEM. The fractured surfaces of the pure polymers, nanocomposites and freeze dried nanowhiskers were examined using a TESCAN VEGA3 scanning electron

microscope. The samples were fractured using liquid nitrogen, mounted, and coated with gold under argon flow. The samples were dried for two hours before examination. The analyses of the dried specimens were carried out at an accelerating voltage of 15 kV.

3.4.3 Fourier transform infrared (FTIR) spectroscopy

FTIR spectroscopy is a powerful technique for rapid identification of small materials. An infrared spectrum results from absorption of the electromagnetic radiation at the frequencies corresponding to the vibrations between chemical bonds of atoms making up the material. This results in a positive identification of the material and the size of peaks gives direct indication of the number of molecules present [4,5]. In ATR-FTIR a beam of IR is passed through a high refractive index crystal which is in contact with the sample. The resulting internal reflectance forms an evanescent wave which extends into the sample (0.5-2 μm) and on the other end of the crystal the beam is collected by a detector in which the spectrum is generated [4,5].

The molecular structure and chemical bonding in the sisal nanowhiskers, the neat polymers and the nanocomposites were studied by FTIR-ATR. FTIR spectra were recorded using a Perkin Elmer Spectrum 100 FTIR spectrometer fitted with PIKE Miracle$_{TM}$ ATR, equipped with a diamond crystal. Spectra of thin films of the samples were recorded using 32 scans and a resolution of 4 cm^{-1}over a range of 600-4000 cm^{-1}.

3.4.3 Wide-angle X-ray diffractometry (WAXD)

X-ray diffractometry is an important technique for determining crystal structures. The X-rays are directed onto the sample which is rotating with the detector. When the geometry of the incident beam of X-rays hitting the sample satisfies the Bragg's equation, interference occurs and the peak intensity is recorded. A detector processes the X-ray signals and converts them into a count rate. Peaks appear where the X-ray beam is diffracted by the crystal lattice. The d-spacings between the lattices and their distribution in the crystalline structure is unique for each material, therefore the angular distribution of the diffraction peaks and their intensities (the diffraction pattern) serve as a fingerprint of that material. From the peak intensities on

the diffraction patterns, which are directly proportional to the number of atoms in the material, the concentration of the phases in the material can be obtained [2,3].
Changes in the crystalline structure of the cellulose nanowhiskers, neat PE and the nanocomposites were investigated by WAXD. The WAXD experiments were carried out at room temperature with a Bruker D8 Advance spectrometer operated with a CuK_{α} anode (λ = 1.54 nm) with 2θ ranging from 5 to 50°on the freeze dried whiskers and on thin films of the untreated and treated nanocomposites.

3.4.4 Differential scanning calorimetry (DSC)

DSC is a technique in which the difference in heat flow (power) to a sample and to a reference material is monitored against time or temperature while the temperature of the sample, in a specified atmosphere, is increased or decreased at a constant rate. There are two types of DSC. In power-compensated DSC, the sample and reference are heated separately and the difference in power required to maintain them at the same temperature throughout the thermal cycle is recorded. In heat flux DSC, the sample and reference are heated from the same source and the temperature difference is measured. This signal is converted to a power difference using the calorimetric sensitivity. DSC quantitatively measures the transitions that occur in the sample, and as a result characterizes a material according to its melting, crystallization and glass transitions [6].

The influence of the treatment of the nanowhiskers, and their incorporation into the PE matrices, on the crystallization and melting behaviour of the polymers were studied by DSC. The analyses were performed using a Perkin Elmer DSC7 differential scanning calorimeter. Samples with masses between 5 and 10 mg were sealed in aluminium pans and heated under a nitrogen flow of 20 ml min^{-1} from 35 to 180 °C at heating rate of 10 °C min^{-1}, kept at this temperature for 1 min to erase the thermal history, cooled to 35 °C at the same rate, and re-heated under the same conditions. The melting enthalpies and temperatures were determined from the second heating curve, while the crystallization enthalpies and temperatures of the samples were determined from the first cooling curve. Three individual measurements were performed to ensure reproducibility.

3.4.5 Thermogravimetric analysis (TGA)

TGA is used to measure mass loss as a function of temperature at a given heating rate, and under a specified atmosphere. TGA is used to characterize the decomposition and thermal stability of materials under a variety of conditions, and to examine the kinetics of physico-chemical processes occurring in the sample. The mass change features of a material depend on the experimental conditions employed. Factors such as sample mass, volume and physical form, the shape and nature of the sample holder, the nature and pressure of the atmosphere in the sample chamber, and the scanning rate all have an important influence on the characteristics of the recorded TGA curve [2,7,8].

Thermogravimetric analysis (Perkin Elmer TGA7 thermogravimetric analyzer) was used to study the thermal stabilities of the nanocomposites compared to those of the neat polymers and the sisal nanowhiskers. Samples with masses in the range of 5 to 10 mg were heated under a nitrogen flow of 20 ml min^{-1} from 30 ºC to 600 ºC at a heating rate of 10 ºC min^{-1}, and the corresponding mass loss was recorded.

3.4.6 Tensile testing

Tensile testing is the most frequently used test method to characterize the material strength. The tests are performed on either dumbbell-shaped or rectangular specimens under defined conditions of pretreatment, temperature, humidity and deformation rate. The shapes may be cut from thin films of uniform thickness or molded samples. Tensile stress, strain, and Young's modulus are generally determined. Stress is defined as the force applied per unit cross sectional area, and has the basic dimensions of N m^{-2} in SI units. On the other hand, strain is a dimensionless quantity, defined as the increase in the length of the specimen per unit original length. It represents the response of the material to the stress applied to it. The ratio of stress to strain is known as Young's modulus, which has dimensions of force per unit area [9-11].

The tensile properties of the polymers and nanocomposites were determined with a Hounsfield H5KS tensile tester at ambient temperature. The experiments were carried on dumbbell shaped samples (Figure 3.1) at a cross-head speed of 50 mm min^{-1}. The stress and elongation at yield, Young's modulus, stress at break, and elongation at break were

determined from the stress-strain curves and the results were the average of three measurements (because of the availability of limited amounts of sample).

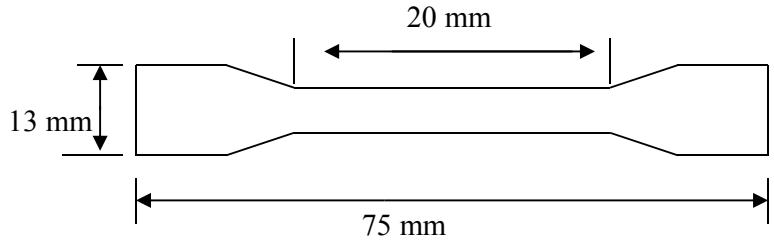

Figure 3.1 Dumbbell shaped tensile testing sample

3.4.7 Dynamic mechanical analysis (DMA)

DMA is a widely used technique to investigate the structure and dynamic properties of polymeric materials. It characterizes the mechanical responses of materials by monitoring property changes with respect to temperature or/and frequency of oscillation. In DMA an oscillating force is applied to a sample and the material's response to that force is analysed. The technique separates the dynamic response of the material in two distinctive parts: an elastic (E') and viscous (E'') part. The elastic part defines the energy stored in the system, while the viscous part describes the energy dissipated during the process. The ratio of the loss modulus to storage modulus is tan δ, and is often called damping. It is a measure of the internal friction of the material and indicates the amount of energy lost in the material as dissipated heat. DMA is used to study molecular relaxation processes (glass transition temperature and secondary transitions) as well as to determine inherent mechanical (e.g. storage modulus, loss modulus, damping factor) and flow properties as a function of time, temperature, or frequency [12-14].

The dynamic mechanical properties of the samples were determined using a Perkin Elmer Diamond DMA in the dual cantilever mode. The samples were scanned for their viscoelastic responses including storage modulus (E'), loss modulus (E") and loss factor (tan δ) to evaluate the effect of the addition of treated and untreated sisal nanowhiskers to the PEs on these properties. The settings for the analyses were as follows:

Frequency	1 Hz
Amplitude	20 μm
Temperature range	-100 to +100 ºC
Temperature programme mode	Ramp
Measurement mode	Bending (dual cantilever)
Heating rate	5 °C min^{-1}
Preloading force	0.02 N
Sample length	20 mm
Sample width	12.0 – 12.5 mm
Sample thickness	1.0 – 1.3 mm

3.5 References

1. D. Campbell, R.A. Pethrick, J.R. White, S. Thornes. Polymer Characterization: Physical Techniques. Stanley Thornes Publishers Ltd., Cheltenham (2000).
2. Y. Leng. Materials Characterization: Introduction to Microscopic and Spectroscopic Methods. John Wiley & Sons Pty. Ltd., Singapore (2008).
3. I.L. Hosier, A.S. Vaughan, G.R. Mitchell, J. Siripitayananon, F.J. Davis. Polymer characterization. In: F.J. Davis (Ed). Practical Approach in Chemistry: Polymer Chemistry. Oxford University Press, Inc., New York (2004).
4. T. Buffeteau, B. Desbat, D. Eyquem. Attenuated total reflection Fourier transform infrared microspectroscopy: Theory and application to polymer samples. Vibrational Spectroscopy 1996; 11:29-36.
5. B.C. Smith. Fundamentals of Fourier Transform Infrared Spectroscopy. CRC Press, New York (2011).
6. J.D. Menczel, L. Judovits, R.B. Prime, H.E. Bair, M. Reading, S. Swier. Differential scanning calorimetry (DSC). In: J.D. Menczel, R.B. Prime (Eds.). Thermal Analysis of Polymers: Fundamentals and Applications. John Wiley& Sons, Inc., Hoboken, New Jersey (2009).
7. J.D. Menczel, H.E.Bair, S. Vyazovkin, P.K. Gallagher, A. Riga. Thermogravimetric analysis(TGA). In: J.D. Menczel, R.B. Prime (Eds.). Thermal Analysis of Polymers: Fundamentals and Applications. John Wiley &Sons, Inc., Hoboken, New Jersey (2009).
8. B. Wunderlich. Thermal Analysis of Polymeric Materials. Springer, Berlin (2005).

9. H.F. Brinson, L.C. Brinson. Polymer Engineering Science and Viscoelasticity: An Introduction. Springer, New York (2008).
10. R.O. Ebewele. Polymer Science and Technology. CRC Press LLC, Boca Ranton, Florida (2000).
11. S. Kamel. Nanotechnology and its applications in lignocellulosic composites, a mini review. eXPRESS Polymer Letters 2007; 1:546-575.
    DOI: 10.3144/expresspolymlett.2007.78.
12. R.P. Chartoff, J.D. Menczel, S.H. Dillman. Dynamic mechanical analysis (DMA). In: J.D. Menczel, R.B. Prime (Eds.). Thermal Analysis of Polymers: Fundamentals and Applications. John Wiley & Sons, Inc., Hoboken, New Jersey (2009).
13. H.A. Khonakdar, U. Wagenknecht, S.H. Jafari, R. Hässler, H. Eslami. Dynamic mechanical properties and morphology of polyethylene/ethylene vinyl acetate copolymers blends. Advances in Polymer Technology 2004; 23:307-315.
    DOI: 10.1002/adv.20019
14. P.V. Joseph, G. Mathew, K. Joseph, G. Groeninckx, S. Thomas. Dynamic mechanical properties of short sisal fibre reinforced polypropylene composites. Composites: Part A 2003; 34:275-290.
    DOI: 10.1016/S1359-835X(02)00020-9.

Chapter 4: Results and discussion

4.1 Fourier-transform infra-red (FTIR) spectroscopy

Figure 4.1 shows the FTIR spectra of LDPE, HDPE, sisal nanowhiskers (SNW) and sisal fibre. Table 4.1 lists the typical band assignments. All the characteristic absorption peaks of the neat LDPE at 2919 cm^{-1} (CH_2 asymmetric stretching), 2842 cm^{-1} (CH_2 symmetric stretching), 1473 and 1463 cm^{-1} (C-H bending deformation), 1378 cm^{-1} (CH_3 symmetric deformation) and 720-730 cm^{-1} (rocking deformation) are observed. The peaks at 2910 and 2852 cm^{-1} belong to the CH_2 asymmetric and symmetric stretching, respectively, 1472 cm^{-1} (bending deformation), 1368 cm^{-1} (CH_3 symmetric deformation), 720 and 740 cm^{-1} which are assigned to C-H rocking deformation are clearly noticed in HDPE spectrum.

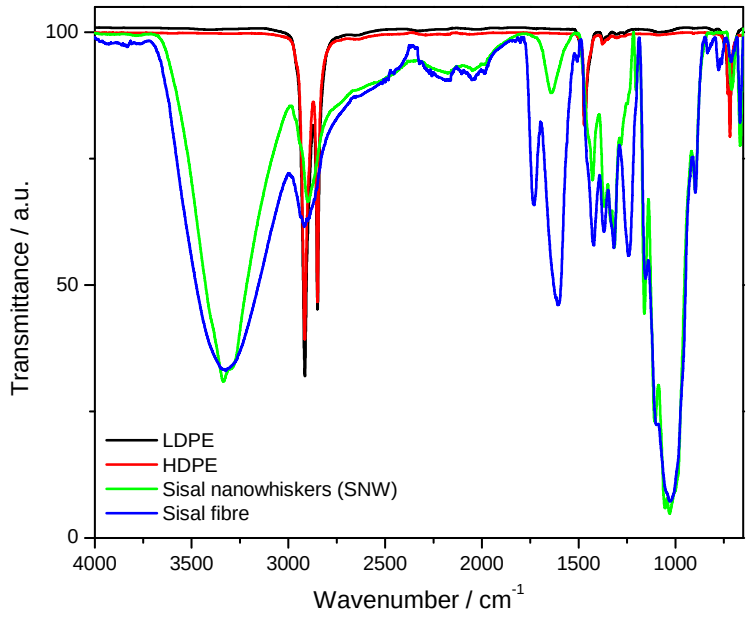

Figure 4.1 FTIR spectra of LDPE, HDPE, sisal nanowhiskers and sisal fibre

Table 4.1 Assignments of characteristics bands of PE and PE/sisal nanowhiskers nanocomposites

Band (cm^{-1})	Assignment	Intensity
2919	CH_2 asymmetric stretching	Strong
2842	CH_2 symmetric stretching	Strong
1473 and 1463	CH bending deformation	Strong
1377	CH_3 symmetric deformation	Weak
1366 and 1351	CH wagging deformation	Medium
1035	Si-O-Si overlapping C-O	Weak
800	Si-C	Weak
730-720	Rocking deformation	Strong

Both the sisal fibre and SNW display the characteristic bands of cellulose I – a broad band in the 3700-2990 cm^{-1} range is the O-H stretching vibrations, and the band at 2900 cm^{-1} is the C-H stretching vibration from $–CH_2$. The wagging and twisting modes of the anhydroglucopyronose unit are observed at 1800 to 600 cm^{-1}. Sisal fibre shows peaks at 1735, 1605 and 1243 cm^{-1} assigned to a carboxylic acid or ester, and acetyl and methyl ester groups, respectively. These peaks are, as expected, not observed in the SNW spectrum, confirming the removal of hemicelluloses and lignin. A new peak is observed at 1655 cm^{-1}, which can be assigned to an O-H stretching due to water absorbed by the nanowhiskers. There were similar observations by Pandey *et al*. [1] in their study of the bio-nano reinforcement of an environmentally degradable polymer matrix by cellulose whiskers from grass.

Figures 4.2 and 4.3 depicts the FTIR spectra of PE's, SNW, and vinyl triethoxysilane (VTES) treated and the untreated PE/SNW nanocomposites prepared through melt mixing. The untreated 95/5 LDPE/SNW nanocomposites display all the characteristic absorption bands of LDPE, and weak absorptions between 1201 and 929 cm^{-1} (C-O stretching) which may be due to the presence of SNW. The characteristic peaks of the Si-O-Si and Si-O-C bonds at 1162 and 1035 cm^{-1} are noticed in the treated LDPE/SNW. Two new peaks are observed at 800 and 1265 cm^{-1} which are assigned to Si-C and $Si-CH_3$, respectively. It seems as if the vinyl

group of VTES grafted onto LDPE, whereas the silanol group interacted with the –OH groups on the nanowhiskers [2,3].

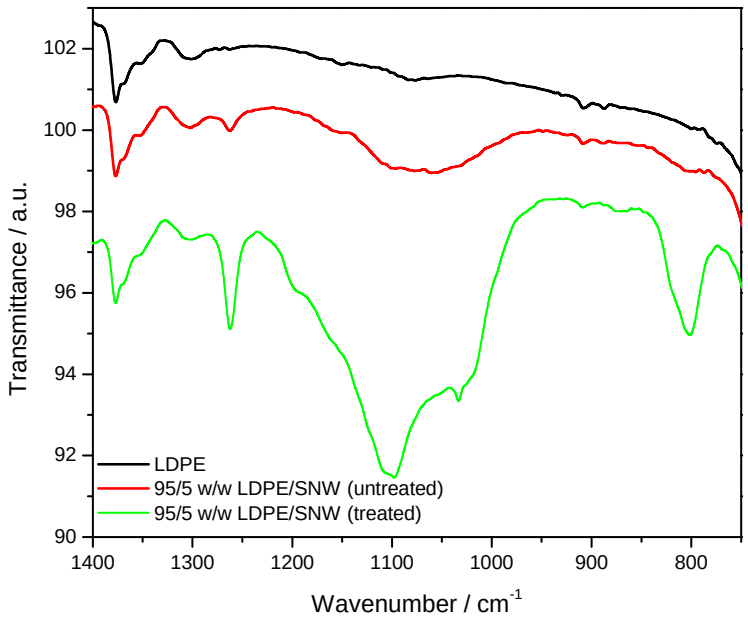

Figure 4.2 FTIR spectra of LDPE and LDPE/sisal nanowhiskers prepared by melt mixing

In the case of the untreated HDPE nanocomposites (Figure 4.3), there is a weak peak between 1163 and 965 cm^{-1} assigned to the C-O stretching of cellulose, which may be due to the presence of SNW. The intensity of this peak increases in the treated HDPE nanocomposites, with small peaks at 1104, 1099, 1084 cm^{-1}, assigned to Si-O-C, and at 1056, 1028 cm^{-1}, related to Si-O-Si overlapping the C-O stretching of cellulose. The peaks at 1263 and 803 cm^{-1}, assigned to Si-CH_3 and Si-C stretching, respectively, are also observed in the treated HDPE nanocomposite spectrum. The intensity of the peak at 1377 cm^{-1} (CH_3 symmetric stretching) decreased and the peaks at 889 (vinylidene groups) and 909 cm^{-1} (vinyl groups) disappeared, which may be due to the DCP initiated radicals that are consumed during silane grafting. The treated LDPE nanocomposites show more intense peaks between 1163 and 965 cm^{-1} than the treated HDPE nanocomposites. This may be due to fewer branches in case of HDPE. It is worth noting that not only the number of branches contributes to the grafting efficiency of silane to polyethylenes. The average molecular weight, as well as vinyl and vinylidene bonds and MFI also contribute to level of silane grafting [3,4].

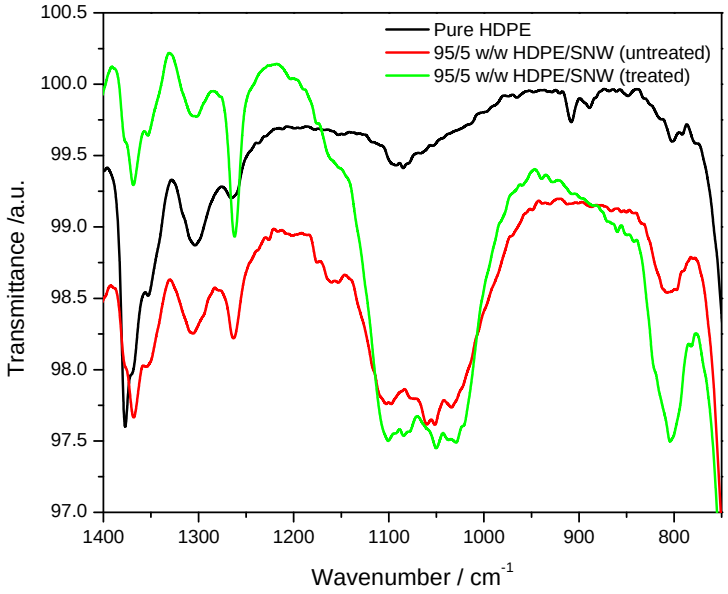

Figure 4.3 FTIR spectra for HDPE and HDPE/ sisal nanowhiskers nanocomposites.

4.2 Morphology of sisal nanowhiskers and PE/sisal nanowhiskers nanocomposites

Figure 4.4 (a,b) shows the TEM micrographs of the sisal whiskers at different magnifications in water. The sisal whiskers appear as rod-like particles. This is the result of successful removal of the amorphous regions of the sisal fibre through sulphuric acid hydrolysis and subsequent treatment. These rod-like whiskers have average lengths of 197 ± 75 nm and diameters of 12.2 ± 3.7 nm. The aspect ratio was calculated to be around 16. The whiskers were well dispersed on the grid, as expected, due to surface charges introduced by the sulphuric acid hydrolysis. These results correlate with the results obtained by De Rodiguez *et al*. [5]. These authors, however, obtained smaller diameters and the aspect ratio was 43. There may be several reasons for this difference, including the growth conditions of the sisal and the conditions under which the sisal fibre was ground.

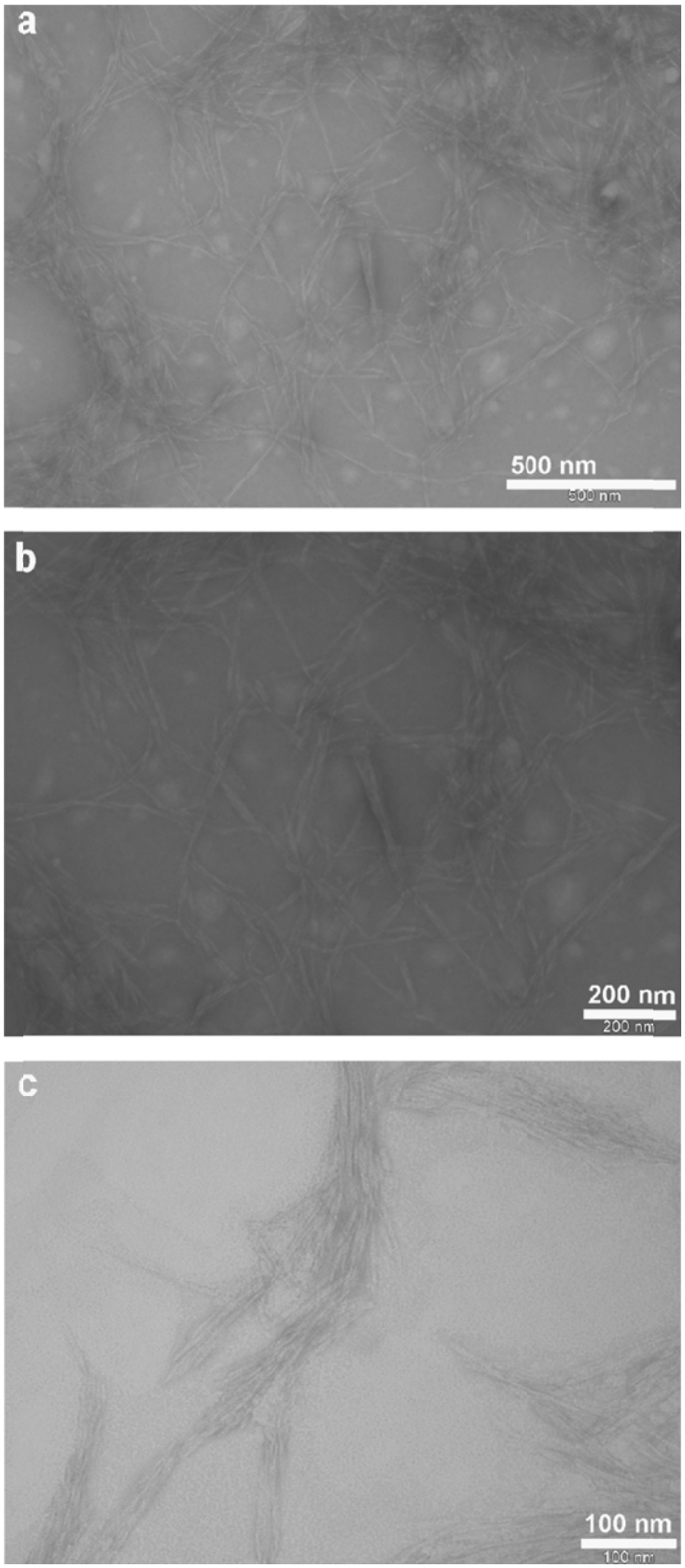

Figure 4.4 TEM micrographs of sisal whiskers

Figure 4.4c shows the TEM micrographs of the whiskers in toluene. The whiskers showed slight agglomeration. The bright circular areas, as observed in the TEM micrographs of the whiskers in water, are not observed. These brighter areas are related to artifacts resulting from the staining agent when exposed to an electron beam [6]. The whiskers' agglomeration may be the result of either solvent exchange of the whiskers from water to toluene or a reaction between the staining reagent and toluene. In addition, evaporation of the toluene which was observed during the analysis, may have led to more agglomeration. It is therefore difficult to conclude whether the aggregation of the whiskers was due to solvent exchange or not.

Figure 4.5 shows the SEM micrographs of 95/5 w/w LDPE/sisal whiskers nanocomposites prepared under different conditions. It was not possible to see individual whiskers in the case of the melt mixed (untreated and treated) LDPE nanocomposites (Figure 4.5(a,b)), which usually appear as white dots [7]. This may have been the result of either the polymer matrix covering the whiskers, or the sizes of the whiskers that were too small to be observable at the sensitivity used in the analysis. Wang *et al*. [8], in their study of the isolation of nanofibres from soybean, also found it difficult to see any nanofibers in the PE matrix. They did, however, observe white spots and related them to the nanofibres that were not uniformly dispersed in the matrix. They pointed out that the cellulose may have degraded during processing, and that further work was needed to understand the dispersion mechanism of nanofibres into a solid matrix through melt-mixing. In our case we can clearly see white dots uniformly dispersed in the matrix. These white dots probably represent the whiskers in the nanocomposite film [7]. It is worth noting that for solution casting, solvent exchange from water to acetone and then to toluene was used. This method avoids the drying step, thus reducing the probability of the whiskers' reaggregation. This may lead to a good dispersion of the whiskers in the matrix.

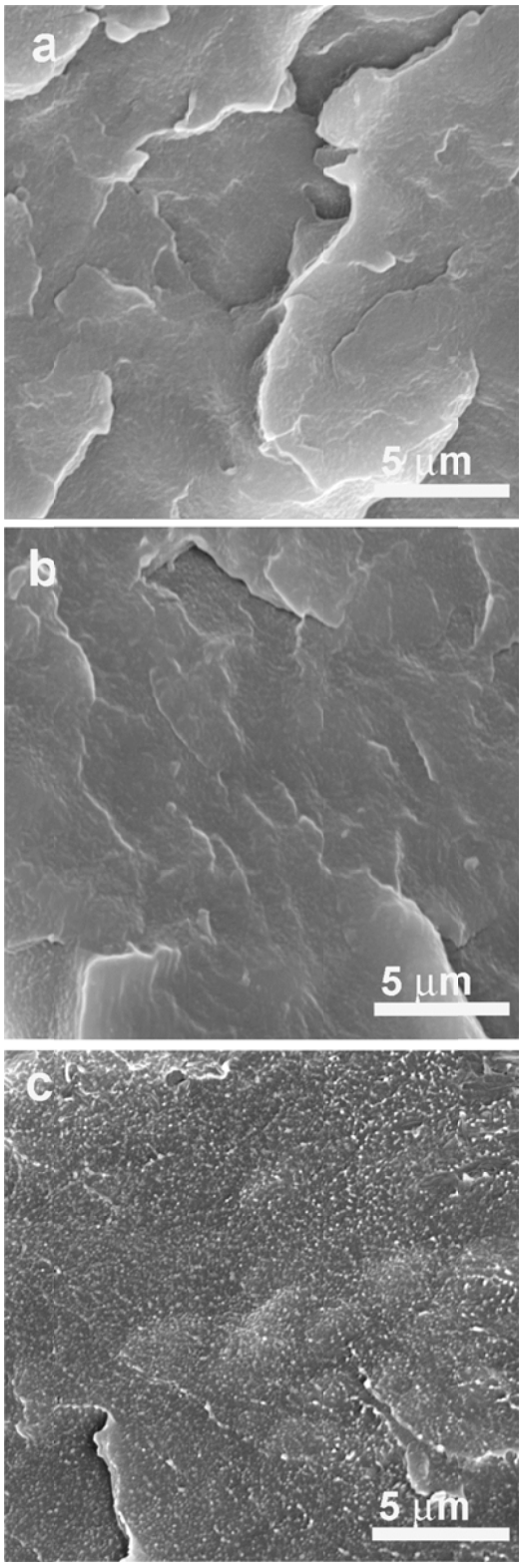

Figure 4.5 SEM micrographs of untreated and treated LDPE/sisal whiskers nanocomposites at 10000x magnification: (a) untreated (95/5 w/w), (b) treated (95/5), and (c) untreated solution mixed (95/5 w/w)

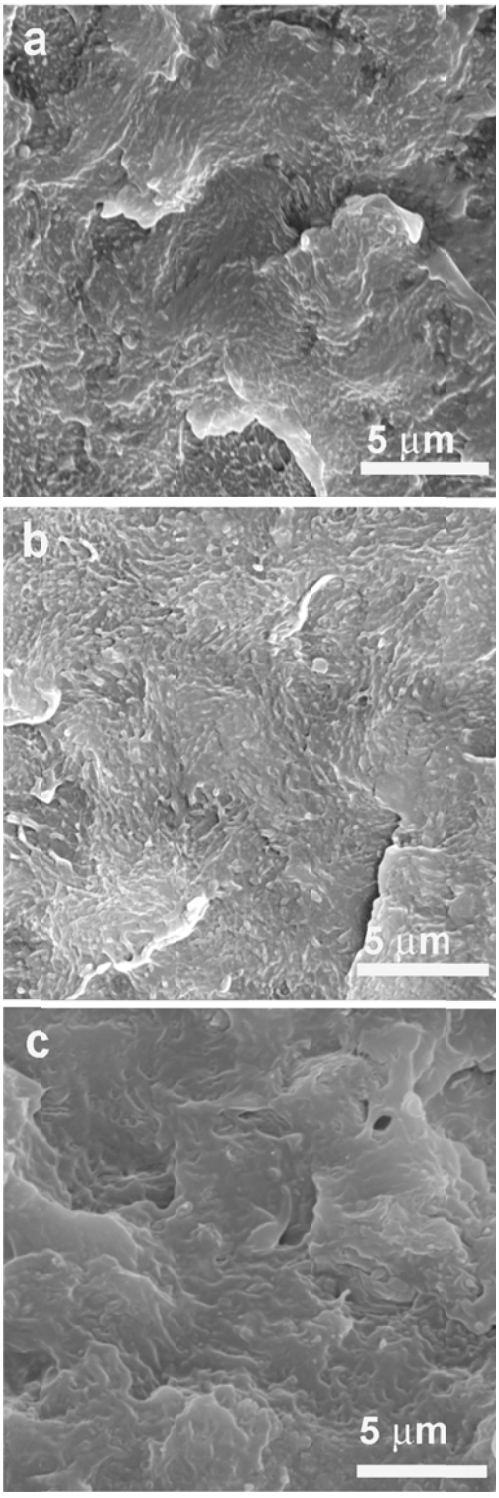

Figure 4.6 SEM micrographs of untreated and treated HDPE/sisal whiskers nanocomposites at 10000x magnification: (a) untreated (95/5 w/w), (b) treated (95/5), and (c) untreated solution mixed (95/5 w/w)

Figure 4.6 shows the SEM micrographs of melt mixed 95/5 w/w HDPE/sisal whiskers nanocomposites prepared under different conditions. The whiskers were uniformly dispersed as white dots in the HDPE matrix (Figure 4.6a). This may be due to the high viscosity of the matrix and the large stresses during melt compounding. Similar dispersion was found for the VTES treated sample (Figure 4.6b). This can additionally be due to the VTES grafted onto the whiskers' surfaces and the improved interaction with the HDPE, as confirmed by FTIR (Section 4.1), resulting in improved interaction and dispersion. In Figure 4.6c, it is difficult to see individual whiskers in the matrix. This may also be attributed to either the polymer matrix covering the whiskers or the sizes of the whiskers that were too small to be observable at the sensitivity used in the analysis. Thus, the dispersion of the whiskers in the matrices needs further verification with other analysis techniques like TEM.

The dispersion of the sisal whiskers in the polyethylene matrices was also investigated by TEM. The TEM micrographs of the untreated and VTES treated 95/5 LDPE/sisal whiskers nanocomposites are shown in the appendix. The images were dark and it is difficult to comment on the dispersion of the nanowhiskers in the matrix. Figure 4.7 shows the TEM micrograph of the untreated solution mixed 95/5 w/w LDPE/sisal nanocomposite. The whiskers were fairly well dispersed in the matrix. As discussed earlier in the SEM analysis, the solvent exchange method avoids the drying step, thus reducing the probability of the whiskers' reaggregation. Similar observations were made in the case of the 99/1 w/w PE/sisal whiskers nanocomposite (not shown).

In Figure 4.8a it can be seen that the whiskers were separated and fairly well dispersed without noticeable agglomerates. This may also be due to the high viscosity of the matrix and large stresses during melt compounding. Similar dispersion was found for the VTES treated sample (Figure 4.8b). This can additionally be due to the VTES grafted onto the nanowhiskers' surfaces of the whiskers and improved interaction with the HDPE, as confirmed by FTIR (Section 4.1), resulting in improved interaction and dispersion. The treatment reduced the interactions between the whiskers, and increased the wettability, giving rise to improved adhesion between HDPE and the whiskers, thus preventing agglomeration. In the case of the nanocomposites prepared from toluene solution casting, a fairly good dispersion was observed (Figure 4.8c). As observed and discussed earlier in the case of the LDPE nanocomposites, it may be due to solvent exchange that reduced the possibility of the whiskers' reaggregation. The darker areas in all the TEM micrographs are due to negative

staining by uranyl acetate. Similar observations were made for the 99/1 w/w PE/sisal whiskers nanocomposites (not shown).

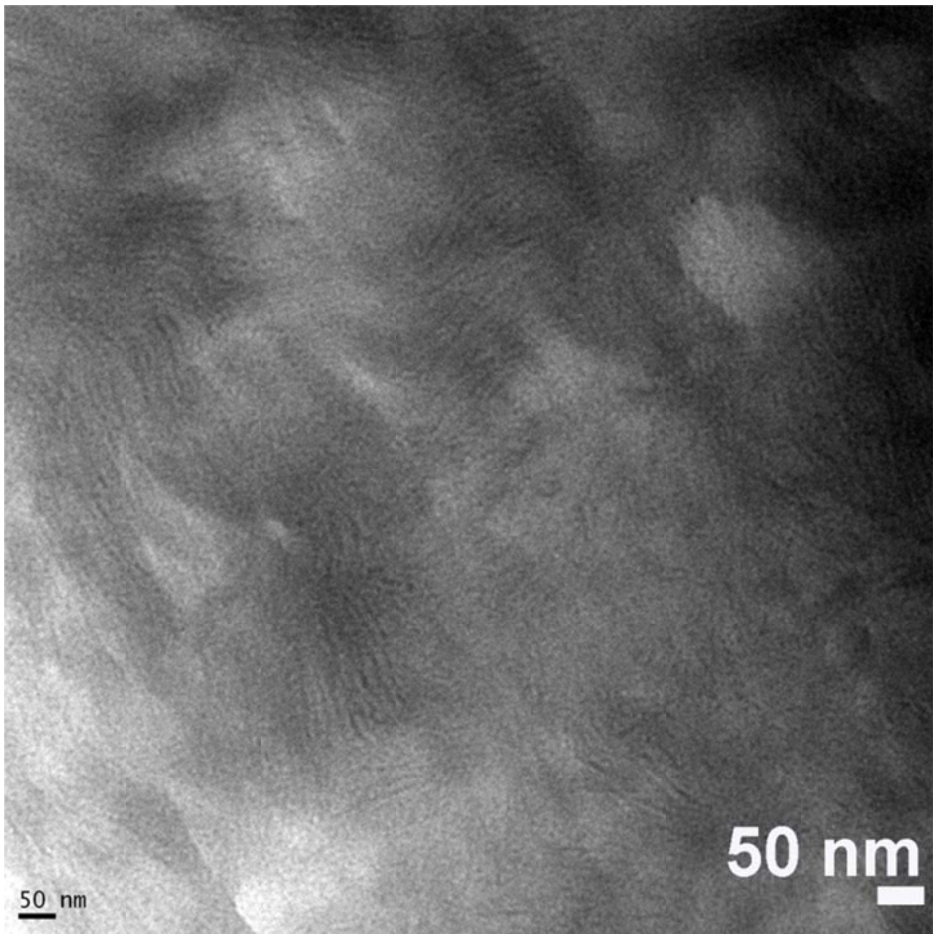

Figure 4.7 TEM micrograph of untreated solution mixed 95/5 LDPE/sisal whiskers nanocomposite

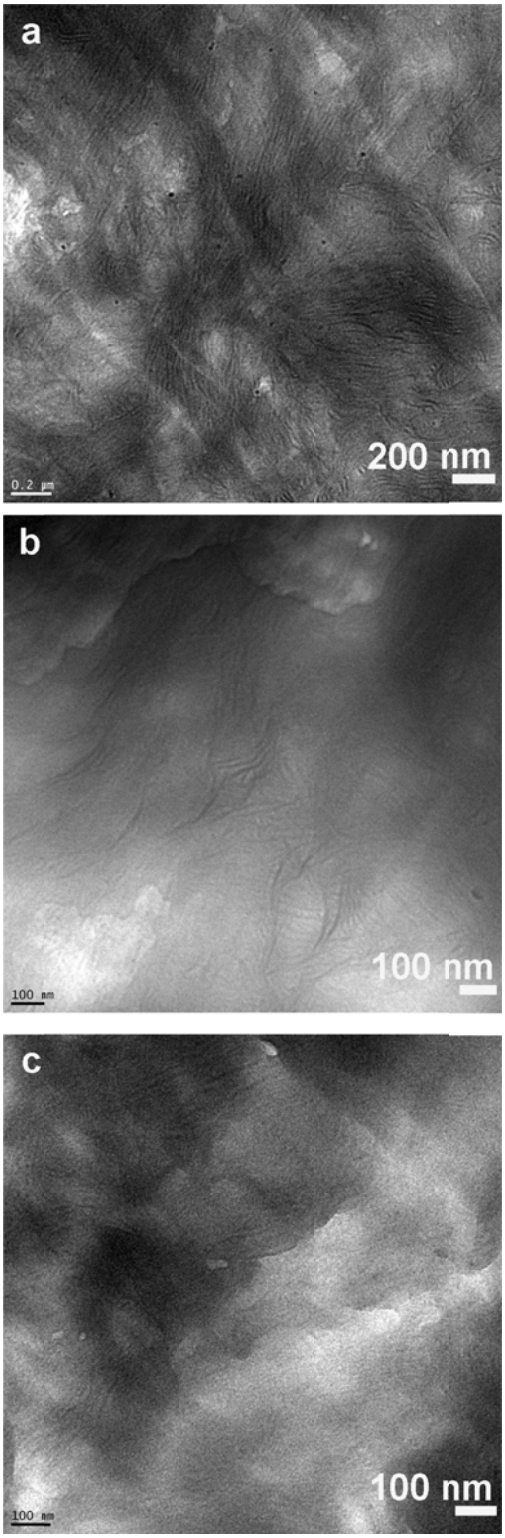

Figure 4.8 TEM micrographs of HDPE/sisal whiskers nanocomposites: (a) untreated melt mixed 95/5 w/w HDPE/sisal, (b) VTES treated melt mixed 95/5 w/w HDPE/sisal, and (c) untreated solution mixed 95/5 w/w HDPE/sisal

4.3 Wide angle X-ray diffractrometry (WAXD)

Figure 4.9 shows the WAXD patterns of the isolated sisal whiskers (SNW) and the sisal fibre. Both the sisal fibre and sisal whiskers patterns display similar peaks at 2θ = 22.3 and 34.4°, respectively corresponding to the reflections of the (200) and (004) lattices planes, as well as the overlapping (110) and (11'0) planes at 2θ = 15.0°. These peaks are characteristic of cellulose I, which was also confirmed by the absence of a doublet in the main peak (2θ = 22.3°) [9,10]. The crystallinity index of the fibre was calculated from the X-ray diffraction patterns according to Equation 4.1.

$$CI = \frac{I_{(002)} - I_{(am)}}{I_{(002)}} \times 100 \qquad (4.1)$$

where $I_{(002)}$ and I_{am} are the peak areas of the crystalline and amorphous peaks, respectively [9].

The crystallinity indices of the sisal whiskers and the sisal fibre were found to be 89% and 65%, respectively. This is also confirmed by the WAXD diffraction pattern of the whiskers, where the diffraction peaks at 2θ = 22.3° and 15.0° became more intense and sharper indicating an increase in crystallinity (Figure 4.9). This is the result of the removal of the amorphous regions through acid attack, leaving behind more crystalline particles. This is further in line with the FTIR data (Section 4.1), where the characteristic peaks of the lignin and hemicelluloses, which exist in the amorphous regions, disappeared.

Figure 4.10 to 4.13 show the X-ray scattering patterns of the PE/sisal whiskers nanocomposites. The full width at half maximum (FWHM) and the unit cell parameter are tabulated in Tables 4.2 and 4.3. LDPE shows two distinct (110) and (200) reflection peaks and a weak (004) reflection peak, respectively at 2θ angles of 21.5, 23.8 and 36.3°, corresponding to d-spacings of 4.12, 7.48 and 2.47 Å (Figure 4.10). This is related to the orthorhombic crystal structure of polyethylene [11]. A broad halo peak at a 2θ angle of about 20°, corresponding to the noncrystalline fraction of LDPE, is overlapped by a sharp peak (at 21.5°). Similar reflection peaks were observed for all nanocomposites' WAXD patterns. The reflection peaks of sisal whiskers are overlapped by sharp and intense peaks of LDPE. In Table 4.2, it can be clearly seen that the FWHM slightly decreases upon the addition of the whiskers, while the d-spacings slightly increase for all the LDPE nanocomposites. Thus, the

lamellar thickness and thickness distribution did not significantly change upon the addition of the whiskers. FWHM is related to the lattice perfection and dimensions of the crystallites [11].

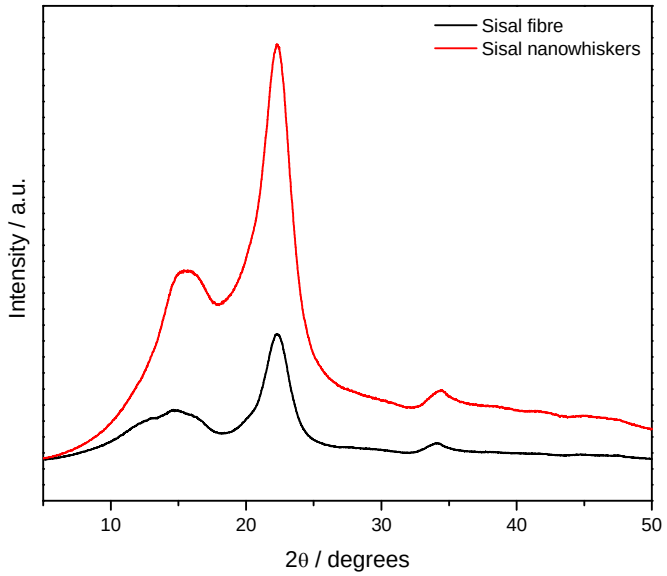

Figure 4.9 WAXD patterns of sisal fiber and whiskers

Table 4.2 Unit cell parameters of LDPE and LDPE/sisal whiskers nanocomposites

Sample	110			200		
LDPE/SNW (w/w)	2θ / deg	d-spacing / Å	FWHM	2θ / deg	d-spacing / Å	FWHM
Untreated LDPE nanocomposites – melt mixed						
100/0	21.4	4.12	0.74	23.8	7.48	0.87
99/1	21.3	4.17	0.65	23.5	7.56	0.81
95/5	21.3	4.16	0.65	23.6	7.54	0.79
VTES treated LDPE nanocomposites – melt mixed						
99/1	21.3	4.17	0.66	23.6	7.54	0.80
95/5	21.4	4.15	0.67	23.7	7.51	0.79
Untreated LDPE nanocomposites – solution mixed						
99/1	21.3	4.17	0.65	23.6	7.54	0.78
95/5	21.3	4.16	0.65	23.6	7.55	0.78

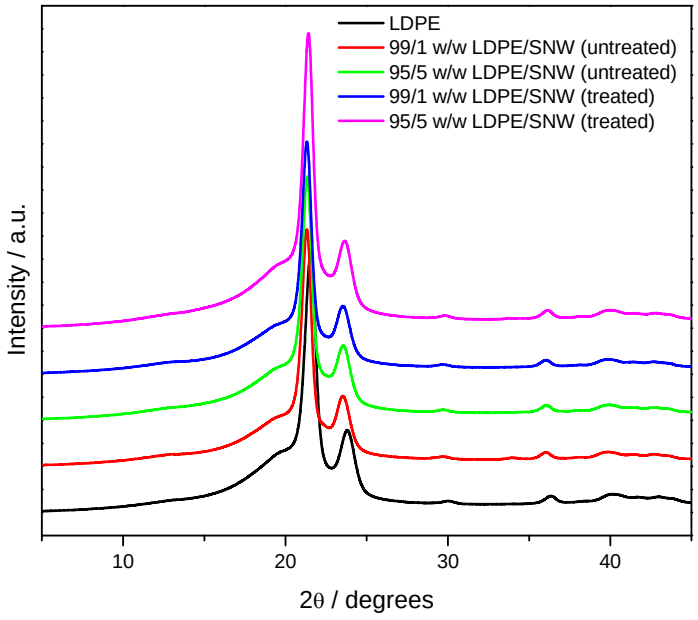

Figure 4.10 WAXD patterns of LDPE, untreated and VTES treated melt mixed LDPE nanocomposites

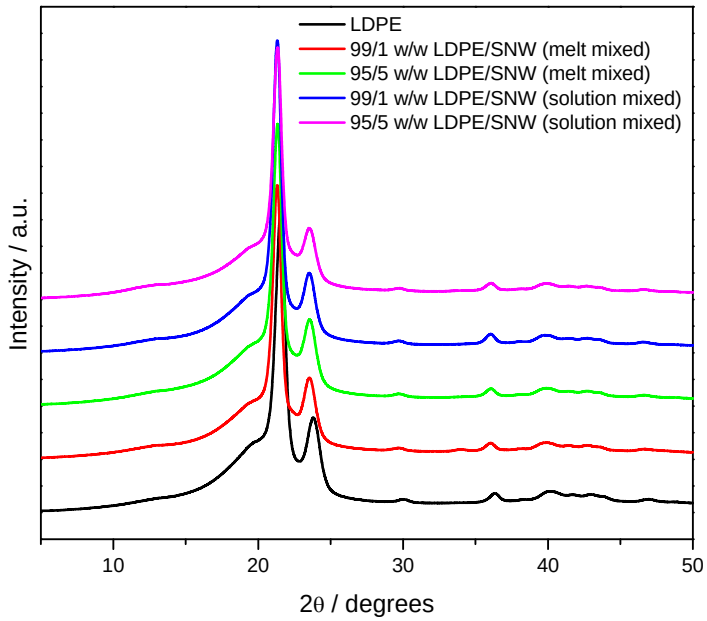

Figure 4.11 WAXD patterns of LDPE, untreated melt and solution mixed LDPE nanocomposites

It can be seen in Figures 4.12 and 4.13 that HDPE also displays two distinct (110) and (200) reflection peaks and a weak (004) reflection peak, respectively at 2θ angles of 21.4, 23.8 and 36.1°, corresponding to d-spacings of 4.14, 7.74 and 2.48 Å. Similar observations were seen for all the nanocomposite samples. As discussed earlier for LDPE, this can be related to the orthorhombic crystal structure of polyethylene. There are, however, differences between the scattering patterns of HDPE and LDPE. HDPE shows more intense and sharp peaks, and the broad halo peak around 20° is quite small. The treated HDPE nanocomposites show more intense sharp peaks at the110 and 200 reflections when compared to the untreated samples (Figure 4.12). In Figure 4.13, similar behaviour can be observed for the untreated solution mixed nanocomposites. It seems as if the whiskers nucleated the polymer matrix, and that this was dependent from the treatment and preparation method. It can be clearly seen in Table 4.3 that the FWHM and d-spacing values change only slightly upon the addition of the whiskers. This indicates that the crystallites' perfection and dimensions were not significantly influenced.

Table 4.3 Unit cell parameters of HDPE and HDPE/sisal whiskers nanocomposites

Sample	**110**			**200**		
HDPE/SNW (w/w)	**2θ / deg**	**d-spacing / Å**	**FWHM**	**2θ / deg**	**d-spacing / Å**	**FWHM**
Untreated HDPE nanocomposites – melt mixed						
100/0	21.4	4.14	0.55	23.8	7.47	0.62
99/1	21.4	4.14	0.55	23.8	7.47	0.62
95/5	21.4	4.14	0.54	23.8	7.48	0.61
VTES treated HDPE nanocomposites – melt mixed						
99/1	21.4	4.15	0.56	23.8	7.49	0.63
95/5	21.4	4.14	0.54	23.8	7.48	0.61
Untreated HDPE nanocomposites – solution mixed						
99/1	21.6	4.11	0.56	23.9	7.43	0.63
95/5	21.6	4.12	0.56	23.9	7.44	0.62

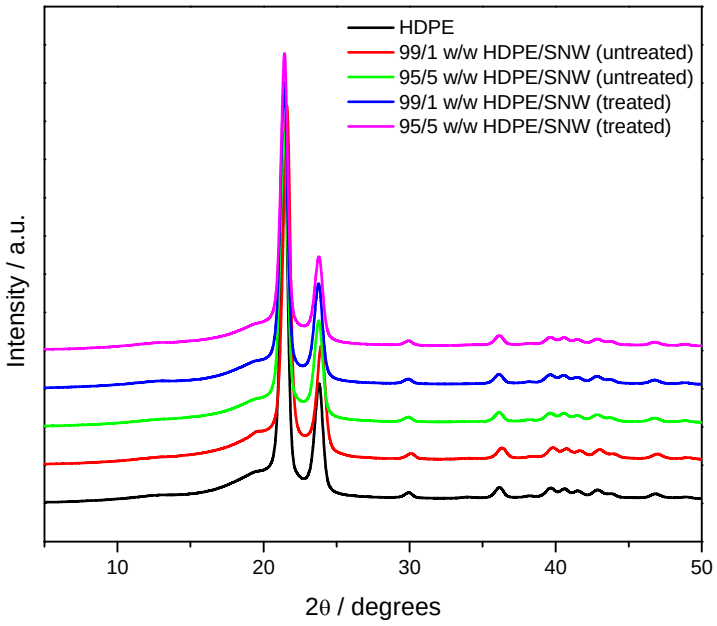

Figure 4.12 WAXD patterns of HDPE, untreated and VTES treated melt mixed HDPE nanocomposites

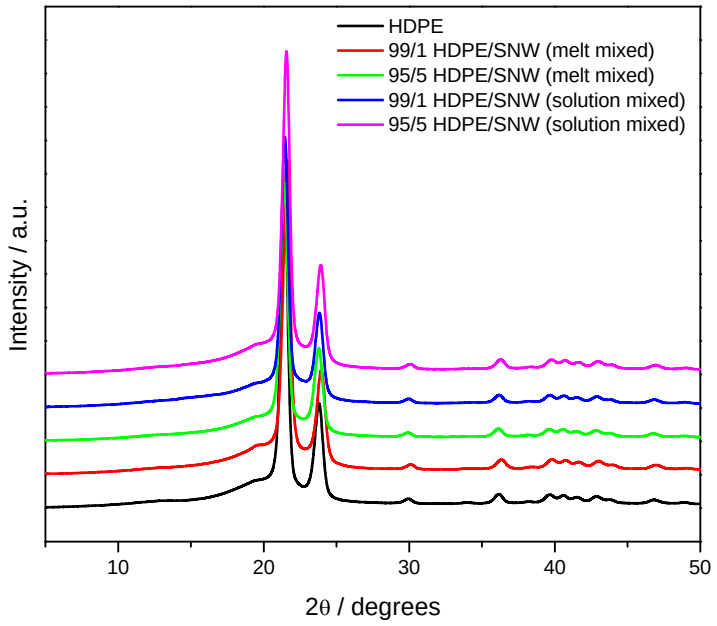

Figure 4.13 WAXD patterns of HDPE, untreated melt and solution mixed HDPE nanocomposites

4.4 Differential scanning calorimetry (DSC)

Figures 4.14 to 4.17 depict the DSC curves for neat PE and PE/sisal whiskers nanocomposites. The characteristics of the nanocomposites from the DSC curve measurements are summarized in Tables 4.4 and 4.5. The degree of crystallinity, χ_c, of the samples was calculated according to the Equation 4.2.

$$\chi_c = \frac{\Delta H_m}{\Delta H_\infty} \times \frac{100}{w} \qquad (4.2)$$

The melting enthalpy of 100% crystalline polymer, ΔH_∞, was taken as 290 J g^{-1} for PE [12]. A correction for the dilution effect linked to the filler incorporation in the matrix was made while calculating the melting enthalpy of the nanocomposites, where *w* is the weight fraction of the polymeric matrix.

In Figures 4.15 and 4.16 it can be seen that the melting of the LDPE and all the LDPE nanocomposites was similar without any significant shifting, independent of the surface nature of the whiskers, the content and the preparation method. In Table 4.4 it can be clearly seen that the melting temperature (T_m), normalized enthalpy of fusion (H_m^{norm}) and crystallinity (χ_c) were roughly constant, regardless of the content, treatment and preparation method. This is an indication that both the size and amount of crystalline domains, which are respectively related to the melting temperature and enthalpy of fusion, of the polymer are retained. These results are in line with the WAXD results discussed earlier, where the unit parameters did not significantly change in all the analysed LDPE nanocomposites. De Menezes *et al*. [12] also found that the melting temperature remains roughly constant upon the addition of the whiskers, regardless of their state of modification. The authors did, however, find that the degree of crystallinity of the LDPE matrix increased with an increase in whiskers content. They observed no changes in the WAXD diffraction patterns of the nanocomposites, and pointed out that the crystallinity of the matrix was not affected by whiskers addition. They did, however, mention that there might have been changes in crystallinity, which may not have been spatially resolved by the diffractometer.

Table 4.4 Melting characteristics of LDPE nanocomposites: melting temperature (T_m), observed melting enthalpy (ΔH_m^{obs}), normalised melting enthalpy (ΔH_m^{norm}), and degree of crystallinity (χ_c)

LDPE/SNW (w/w)	T_m/ °C	ΔH_m^{obs} / J g^{-1}	H_m^{norm} / J g^{-1}	χ_c / %
Untreated LDPE nanocomposites – melt mixed				
100/0	107.0 ± 0.3	93.9 ± 1.0	93.9	32.5
99/1	107.2 ± 0.7	94.4 ± 1.4	95.4	33.0
95/5	107.5 ± 0.4	90.2 ± 1.0	95.0	32.8
Vinyl triethoxysilane treated LDPE nanocomposites – melt mixed				
100/0	106.9 ± 0.3	93.2 ± 2.4	93.2	32.3
99/1	107.3 ± 0.3	93.1 ± 0.5	94.0	32.6
95/5	107.1 ± 0.3	89.4 ± 2.0	94.1	32.6
Untreated LDPE nanocomposites – solution mixed				
100/0	107.5 ± 0.2	96.4 ± 0.2	96.4	33.4
99/1	107.8 ± 0.7	92.4 ± 2.5	93.3	32.3
95/5	107.4 ± 0.2	87.7 ± 0.2	92.3	32.0

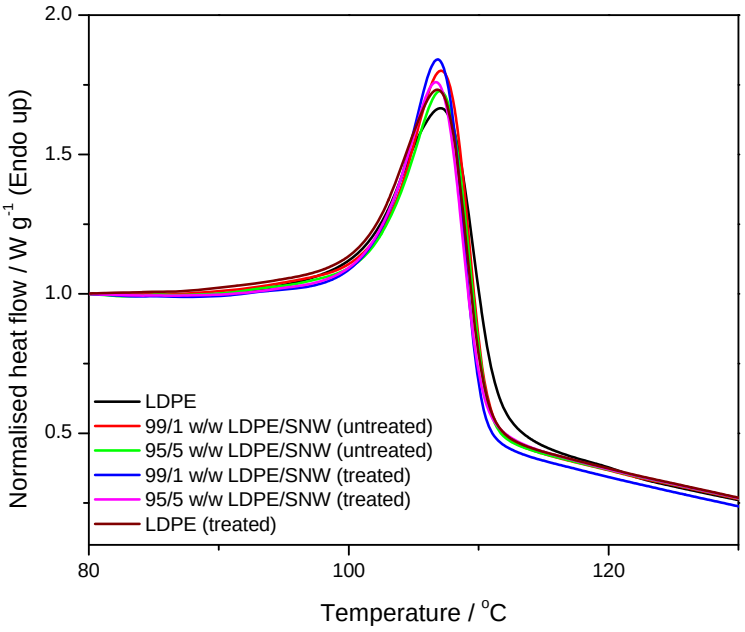

Figure 4.15 DSC melting curves for neat LDPE, untreated and VTES treated LDPE/sisal whiskers nanocomposites

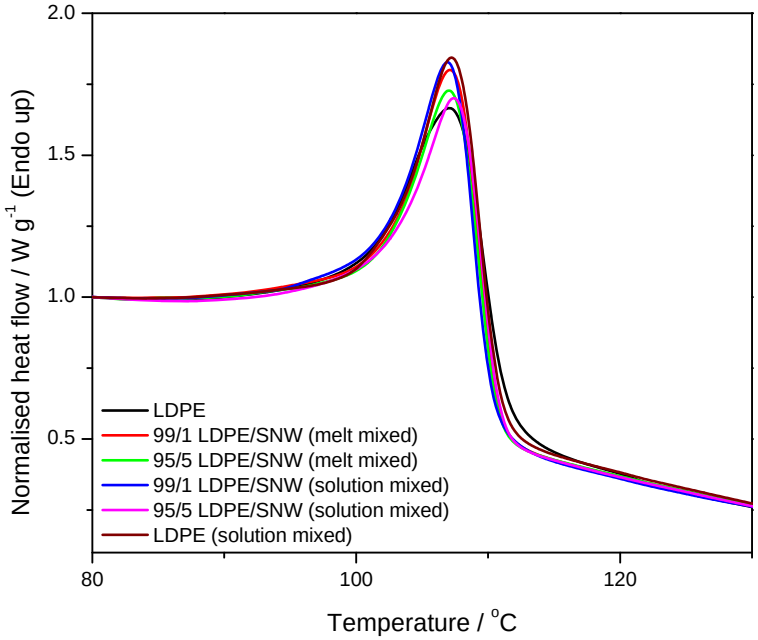

Figure 4.16 DSC melting curves for neat LDPE, untreated melt and solution mixed LDPE/sisal whiskers nanocomposites

There was a slight decrease in melting peak temperature of the treated HDPE nanocomposites as well as the 99/1 w/w untreated HDPE nanocomposites (Figure 4.17). Similar behaviour was observed for the untreated solution mixed nanocomposites. This shift was not significant enough to relate it to any morphological changes. It can be seen clearly in Table 4.4 that the T_m for all the nanocomposite samples remains fairly constant (128-130°C), indicating that the size of the crystalline domains did not change significantly. The observed melting enthalpy, as expected, decreased with an increase in whiskers content for the untreated melt mixed nanocomposites. This was the result of a decrease of the amount of polymer in the nanocomposites. The χ_c and normalized enthalpy values for the untreated melt mixed HDPE/sisal whiskers nanocomposites remain fairly constant, regardless of the sisal whiskers content. The normalized melting enthalpy values generally increased with the nanowhiskers content, indicating a slight increase in the amount of the crystalline domains. This may be due to the nucleation effect of the whiskers. This increase is more obvious for the treated and solution mixed samples, probably because of favourable adhesion between the filler and the matrix. Grunert *et al*. [13] found that heat of fusion (ΔH_f) increased with an increase in silylated whiskers content, and stayed the same for the untreated samples. The authors

pointed out that the silylated whiskers acted as nucleating agents and promoted the crystallization of the cellulose acetate butyrate matrix. They did, however, find that the melting temperature also increased with increasing silylated whiskers content as a result of stronger filler-matrix interaction. Ljungberg *et al*. [14] found that nanocomposites prepared from toluene solution casting and filled with untreated whiskers nucleated the β-phase of the iPP matrix. They pointed out that this could be due to hydrophilicity of the whiskers.

Table 4.5 Melting characteristics of HDPE nanocomposites: melting temperature (T_m), observed melting enthalpy (ΔH_m^{obs}), normalised melting enthalpy (ΔH_m^{norm}), and degree of crystallinity (χ_c)

HDPE/SNW (w/w)	T_m / °C	ΔH_m^{obs} / J g^{-1}	H_m^{norm} / J g^{-1}	χ_c / %
Untreated HDPE nanocomposites – melt mixed				
100/0	130.1 ± 0.4	185.2 ± 4.2	185.2	64.1
99/1	129.7 ± 0.3	181.0 ± 7.2	182.8	63.3
95/5	130.0 ± 0.3	177.0 ± 3.8	186.3	64.5
Vinyl triethoxysilane HDPE treated nanocomposites – melt mixed				
100/0	129.0 ± 0.7	176.4 ± 3.5	176.4	61.1
99/1	129.2 ± 0.7	194.9 ± 1.1	196.9	68.1
95/5	128.7 ± 0.5	186.6 ± 2.4	196.4	68.0
Untreated HDPE nanocomposites – solution mixed				
100/0	128.7 ± 0.2	185.0 ± 3.4	185.0	64.1
99/1	128.9 ± 0.1	186.4 ± 3.3	188.3	65.2
95/5	129.6 ± 1.5	183.3 ± 0.7	193.0	66.8

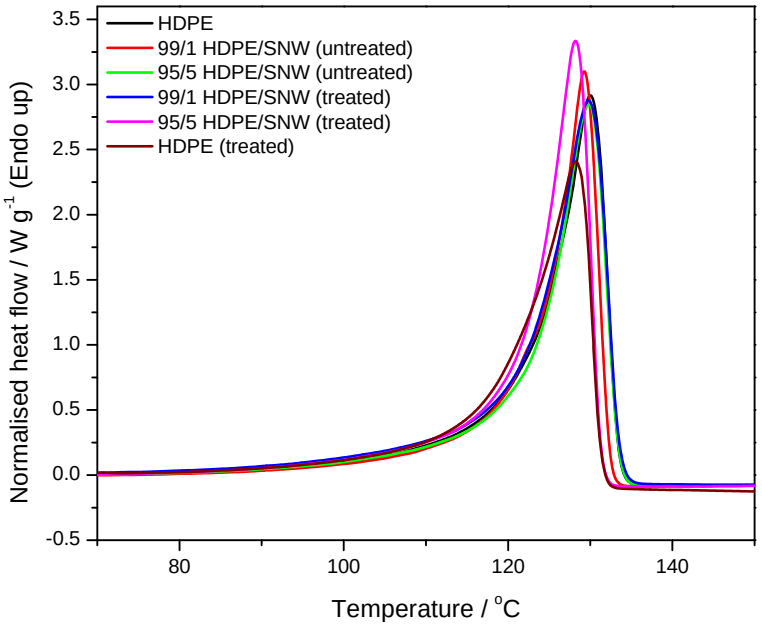

Figure 4.17 DSC melting curves for neat HDPE, untreated and VTES treated HDPE/sisal whiskers nanocomposites

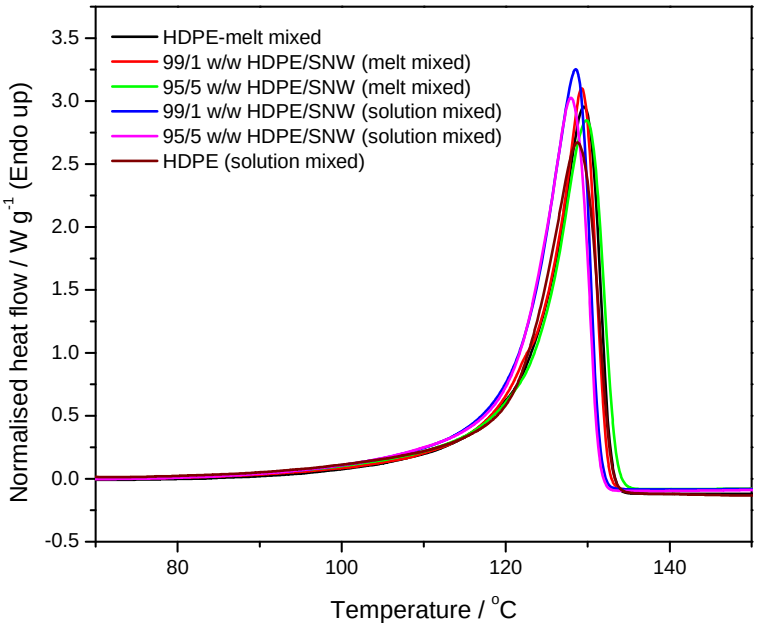

Figure 4.18 DSC melting curves for neat HDPE, untreated melt and solution mixed HDPE/sisal whiskers nanocomposites

4.5 Thermogravimetric analysis (TGA)

Figures 4.19 to 4.26 show the thermal degradation curves of the investigated samples. The relevant temperature values from these curves are tabulated in Tables 4.6 and 4.7. Sisal whiskers displayed three pyrolysis steps up to 600 °C (Figure 4.19). The small mass loss below 100°C is attributed to moisture evaporation. The decomposition of the whiskers occurred between 220 and 350°C. This pyrolysis process is related to processes such as depolymerisation, dehydration and decomposition of glycosyl units followed by the formation of char above 350 °C [10,15,16]. There is no separate decomposition of hemicellulose above 280 °C, which further confirms its removal during the preparation of the whiskers [4].

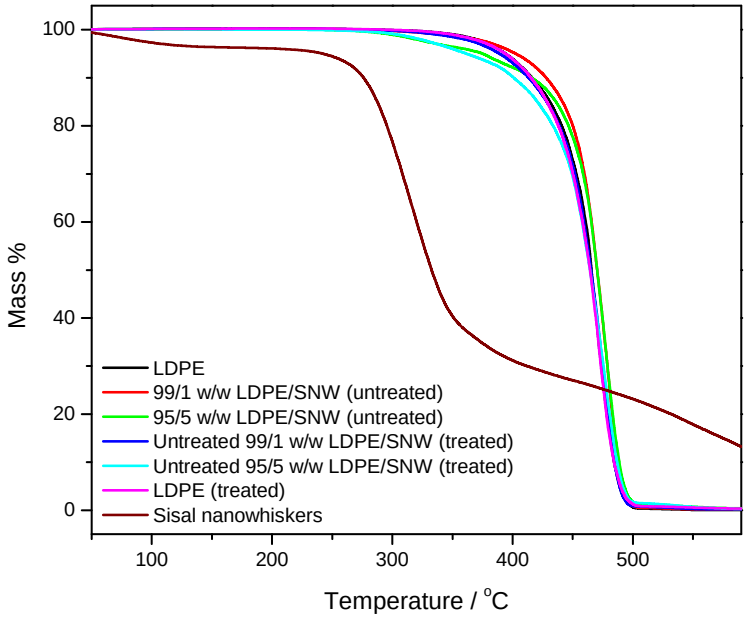

Figure 4.19 TGA curves of LDPE, VTES treated LDPE, and untreated and VTES treated nanocomposites

Table 4.6 Thermal degradation characteristics ($T_{20\%}$: decomposition temperature associated with a 20% mass loss, $T_{50\%}$: decomposition temperature associated with a 50% mass loss, and T_d: temperature maximum from derivative TGA curves) for LDPE/sisal whiskers nanocomposites

LDPE/sisal whiskers(w/w)	$T_{20\%}$ / ºC	$T_{50\%}$ / ºC	T_d / ºC
Untreated LDPE nanocomposites – melt mixed			
100/0	441.3	465.5	471.4
99/01	450.1	469.7	479.9
95/05	450.1	470.4	479.0
Vinyl triethoxysilane treated LDPE nanocomposites – melt mixed			
100/0	438.1	464.1	471.0
99/01	439.3	465.4	476.3
95/05	434.5	464.2	476.4
Untreated LDPE nanocomposites – solution mixed			
100/0	439.0	466.5	477.7
99/01	444.8	467.9	477.7
95/05	436.7	469.5	478.1

The LDPE shows a single decomposition step at about 466°C, regardless of its treatment and preparation method, as observed in Figure 4.19 and 4.21. There is a development of a separate mass loss step on the lower temperature before the main loss step of the LDPE matrix degradation for all prepared nanocomposites. The height of this separate mass loss is close to the amount of whiskers in the composition. This may be attributed to whiskers' decomposition processes, as discussed earlier. These processes include dehydration, rearrangement, formation of carbonyl and carboxylic groups, evaporation of water, carbon dioxide and carbon monoxide, and formation char residue. In Figure 4.19, the untreated LDPE nanocomposites show a slight increase in thermal stability compared to neat LDPE, as can clearly seen in Table 4.6 and Figure 4.20. This may be attributed to the char residue formed during whiskers decomposition acting as thermal barrier, reducing heat transfer to the interior, and also trap or restrict the release of volatile products hence slightly improve thermal stability of the composite material. Similar observations were reported by Panaitescu *et al*. [17]. They found that microfibrils at low content (10 wt%) act as scavengers consuming free radicals hence improve thermal stability of the polymer. Bahar *et al.* [18] reported an

increase thermal stability with an increase in whiskers' content. The authors pointed out that this was the result of whiskers increasing the thermal resistance of the composites. The treated LDPE nanocomposites did not significantly influence the degradation behaviour of the polymer. As can be seen in Table 4.6, the temperature associated with 20% and 50% weight loss remained roughly constant with an increase in whiskers' content, where as T_d maximum slightly increases. This may be attributed to interaction between the whiskers and polymer which led to both degrading together. De Menezes *et al.* [12] also reported that the T_d maximum remained roughly constant regardless of whiskers' modification and/or content. They did, however, found that the onset temperature of the weight loss process was systematically lower for composites than for neat polymer. They pointed out that this may be due to water content in the cellulose whiskers.

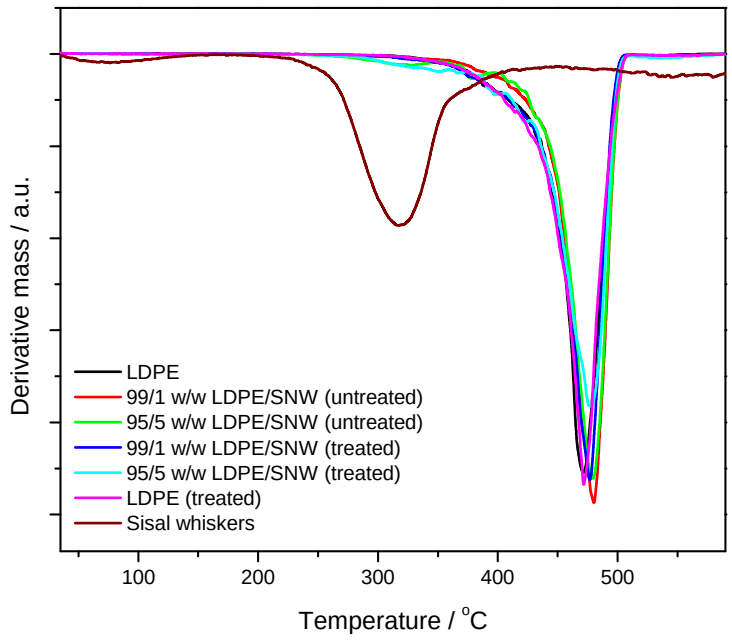

Figure 4.20 dTGA curves of LDPE, VTES treated LDPE, and untreated and VTES treated nanocomposites

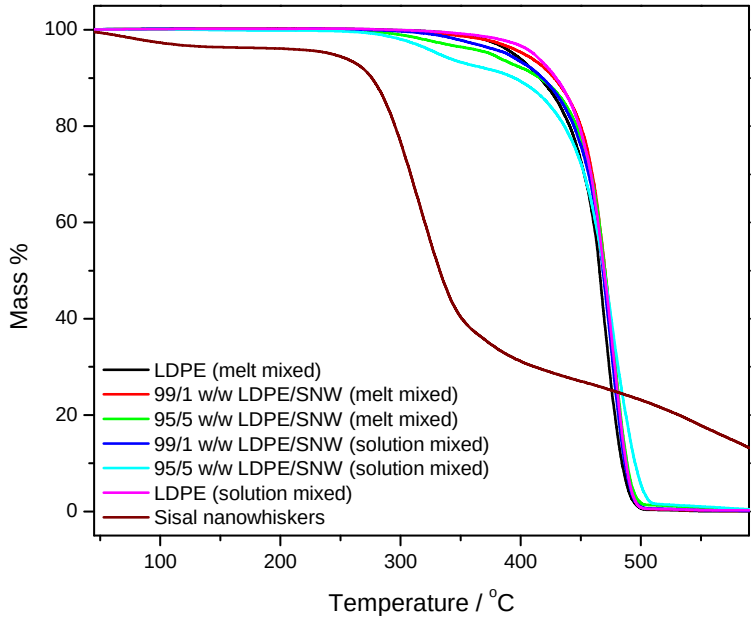

Figure 4.21 TGA curves of sisal whiskers, LDPE, and melt and solution mixed LDPE nanocomposites

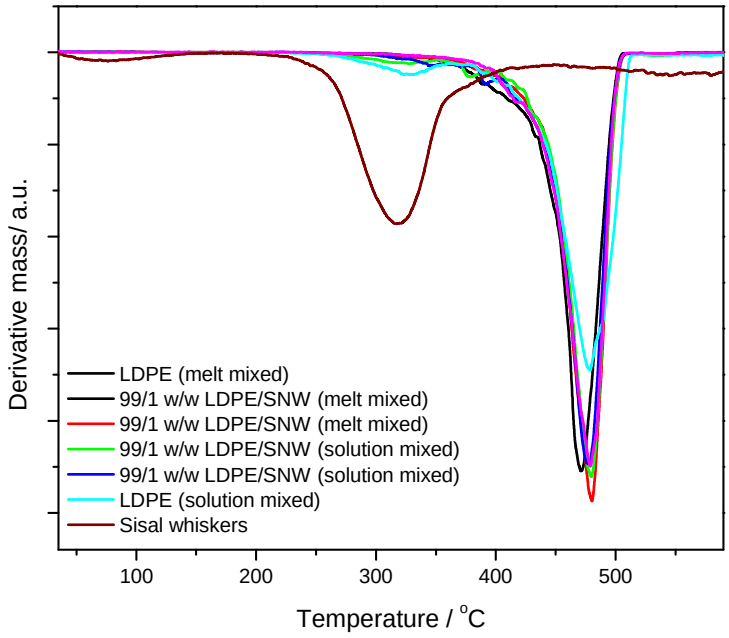

Figure 4.22 dTGA curves of sisal nanowhiskers, LDPE, and melt and solution mixed LDPE nanocomposites

Figure 4.21 and 4.22 depict respectively the TGA and dTGA curves for untreated melt and solution mixed LDPE nanocomposites. It is clear from the curves and Table 4.6 that both the untreated melt and solution mixed LDPE nanocomposites slightly increases the thermal stability of the neat polymer. The temperature associated with 20% weight loss for solution mixed nanocomposites decreases slightly with an increase in whiskers content, whereas the temperature associated with 50% and T_d maximum slightly increase. As discussed earlier this may be attributed to whiskers trapping free radicals and reducing heat transfer to the interior of the composite materials.

Table 4.7 Thermal degradation characteristics ($T_{20\%}$: decomposition temperature associated with a 20% weight loss, $T_{50\%}$: decomposition temperature associated with a 50% weight loss, and T_d: temperature maximum from derivative TGA curves)for HDPE/sisal whiskers nanocomposites

HDPE/sisal whiskers(w/w)	$T_{20\%}$ / ºC	$T_{50\%}$ / ºC	T_d / ºC
Untreated HDPE nanocomposites-melt mixed			
100/0	453.1	472.4	478.5
99/01	452.4	473.5	482.2
95/05	448.4	473.9	485.9
Vinyl triethoxysilane treated HDPE nanocomposites-melt mixed			
100/0	456.4	473.3	477.6
99/01	454.5	475.1	480.2
95/05	442.7	472.4	480.5
Untreated HDPE nanocomposites-solution mixed			
100/0	455.1	474.5	482.0
99/01	446.6	474.5	485.3
95/05	447.4	474.6	483.5

In Figure 4.23 and 4.25, untreated and treated melt mixed HDPE as well as solution mixed HDPE show a single degradation step. Furthermore, there was slight increment in thermal stability for treated melt mixed HDPE compared to neat HDPE, whereas the solution and melt mixed HDPE overlap each other. The former may be due to silane grafting and/or crosslinking reactions inducing thermal stability of the neat polymer [19]. The development of a separate mass loss step for all prepared nanocomposites samples at lower temperature

before the main weight loss degradation step is also observed in Figure 4.23 and 4.25. The height of this mass loss step also is close to the quantity of whiskers in the composition. As discussed earlier for LDPE nanocomposites, this may be attributed to the whiskers decomposition processes. In Figure 4.23 and 4.25, the untreated and treated melt mixed as well as solution mixed HDPE nanocomposites almost overlap each other, depending on the whiskers' content, over the whole investigated temperature. Moreover, there is no significant influence on the thermal degradation behaviour of the polymer, regardless of the preparation method and treatment, as can clearly be seen in Figure 4.24 and 4.26 as well as Table 4.7. Samir *et al*. [20] also reported that there was no influence on the thermal stability of the poly(oxyethylene) matrix upon the addition of the whiskers despite strong interaction found between the polymeric matrix and whiskers. Alloin *et al*. [21] also reported that there was no effect of processing method on thermal degradation under inert atmosphere. They did, however, found that the extruded films have lower degradation temperature compared to cast/evaporated ones in oxidative atmosphere.

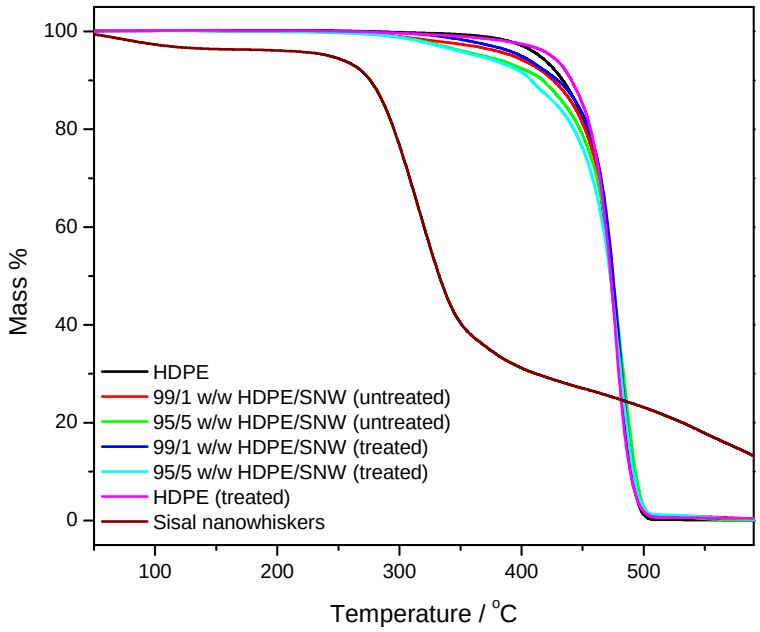

Figure 4.23 TGA curves of HDPE, VTES treated HDPE, and untreated and VTES treated nanocomposites

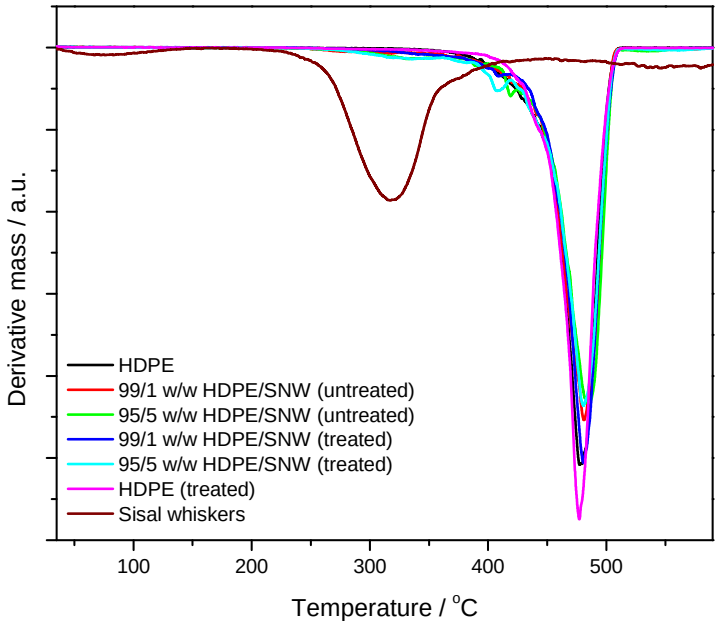

Figure 4.24 dTGA curves of HDPE, VTES treated HDPE, and untreated and VTES treated nanocomposites

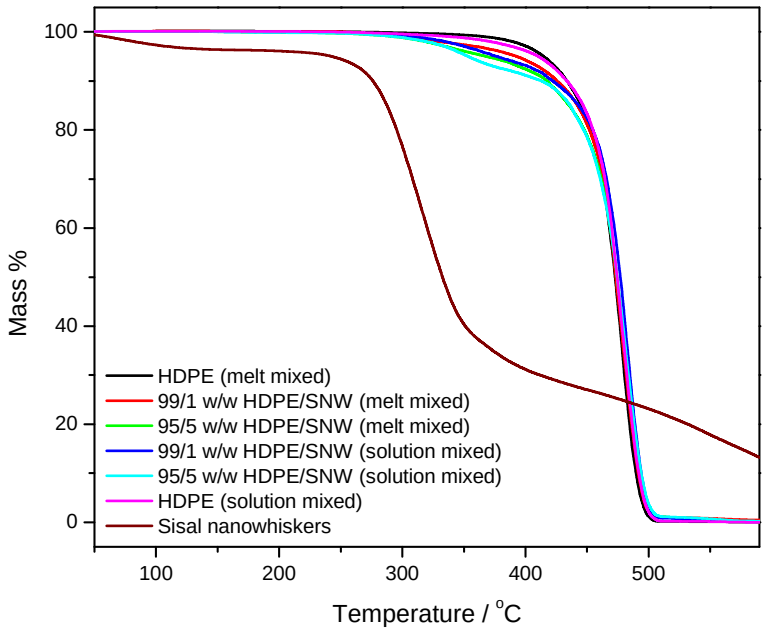

Figure 4.25 TGA curves of sisal nanowhiskers, HDPE, and melt and solution mixed HDPE nanocomposites

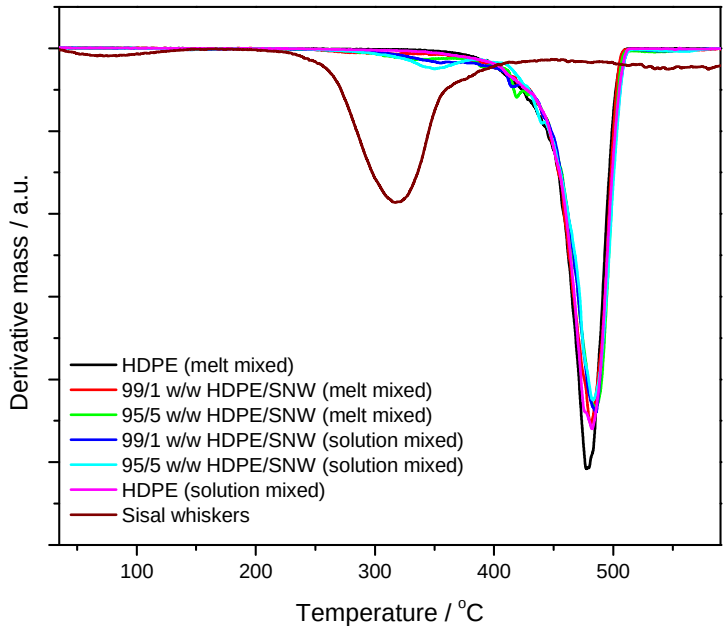

Figure 4.26 dTGA curves of sisal nanowhiskers, HDPE, and melt and solution mixed HDPE nanocomposites

4.6 Dynamic mechanical analysis (DMA)

The dynamic mechanical behaviour of all the investigated samples is shown in Figures 4.27 to 4.34. All the loss modulus curves are presented in the Appendix. LDPE shows the typical behaviour of a semicrystalline polymer (Figure 4.27), but there is an unusual peak around 70 °C. The untreated melt mixed 99/1 w/w LDPE/SNW nanocomposite also shows this behaviour. This phenomenon can be clearly seen in Figure 4.29, where the transition splits into two peaks around 56 and 68 °C. These transitions are normally called α and α′. The latter is related to the slippage of the crystallites past each other, while the former is related to the movement of amorphous chain segments within the crystalline phase [22]. Interestingly, this peak disappeared upon the addition of the whiskers. This may have been caused by the whiskers influencing the interlamellar chain motion, because the polymer crystallization probably started at the surfaces of the whiskers. Similar observations were reported by Molefi *et al.* [23], who also observed this unusual peak for both LLDPE and LDPE, which then disappeared upon the addition of the fillers. Both the untreated and VTES treated melt mixed

LDPE nanocomposites' storage modulus curves were higher than that of the neat polymer over the whole temperature range investigated. At low temperatures (below 0 °C) the curves almost overlap each other. As the temperature increases (above the glass transition), these curves start separating and the effect of the whiskers' presence is clearly observed. This can be attributed to the higher modulus of the whiskers compared to that of the polymeric matrix. The curves for the treated nanocomposites are very similar to those of their untreated counterparts. It seems as if the treatment did not influence the storage modulus of the nanocomposites. These observations are in agreement with the ones reported by de Menezes *et al.* [12], who also observed no influence of the treatment on the storage modulus of the treated nanocomposites. They pointed out that the treatment may have reduced the possibility of interwhiskers interactions, which would have increased the storage modulus.

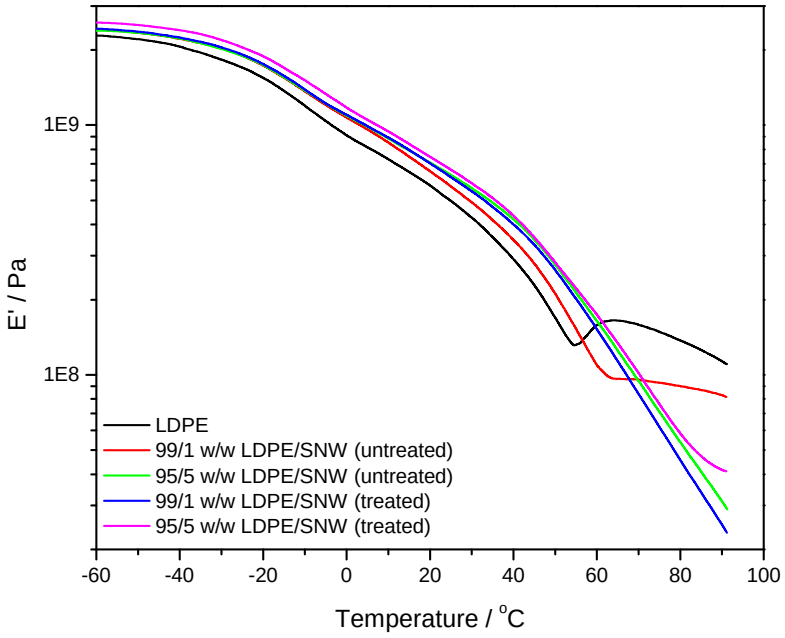

Figure 4.27 Storage modulus versus temperature for LDPE and its untreated and VTES treated sisal whiskers nanocomposites

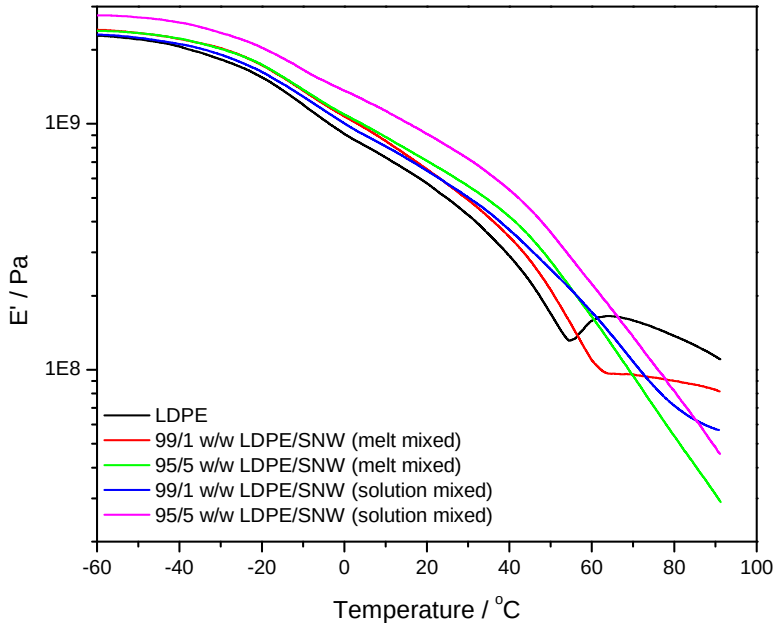

Figure 4.28 Storage modulus versus temperature for LDPE and its melt and solution mixed sisal whiskers nanocomposites

Figure 4.28 also shows that the reinforcing effect was more significant at higher temperatures. Generally, the storage modulus of both untreated melt and solution mixed nanocomposites increased with an increase in whiskers' content. This may be attributed to the higher modulus of the whiskers. Furthermore, the storage modulus values for the untreated solution mixed nanocomposites are higher than those for the melt mixed samples. This was probably be due to interactions between the whiskers, improving their reinforcing efficiency. However, these interactions were not observable in the TEM and SEM results (Section 4.2). During solution casting, the whiskers have enough time to interact with each other which may have resulted in a hydrogen bonding network. This is as the result of the low viscosity of the polymer matrix and the slow processing conditions. As discussed earlier, the formation of a hydrogen bonding network was reported to be the major cause of the reinforcing efficiency in cellulose whiskers reinforced nanocomposite materials [21,24]. On the contrary, during melt compounding, the high viscosity of the polymer, fast processing and the mechanical stresses involved counteracted the formation of a hydrogen bonded network between the whiskers, resulting in either a limited or no hydrogen bonded network.

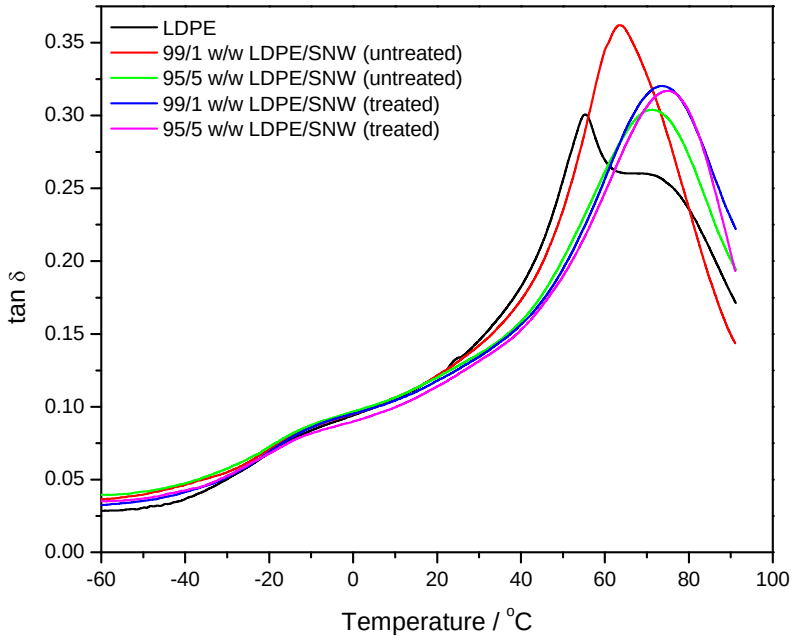

Figure 4.29 tan δ versus temperature for LDPE and its untreated and VTES treated sisal whiskers nanocomposites

The curves of tan δ as a function of temperature for the untreated and VTES treated melt mixed LDPE nanocomposites are shown in Figure 4.29. These curves show two clearly resolved relaxation transitions located around -17 °C (glass transition) and 40-80 °C (α transitions). The same is observed for the untreated solution mixed LDPE nanocomposites (Figure 4.30). The weak transition at -17 °C is known as the β relaxation and usually represents the glass transition of polyethylenes [25,26]. There was no significant shift upon the addition of the whiskers, regardless of whiskers' content, treatment and preparation method. The second transition is associated with the chain segment movement in the crystalline phase which is probably due to the orientation of defect areas in the crystals [25,26]. For neat LDPE this transition splits into two peaks located at temperatures about 56 and 68°C,and are usually called the α and α' transitions. As mentioned earlier, these transitions can be explained as the chain motions of the amorphous chain segments in the crystalline phase, and the slippage of the crystallites past each other, respectively. They may also be explained as being the result of the presence of lamellae with different thicknesses, in the sense that the melting of thinner lamellae may show a transition at lower temperatures followed by interlamellar shear of the larger crystallites [22,23]. The splitting of this

transition vanishes upon the addition of the whiskers. It is clear that the whiskers inhibited this phenomenon resulting in a single transition at higher temperatures. The shift to higher temperatures is an indication that the presence of the whiskers somehow restricted the mobility of the amorphous chains in the crystalline phase and/or the slippage of the crystallites. As mentioned earlier, this may probably be the result of the crystallization of the polymer starting on the surface of the whiskers and thus influencing the chains motions within the crystalline regions.

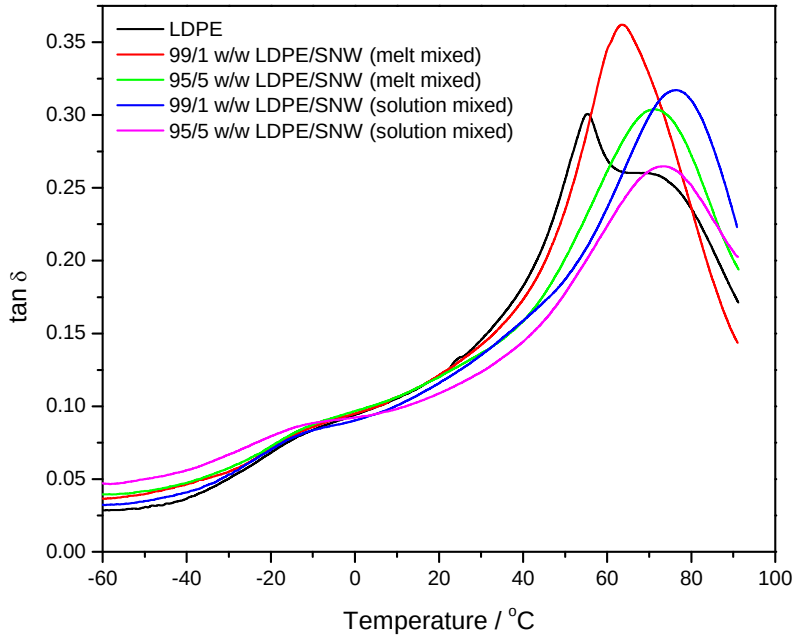

Figure 4.30 tan δ versus temperature for LDPE and its melt and solution mixed sisal whiskers nanocomposites

The storage modulus curves of the untreated and treated HDPE/sisal whiskers nanocomposites are shown in Figure 4.31. At lower temperatures, both the treated and untreated nanocomposites have lower E' values than the neat polymer. The reinforcing effect of the whiskers is more obvious at higher temperatures. This could be related to the reinforcing effect of the whiskers, which restricts the HDPE chain motions when it softens, and to the increase in crystallinity as reported in the DSC results (Section 4.4). Furthermore, the treated nanocomposites displayed lower values compared to the untreated composites. As discussed earlier, this could be the result of the stronger interaction between the whiskers and the matrix, which may have reduced the whisker-whisker interactions, and resulted in a

decrease in storage modulus [12,21,24]. Nair *et al*. [27] reported that the unmodified whiskers based nanocomposites showed a stronger reinforcing effect than the chemically modified whiskers nanocomposites. They pointed out that the increase in filler-matrix interactions resulted in a decrease in the whisker-whisker interactions, that were responsible for the good mechanical characteristics of the unmodified whiskers based nanocomposites

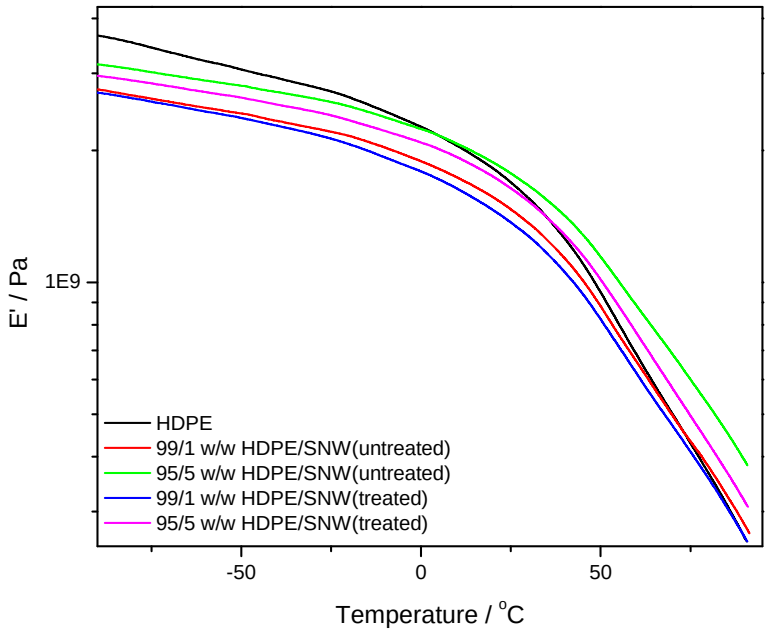

Figure 4.31 Storage modulus versus temperature for HDPE and its untreated and VTES treated sisal whiskers nanocomposites

As can be seen in Figure 4.32, the whiskers generally improved the storage modulus at higher temperatures. This may be attributed to whiskers' higher modulus compared to that of the neat polymer, and/or to the increase in crystallinity reported in DSC results (Section 4.4). The storage modulus in this temperature range also increases with an increase in whiskers content. The solution mixed nanocomposites at 5% whiskers content show higher E' values than all the other nanocomposites and the neat polymer over the whole range of investigated temperatures. As mentioned earlier for the untreated solution mixed LDPE nanocomposites, this may additionally be due to the formation of a hydrogen bonding network between the whiskers leading to improved reinforcing efficiency. However, these interactions were not clearly observed in TEM and SEM results (Section 4.2).

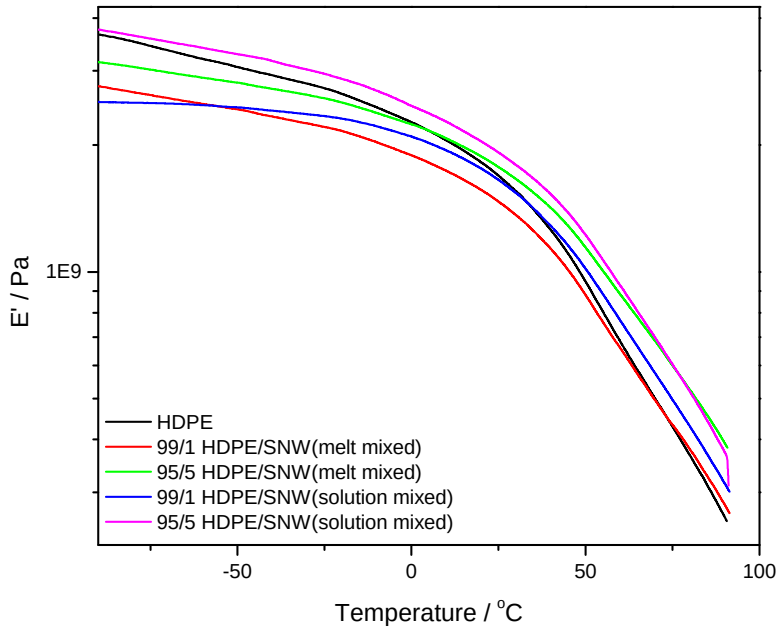

Figure 4.32 Storage modulus versus temperature for HDPE and its melt and solution mixed sisal whiskers nanocomposites

Tan δ as function of temperature for HDPE and the HDPE/sisal whiskers nanocomposites is shown in Figures 4.33 and 4.34. The β relaxation, observed in the tan δ curves of LDPE and its nanocomposites (Figures 4.29 and 4.30), is not visible in the tan δ curves of HDPE and its nanocomposites. This can be attributed to the highly crystalline nature of HDPE [8]. It is interesting that after the onset at about 20 °C the curves start to deviate from each other, and pure HDPE has the highest tan δ values. The VTES treated nanocomposites have the lower values than their untreated counterparts. This is the result of the interfacial bonding between the polymer and the whiskers. The nanocomposites with poor interfacial bonding between the filler and the matrix have higher energy dissipation than those with stronger interfacial bonding [28]. The untreated solution mixed nanocomposites display lower tan δ values than the untreated melt mixed nanocomposites at higher temperatures (Figure 4.34). The whiskers may have immobilized the amorphous chains within the crystalline phase, because the crystallization probably started on the surface of the whiskers.

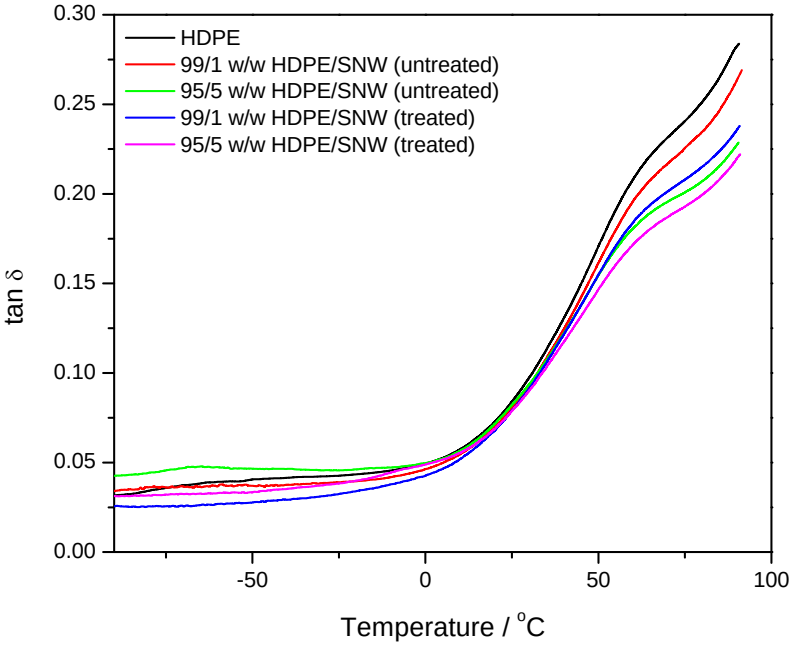

Figure 4.33 tan δ versus temperature for HDPE and its untreated and VTES treated sisal whiskers nanocomposites

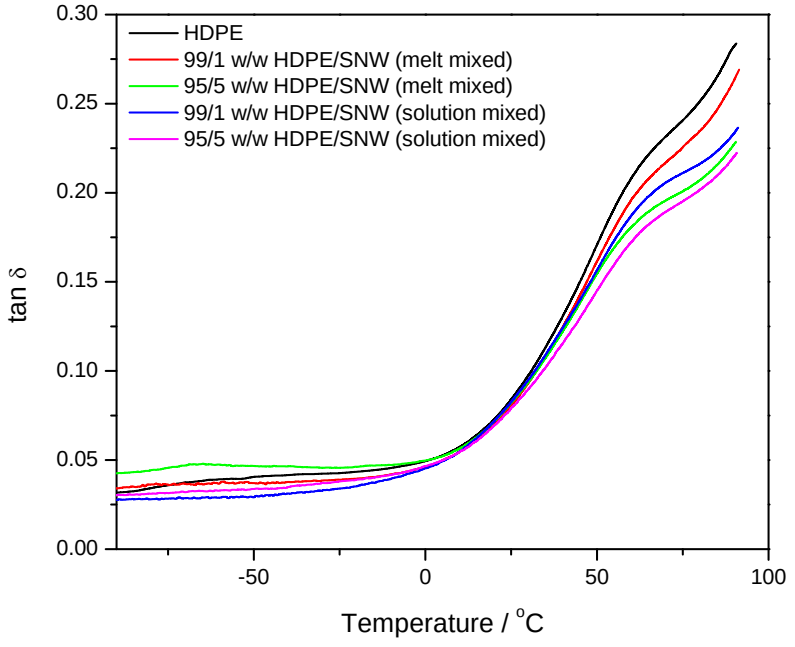

Figure 4.34 tan δ versus temperature for HDPE and its melt and solution mixed sisal whiskers nanocomposites

4.7 Tensile testing

The tensile properties of the investigated samples as a function of sisal whiskers content are summarized in Tables 4.8 and 4.9. All the stress-strain curves are presented in the Appendix. In Table 4.8 the elongation at break decreased upon the addition of the whiskers. There are no significant differences between the treated and untreated melt mixed, as well as the untreated solution mixed samples. This can be explained by the whiskers imparting rigidity and brittleness to the LDPE matrix, and acting as defect points where stress cracking occurs more easily. Generally the tensile modulus increases upon the addition of the whiskers, and further increases with an increase in whiskers content. There were no significant differences between equivalent samples prepared in different ways (Table 4.8). The stress at break was fairly constant within experimental error, regardless of the whiskers content and kind of treatment. The increased tensile modulus may be ascribed to the higher modulus of the whiskers, and to some extent to a reinforcement of the polymer matrix.

Table 4.8 Tensile properties for LDPE, as well as the treated and untreated LDPE nanocomposites

LDPE/SNW (w/w)	Elongation at break / %	E-modulus / MPa	Stress at break / MPa
Untreated LDPE-nanocomposites-melt mixed			
100/0	535 ± 6	172 ± 2	11.2 ± 0.7
99/1	86.3 ± 1.1	206 ± 3	10.8 ± 0.3
95/5	50.5 ± 1.0	213 ± 4	11.0 ± 0.3
VTES treated LDPE nanocomposites-melt mixed			
100/0	363 ± 2	167 ± 2	10.1 ± 0.2
99/1	91.3 ± 6	178 ± 2	10.5 ± 0.1
95/5	-	202 ± 2	-
Untreated LDPE nanocomposites-solution mixed			
100/0	542 ± 12	167 ± 10	10.3 ± 0.8
99/1	-	200 ± 2	-
95/5	44.7 ± 1.4	217 ± 8	10.5 ± 0.4

In Table 4.9, it can be clearly seen that the elongation at break of HDPE significantly decreased upon the addition of the whiskers for all the investigated samples. This can be explained by the whiskers acting as defect points for the initiation and propagation of stress cracking. The elongation at break for melt mixed treated HDPE is lower than the neat melt mixed HDPE. This decrease in elongation at break may be explained by the crosslinking of the polymer chains, which restricted the chain mobility and decreased the extent to which the polymer can elongate before fracturing. Interestingly, the melt mixed VTES treated HDPE nanocomposites showed slightly higher elongation at break values for a given composition than both the untreated counterparts. This effect may be ascribed to the VTES treatment which led to a better adhesion between the whiskers and the polymeric matrix, which enabled stress transfer. The tensile modulus increased significantly with the addition of whiskers, and it further increased with an increase in whiskers content for all the HDPE nanocomposites. The decrease in elongation at break and increase in modulus was more pronounced for the HDPE nanocomposites than the LDPE nanocomposites. This effect may be attributed to the difference in crystallinity of these polymers. Since the whiskers are located in amorphous phase, the concentration of the whiskers would be higher for the highly crystalline HDPE. Thus the addition of the whiskers would increase the rigidity and also influence the drawability, which begin in an amorphous phase. The stress at break significantly increased with the addition of the whiskers (Table 4.8), and this increase depended on the nanocomposite preparation method. For all the nanocomposites this increase may be attributed to a better dispersion, as observed in the TEM and SEM results (Section 4.2). In addition, there may be a good interaction, most probably because the polymer crystallizes on the surface of the whiskers. This was confirmed by an increase in crystallinity observed from the DSC results (Section 4.4). For the treated melt mixed HDPE nanocomposites this effect may additionally be due to a good stress transfer between the whiskers and polymeric matrix.

Table 4.9 Tensile properties for HDPE, as well as the treated and untreated HDPE nanocomposites

HDPE/SNW (w/w)	Elongation at break / %	E-modulus / MPa	Stress at break / MPa
Untreated HDPE nanocomposites – melt mixed			
100/0	832 ± 46	412 ± 7	16.4 ± 1.3
99/1	27.1 ± 0.8	586 ± 7	19.3 ± 3.1
95/5	-	623 ± 5	-
VTES treated HDPE nanocomposites – melt mixed			
100/0	388 ± 12	197 ± 18	14.6 ± 0.7
99/1	129 ± 17	509 ± 8	13.8 ± 1.2
95/5	19.2 ± 2.1	559 ± 9	28.0 ± 0.6
Untreated HDPE nanocomposites – solution mixed			
100/0	951 ± 68	329 ± 16	17.8 ± 1.1
99/1	17.0 ± 1.8	507 ± 13	26.2 ± 0.1
95/5	-	512 ± 13	-

4.8 References

1. J.K. Pandey, W.S. Chu, C.S. Kim, C.S. Lee, S.H. Ahn. Bio-nano reinforcement of environmentally degradable polymer matrix by cellulose whiskers from grass. Composites: Part B 2009; 40:676-680.
   DOI: 10.1016/j.compositesb.2009.04.013
2. A.N. Frone, S. Berlioz, J.-F. Chailan, D.M. Panaitescu, D. Donescu. Cellulose fiber-reinforced polylactic acid. Polymer Composites 2011; 32:977-985.
   DOI: 10.1002/pc.21116
3. J. Morshedian, P.M. Hoseinpour, H. Azizi, R. Parvizzad. Effect of polymer structure and additives on silane grafting of polyethylene. eXPRESS Polymer Letters 2009; 3:105-115. DOI: 10.3144/expresspolmlett.2009.14
4. Y.-T. Shieh, C.-M. Liu. Silane grafting reactions of LDPE, HDPE, and LLDPE. Journal of Applied Polymer Science 1999; 74:3404-3411.
   DOI: 10.1002/(SICI)1097-4628(19991227)
5. N.L.G. de Rodriguez, W. Thielemans, A. Dufresne. Sisal cellulose whiskers reinforced polyvinyl acetate nanocomposites. Cellulose 2006; 13:261-270.

DOI: 10.1007/s10570-005-9039-7

6. D. Bendeson, K. Oksman. Polylactic acid/cellulose whisker nanocomposites modified by polyvinyl alcohol. Composites: Part A 2007; 38:2486-2492.
DOI: 10.1016/j.compositesa.2007.08.0001
7. X. Cao, H. Dong, C.M. Li. New nanocomposite materials reinforced with flax cellulose nanocrystals in waterborne polyurethane. Biomacromolecules 2007; 8:899-904.
DOI: 10.1021/bm0610368
8. B. Wang, M. Sain. Isolation of nanofibers from soybean source and their reinforcing capability on synthetic polymers. Composites Science and Technology 2007; 67:2521-2527.
DOI: 10.1016/j.composcitech.2006.12.015
9. J.I. Morán, V.A. Alvarez, V.P. Cyras, A. Vázquez. Extraction of cellulose and preparation of nanocellulose from sisal fibers. Cellulose 2008; 15:149-159.
DOI: 10.1007/s10570-007-9145-9
10. M.A. Martins, E.M. Teixeira, A.C. Corrêa, M. Ferreira, L.H.C. Mattoso. Extraction and characterization of cellulose whiskers from commercial cotton fibers. Journal of Materials Science 2011; 46:7858-7864.
DOI: 10.1007/s10853-011-5767-2
11. X. Huang, P. Jiang, C. Kim, J. Duan, G. Wang. Atomic force microscopy analysis of morphology of low density polyethylene influenced by Al nano- and microparticles. Journal of Applied Polymer Science 2008; 107:2494-2499.
DOI: 10.1002/app.27357
12. A.J. de Menezes, G. Siqueira, A.A.S. Curvelo, A. Dufresne. Extrusion and characterization of functionalized cellulose whiskers reinforced polyethylene nanocomposites. Polymer 2009; 50:4552-4563.
DOI: 10.1016/j.polymer.2009.07.038
13. M. Grunert, W. Winter. Nanocomposites of cellulose acetate butyrate reinforced with cellulose nanocrystals. Journal of Polymers and the Environment 2002; 10:27-30.
DOI:10.1023/A:1021065905986
14. N. Ljungberg, J.-Y. Cavaillé, L. Heux. Nanocomposites of isotactic polypropylene reinforced with rod-like cellulose nanowhiskers. Polymer 2006; 47:6285-6292.
DOI: 10.1016/j.polymer.2006.07.013

15. M. Roman, W.T. Winter. Effect of sulfate groups from sulfuric acid hydrolysis on the thermal degradation behavior of bacterial cellulose. Biomacromolecules 2004; 5:1671-1677.
DOI: 10.1021/bm034519
16. Q. Liu, C. Lv, Y. Yang, F. He, L. Ling. Study on the pyrolysis of wood derived rayon fiber by thermogravimetry-mass spectrometry. Journal of Molecular Structure 2005; 733:193-202.
DOI: 10.1016/j.molstruc.2004.01.016
17. D.M. Panaistescu, D.M. Vuluga, H. Paven, M.D. Lorga, M. Ghiurea, I. Matasaru, P. Nechita. Properties of polymer composites with cellulose microfibrils. Molecular Crystals and Liquid Crystals 2008; 484:86-98.
DOI: 10.1080/15421400801903502
18. E. Bahar, N. Ucar, A. Onen, Y. Wang, M. Oksüz, O. Ayaz, M. Ucar, A. Demir. Thermal and mechanical properties of propylene nanocomposites materials reinforced with cellulose nano whiskers. Journal of Applied Polymer Science 2012; 125:2882-2889.
DOI: 10.1002/app.36445
19. C. Jiao, Z. Wang, Z. Gui, Y. Hu. Silane grafting and crosslinking of ethylene-octene copolymer. European Polymer Journal 2005, 1204-1211.
DOI: 10.1016/j.eurpolymj.2004.12.008
20. M.A.S.A. Samir, F. Alloin, J.-Y. Sanchez, A. Dufresne. Cellulose nanocrystals reinforced poly(oxyethylene). Polymer 2004; 45:4149-4157.
DOI: 10.1016/j.polymer.2004.03.094
21. F. Alloin, A. D'Aprea, A. Dufresne, N.E. Kissi, F. Bossard. Poly(oxyethylene) and ramie whiskers based nanocomposites: influence of processing: extrusion and casting/evaporation. Cellulose 2011; 18:957-973.
DOI: 10.1007/s10570-011-9543-x
22. K.P. Menard. Dynamic Mechanical Analysis: A Practical Introduction. CRC Press: Boca Raton, Florida (1999).
23. J.A. Molefi, A.S. Luyt, I. Krupa. Comparison of the influence of copper micro- and nano-particles on the mechanical properties of polyethylene/copper composites. Journal of Materials Science 2010; 45:82-88.
DOI: 10.1007/s10853-009-3894-9

24. M.A.S.A. Samir, F. Alloin, A. Dufresne. Review of recent research into cellulosic whiskers, their properties and their applications in nanocomposites field. Biomacromolecules 2005; 6:612-626.
DOI: 10.1021/bm0493685

25. Y.P. Khanna, E.A. Turi, T.J. Taylor, V.V. Vickroy, T.J.F. Abbott. Dynamic mechanical relaxations in polyethylene. Macromolecules 1985; 18:1302-1309.
DOI: 10.1021/ma000148a045

26. I.M. Ward, J. Sweeney. An Introduction to the Mechanical Properties of Solid Polymers. John Wiley & Sons, Hoboken (2004).

27. K.G. Nair, A. Dufresne. Crab shell chitin whiskers reinforced natural rubber nanocomposites. 3. Effect of chemical modification of chitin whiskers. Biomacromolecules 2003; 4:1835-1842.
DOI: 10.1021/bm030058g

28. L.A. Pothan, Z. Oommen, S. Thomas. Dynamic mechanical analysis of banana fiber reinforced polyester composites. Composites Science and Technology 2003; 63:283-293.
DOI: 10.1016/S0266-3538(02)00254-3

Chapter 5: Conclusions

The objective of this work was to prepare nanocomposites from whiskers extracted from sisal fibre as reinforcing phase for semicrystalline polymers, and to investigate the influence of the processing technique on the resulting properties. Two types of polyethylenes, LDPE and HDPE, were chosen as matrices because of the difference in their molecular characteristics. The nanocomposite films were prepared by two different techniques, melt compounding and solution casting from toluene, both followed by melt pressing. In the case of melt mixing, samples were also prepared where the whiskers were chemically modified with silane to improve their dispersion and compatibility with the host polymers. The dynamic mechanical, mechanical and thermal properties as well as the morphologies of these samples were investigated.

The sisal whiskers were obtained from sulphuric acid hydrolysis and subsequent treatments and appeared as elongated rodlike particles. This became evident when the peaks related to the amorphous part of the fibre disappeared in the whiskers' FTIR spectrum, and an increase in the crystallinity was observed in the WAXD analysis. The chemical modification of the whiskers was confirmed by FTIR. A good dispersion of the whiskers and interaction with the polymers were achieved because of the whiskers' surface modification. A similar dispersion was achieved for the untreated nanocomposites from both the processing techniques. The linear mechanical properties of the treated nanocomposites showed that silane treatment gave rise to a weaker reinforcing effect. The solution mixed nanocomposites showed a stronger reinforcing effect, even stronger than the untreated melt mixed nanocomposites. This is because of a rigid cellulosic network formed during the process of solution mixing. It seems as if the surface modification of the whiskers prevented the stronger interaction between the whiskers, because of the stronger interaction between the whiskers and the host matrices. Generally, the tensile properties of all the nanocomposites were improved upon the addition of the whiskers, and this effect was more profound for the HDPE based nanocomposites. This was evidenced by the tensile strength for the LDPE nanocomposites which was roughly constant, regardless of treatment and preparation method, whereas a significant increase was observed for the HDPE based nanocomposites. The crystallization behaviour of LDPE was not significantly influenced by the whiskers, the treatment or the preparation method. This was confirmed by the melting temperature and crystallinity which remained almost constant,

as well as the crystallites' perfection and dimensions that were not significantly influenced. The HDPE based nanocomposites showed an increase in crystallinity with the addition of the whiskers for all the nanocomposites, probably because of the strong nucleation effect of the whiskers in the higher crystallinity polymer. The thermal degradation of both polymers was not significantly influenced by the presence of the whiskers, the treatment or the preparation method.

Recommendations for future work:

Most studies reported in the literature for cellulose reinforced nanocomposites are prepared *via* solution casting/evaporation methods. Our study showed that the melt compounding process is a promising processing method to prepare the cellulose reinforced nanocomposites and to achieve good dispersion and improved mechanical properties comparable to solution casting/evaporation methods. Additionally, our study showed the possibility to prepare cellulose nanocomposites based on highly hydrophobic commodity plastics such as LDPE and HDPE using a melt compounding technique, which is almost not reported in the literature. Thus, the following can be recommended for future work:The utilization of surface modification for cellulose nanowhiskers which does not completely prevent interaction between the whiskers in order to improve the properties of the resulting nanocomposites.

ACKNOWLEDGEMENTS

I would to thank God Almighty for giving me constant strength, courage and endless blessings throughout this work and in my life without which the preparation and assembling of this work would be possible.

I would like to express my deep gratitude to Professor **Adriaan S. Luyt**, my supervisor, for his patient guidance, enthusiastic encouragement and useful critiques of this research work. The help and guidance given by him throughout this work shall carry me a long way in the journey of life on which I am about to embark.

I would also like to extend my thanks to the University of the Free State for the opportunity to study under their umbrella. I would also like this opportunity to thank Mrs Marlize Jackson, the Faculty' secretary for her generous service.

Special thanks to my late parents, Letsatsi Ramateka Mokhena and Maboteng Agnes Nondlala and the entire family of Mokhena, Mmipi and Nondlala. I am grateful for their guidance, support and love.

I would also like to thank:

- My fellow research group and colleagues (Dr Ahmad Essa, Dr Hei Wei, Dr Nagi Greesh, Mr Makgaotsa Jonas Mochane, Mr Teboho Motsoeneng, Mr Mfiso Mngomezulu, Mr Tshwafo Motaung, Mr Thabang Mokhutho, Mr Tladi Mofokeng, Mr Jeremiah Sefadi, Mr Tsietsi Tsotetsi, Mr Neo Moji, Mrs Nomampondomise Molefe, Mrs Moipone Malimabe, Ms Julia Mofokeng, Ms Motshabi Sibeko, Ms Zanele Clarke) for their support and valuable inputs. I am grateful for their cooperation during the period of assignment.
- My siblings, Hlouwe Malaka, Lesuping Mokhina and Madikotsi Mokhina
- My teachers, Ntate Samora Selometsi, Thabo Mpiti, Letuka Tshupane, Keta Tobalete, Sechaba Motloung, Adries Mokoena, Mr Moloi, Jimmy Selometsi, Mr Mokoena, Rashokoe Mpiti , Mpesi Mokhotla, Mrs Tselane Mbhele, Mrs Mokhatla, Mrs Moshoadiba, Mrs Ncanga, Mr Sekhonyane , Mr Rabiki, Mrs Jane Sethabela for their exemplary guidance and support.

- My friends Thabo Molefi, Mpedi Mosia, Manti Lesia, Tumelo Taemane, Essa Ahmad, Tshepo Mokoena, Benny Mokomatsili, Motlatsi Sethabela, Dominic Tomeng, Lotha Lungisa, Setjhaba Mohlakoana, Moeti Taioe, Bongane Salemane, Teboho Motsoeneng, Jonas Mochane for being there for me through hard times and constant encouragement without which this work would not be possible.
- Last but not least, George Diliyannis for providing us with unstabilised HDPE.

Appendix A

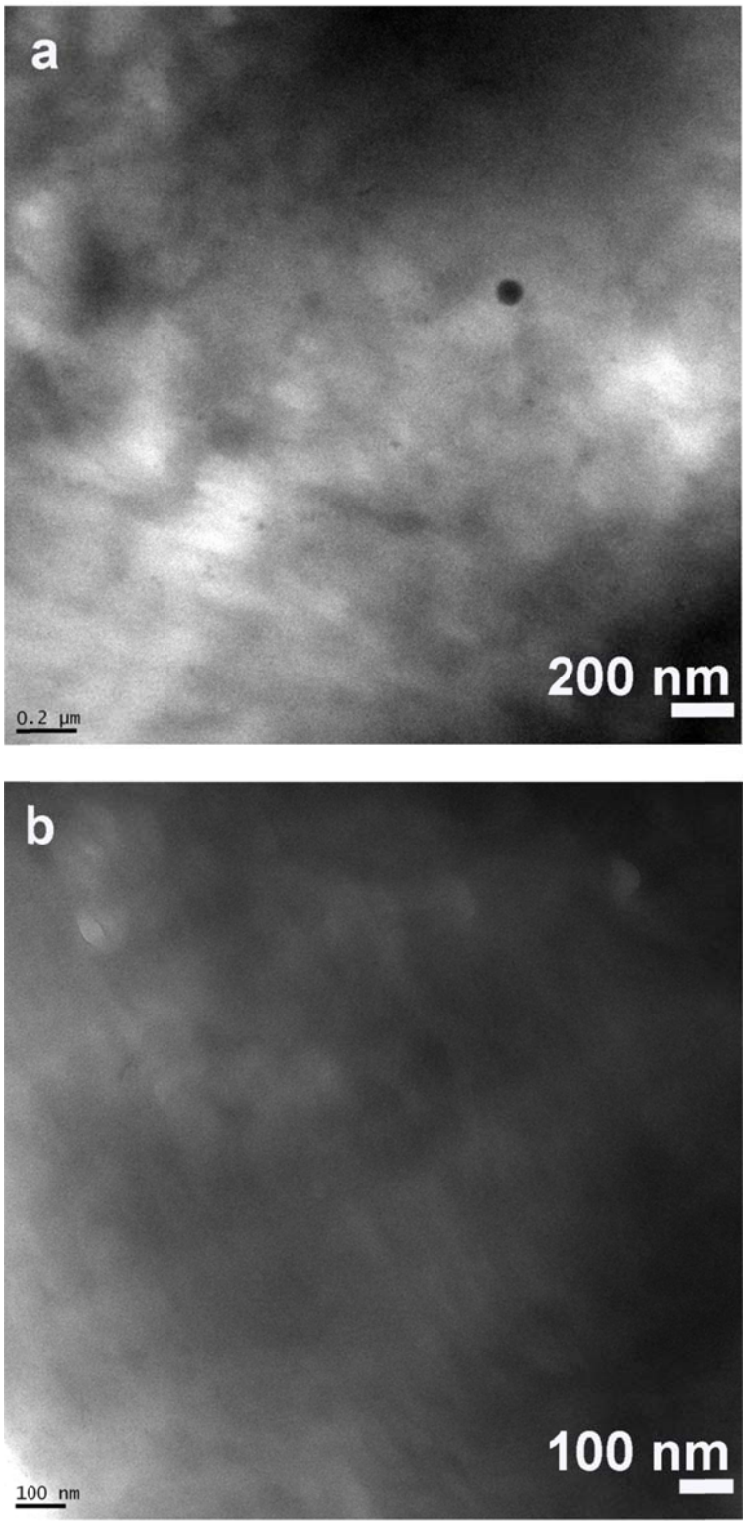

Figure A.1 TEM micrographs of LDPE/sisal whiskers nanocomposites: (a) untreated melt mixed 95/5 LDPE/sisal and (b) VTES treated melt mixed 95/5 LDPE/sisal

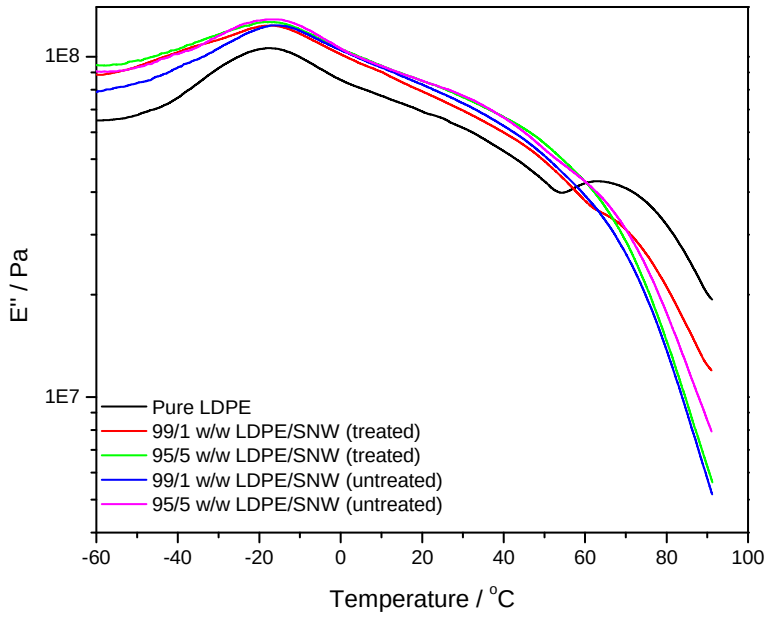

Figure A.2 Loss modulus versus temperature for neat LDPE as well as its untreated and VTES treated sisal nanocomposites

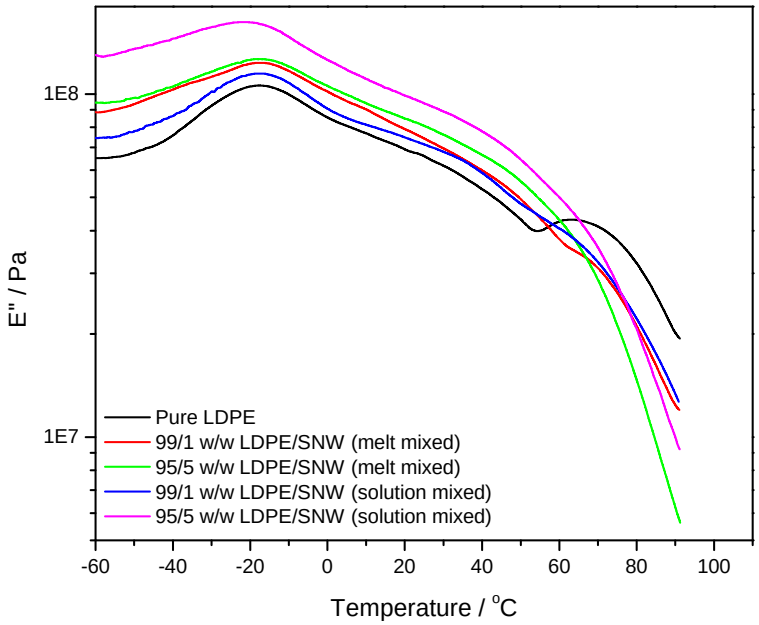

Figure A.3 Loss modulus versus temperature for neat LDPE as well as its melt and solution mixed sisal nanowhiskers nanocomposites

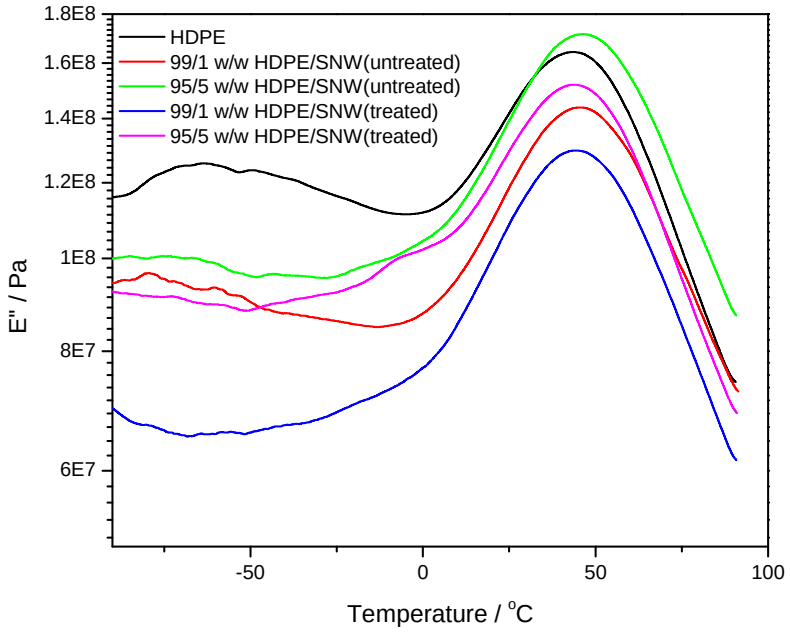

Figure A.4 Loss modulus versus the temperature for neat HDPE as well as its untreated and VTES treated sisal nanocomposites

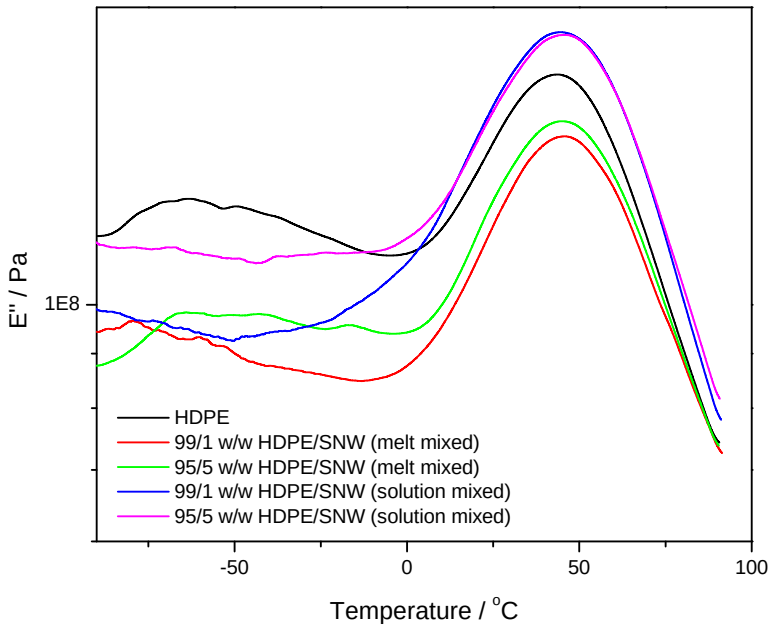

Figure A.5 Loss modulus versus temperature for neat HDPE as well as itsmelt and solution mixed sisal nanowhiskers nanocomposites

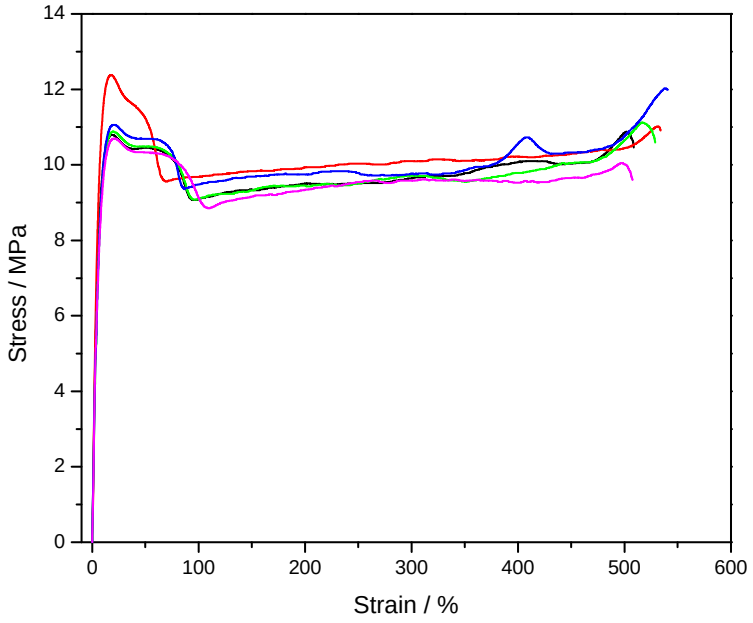

Figure A.6 Stress-strain curves of melt mixed LDPE

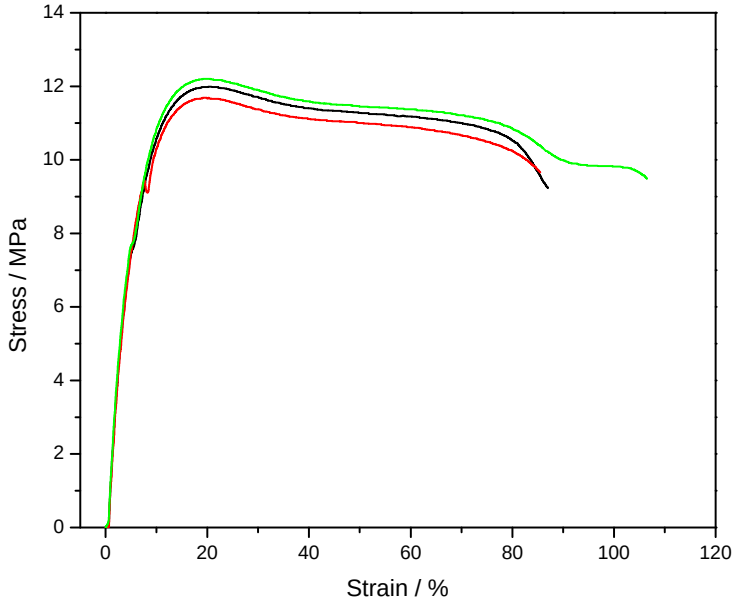

Figure A.7 Stress-strain curves of untreated melt mixed 99/1 w/w LDPE/SNW

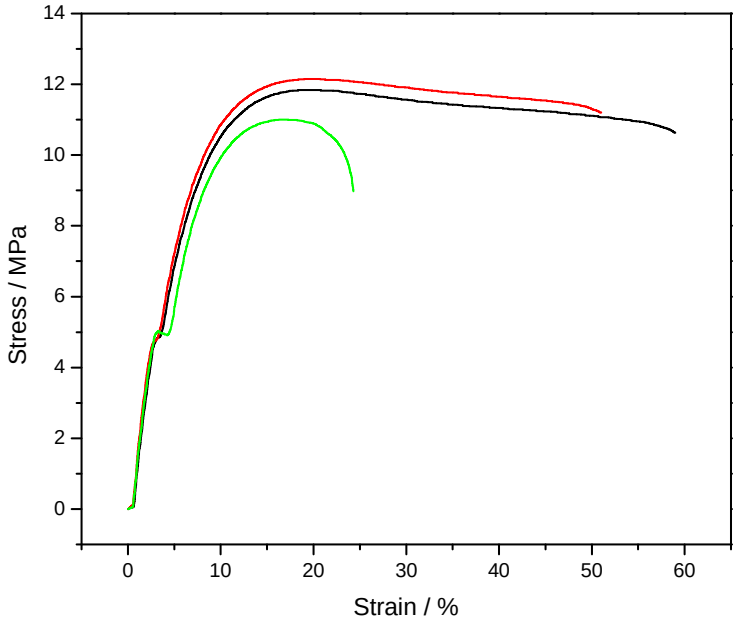

Figure A.8 Stress-strain curves of untreated melt mixed 95/5 w/w LDPE/SNW

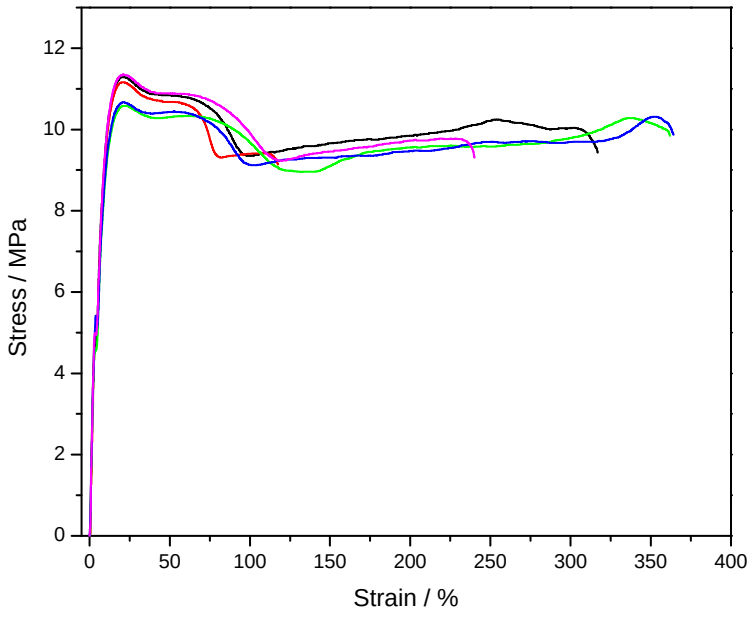

Figure A.9 Stress-strain curves of VTES treated melt mixed LDPE

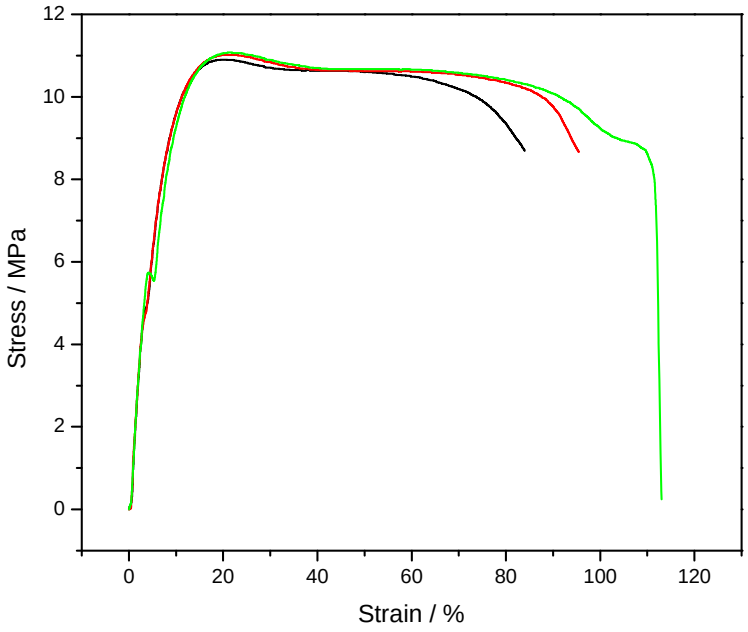

Figure A.10 Stress-strain curves of VTES treated melt mixed 99/1 w/w LDPE/SNW

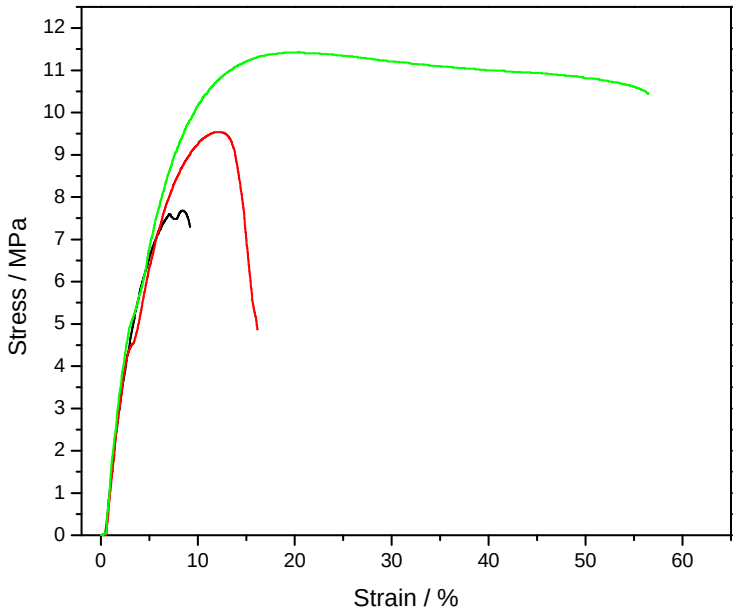

Figure A.11 Stress-strain curves of VTES treated melt mixed 95/5 w/w LDPE/SNW

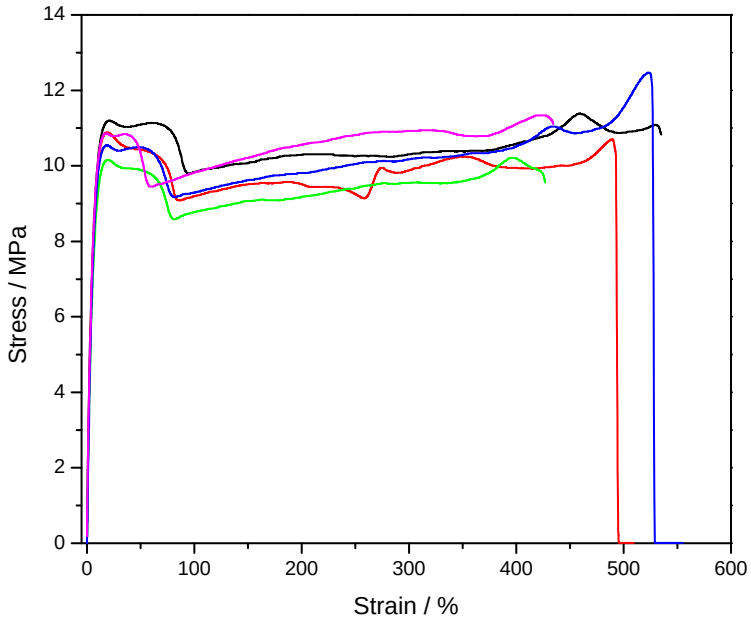

Figure A.12 Stress-strain curves of untreated solution mixed LDPE

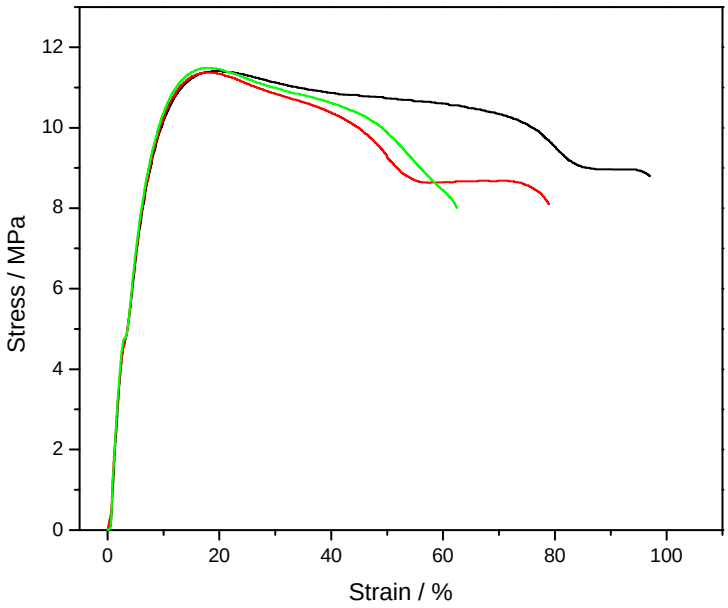

Figure A.13 Stress-strain curves of untreated solution mixed 99/1 w/w LDPE/SNW

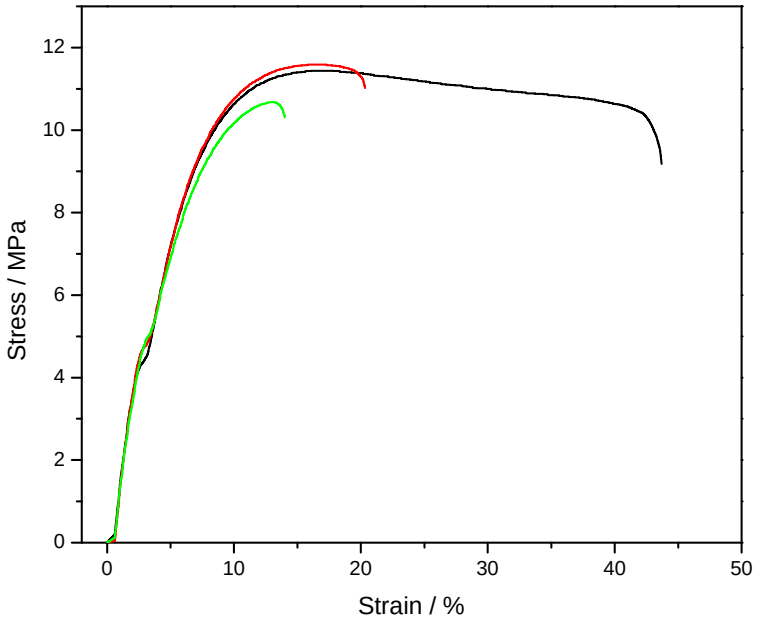

Figure A.14 Stress-strain curves of untreated solution mixed 95/5 w/w LDPE/SNW

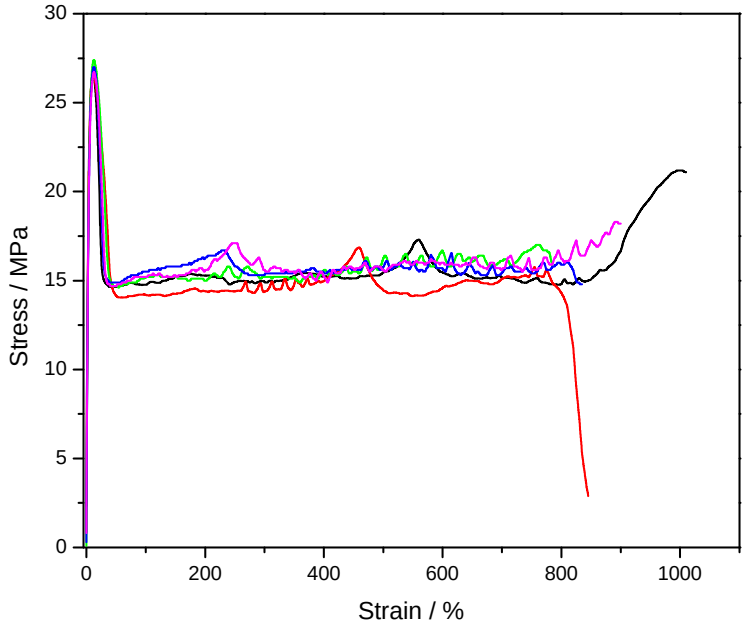

Figure A.15 Stress-strain curves of untreated melt mixed HDPE

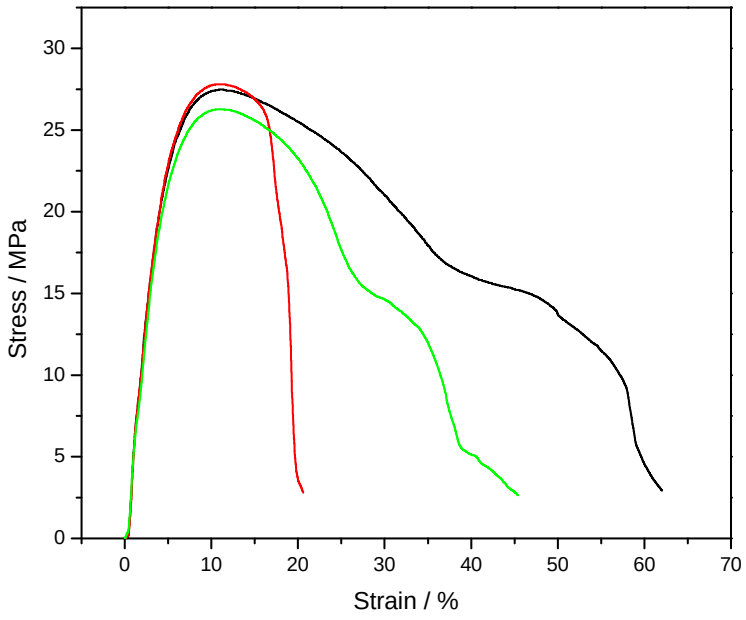

Figure A.16 Stress-strain curves of untreated melt mixed 99/1 w/w HDPE/SNW

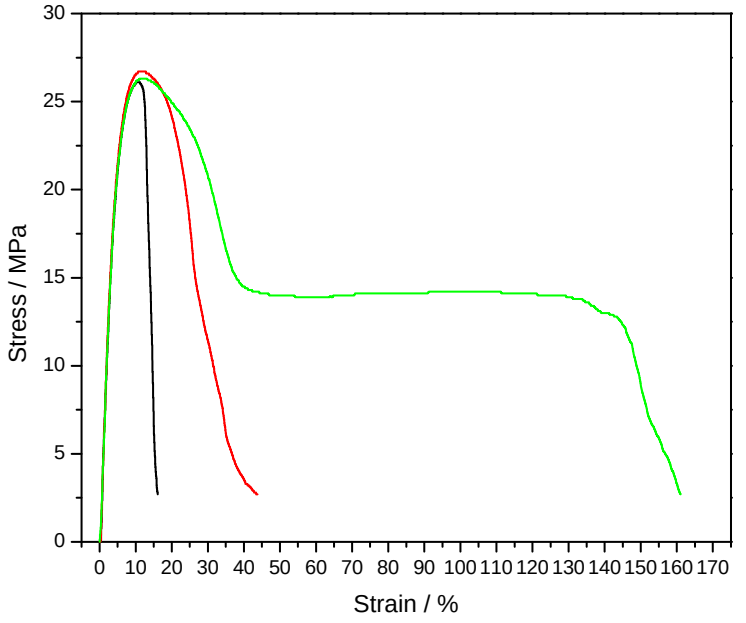

Figure A.17 Stress-strain curves of untreated melt mixed 95/5 w/w HDPE/SNW

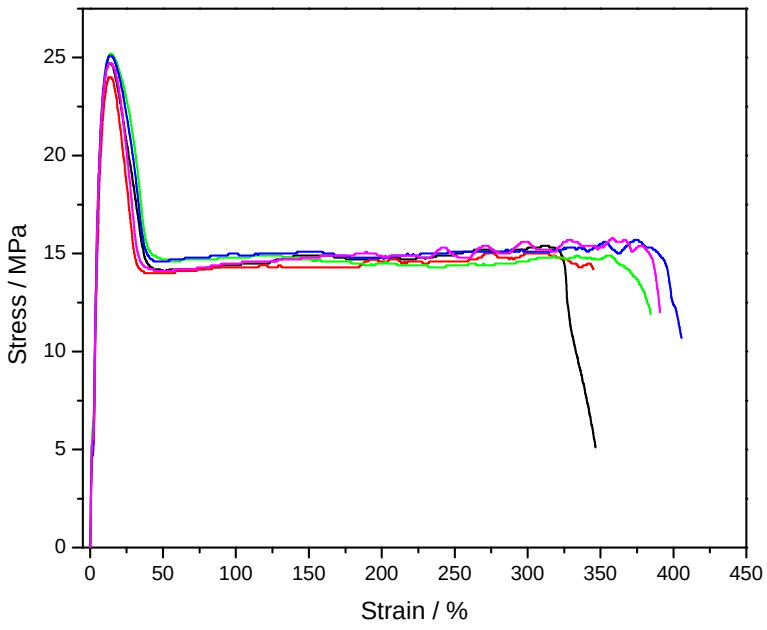

Figure A.18 Stress-strain curves of VTES treated melt mixed HDPE

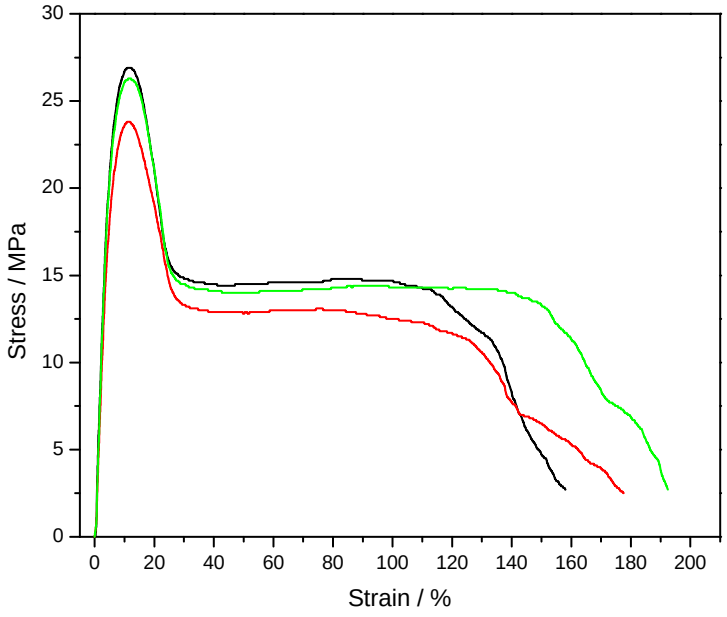

Figure A.19 Stress-strain curves of VTES treated melt mixed 99/1 w/w HDPE/SNW

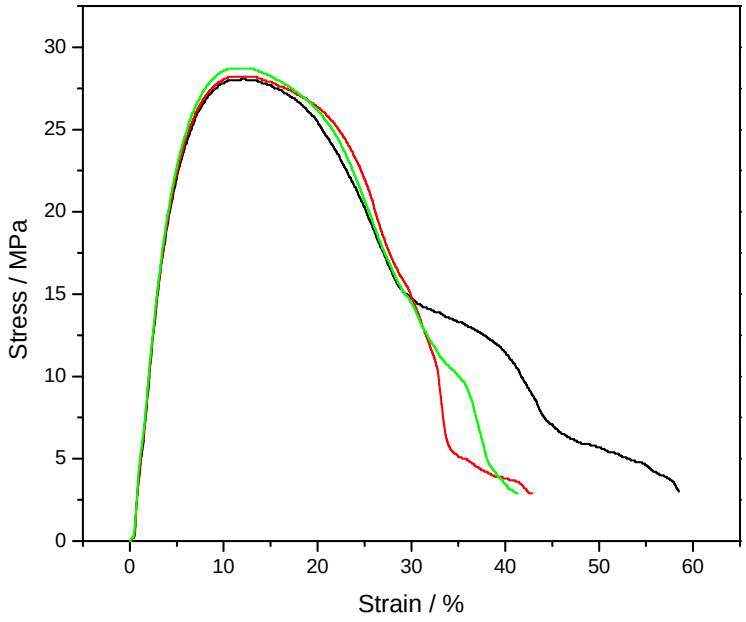

Figure A.20 Stress-strain curves of VTES treated melt mixed 95/5 w/w HDPE/SNW

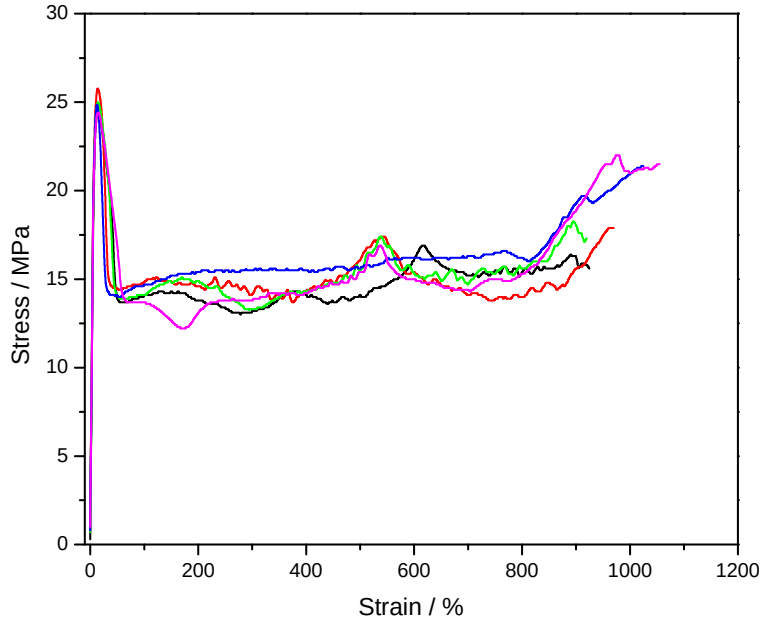

Figure A.21 Stress-strain curves of solution mixed HDPE

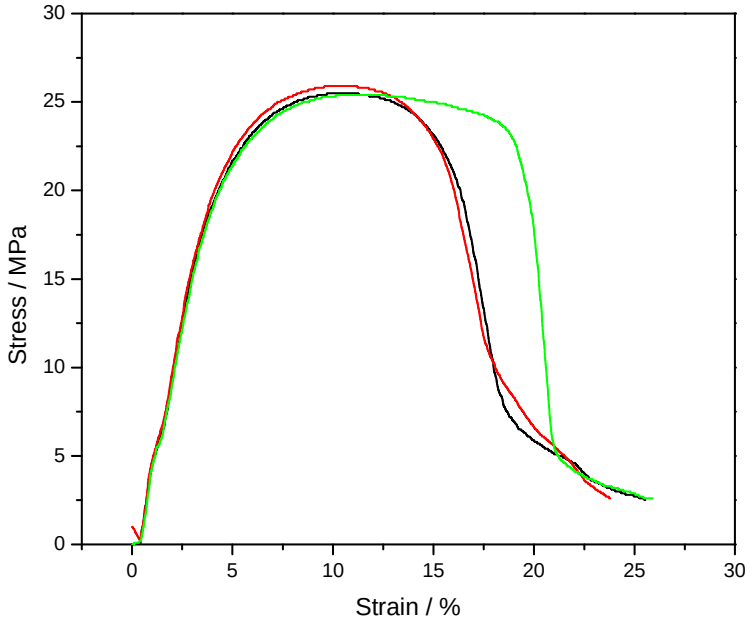

Figure A.22 Stress-strain curves of untreated solution mixed 99/1 w/w HDPE/SNW

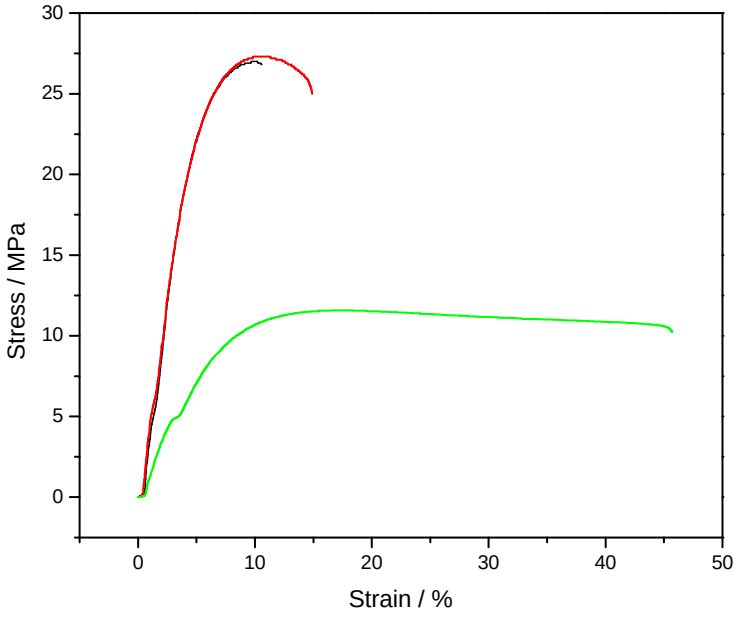

Figure A.23 Stress-strain curves of untreated solution mixed 95/5 w/w HDPE/SNW